UNIVERSITÀ DEGLI STUDI DI TRIESTE

# UNIVERSITÀ DEGLI STUDI DI TRIESTE

## XXXIII CICLO DEL DOTTORATO DI RICERCA IN

Dottorato in Biomedicina Molecolare

**PO FRIULI VENEZIA GIULIA - FONDO SOCIALE EUROPEO 2014/2020**

# Role of TRIM18, the Opitz Syndrome gene product, in the control of ciliogenesis through autophagy

Settore scientifico-disciplinare: **BIO-18**

DOTTORANDO / A
**Martina Mascaro**

COORDINATORE
**PROF. Germana Meroni**

SUPERVISORE DI TESI
**PROF. Germana Meroni**

**ANNO ACCADEMICO 2019/2020**

# Abstract

TRIM18/MID1 is an E3 Ubiquitin ligase belonging to the TRIM family of proteins that localises on microtubules. Loss-of-function mutations in the *MID1* gene have been associated with the X-linked form of Opitz G/BBB syndrome, a genetic disorder characterised by defects in ventral midline development. Within the cell, MID1 exists as a microtubular macromolecular complex, consisting of several MID1 interactors not all identified yet. Among them is α4, one of the regulatory subunits of Protein Phosphatase 2A (PP2A). MID1 has been reported to decrease the microtubular pool of PP2A catalytic subunit (PP2Ac) protein levels, thus leading to hypo-phosphorylation of its target proteins. MID1-lacking cells show increased levels of PP2Ac and a reduced association between mTOR and Raptor, leading to a downregulation of the mTORC1 signalling complex. This suggest that MID1 may act upstream of the mTORC1 signalling. Nevertheless, Opitz syndrome pathogenetic mechanisms have not been understood yet, but some clinical features are shared with another class of pathologies where genes controlling primary cilium dynamics are mutated, i.e. ciliopathies. Given this, we hypothesised that MID1 might be involved in the regulation of processes in which the primary cilium is involved.

The role of MID1 in primary cilium was investigated in a human epithelial cell line and in wild-type and *Mid1*$^{-/Y}$ Mouse Embryo Fibroblasts (MEFs). The data show that MID1 overexpression and *Mid1* depletion both cause impairment in primary ciliogenesis and/or primary cilia length, suggesting a role in the regulation of ciliary assembly. Being primary cilium dynamics regulated by autophagy, also controlled through the mTORC1 signalling, we asked whether primary cilia impairments caused by MID1 could be due to misregulations in the autophagy pathway. By analysing the same cellular models, we observed alterations in basal autophagy and in the starvation-induced autophagy flux in MID1-overexpressing cells and in *Mid1*$^{-/Y}$ MEFs.

My results indicate that MID1 is a negative regulator of both ciliogenesis and ciliary elongation, depending on cell type and culture condition, as well as a regulator of autophagy pathway, as reported for other members of the TRIM family. Taken together the results can give new insights on the Opitz syndrome pathogenetic mechanisms and we can suggest to consider this disease as a new ciliopathy.

# Sommario

**Abstract** ... 3
**1. Introduction** ... 6
**1.1. Opitz G/BBB Syndrome.** ... 6
**1.2. *MID1* gene and protein.** ... 8
**1.2.1. MID1 binds microtubules.** ... 10
**1.2.2. MID1 binds α4 and downregulates PP2Ac.** ... 11
**1.2.3. MID1 crosstalk with Sonic Hedgehog pathway.** ... 12
**1.2.4. MID1 regulation of protein translation.** ... 13
**1.3. Autophagy** ... 14
**1.3.1. Cellular quality control by the ubiquitin-proteasome system and autophagy.** ... 14
**1.3.2. Autophagy pathway.** ... 15
**1.3.3. Autophagy machinery.** ... 19
**1.3.4. Autophagy regulation.** ... 22
**1.4. Ciliogenesis and primary cilium dynamics.** ... 23
**1.4.1. Primary cilium structure.** ... 23
**1.4.2. Primary cilium assembly mechanism.** ... 25
**1.4.3. Intraflagellar transport and ciliary trafficking.** ... 28
**1.4.4. Primary cilium functions.** ... 29
**1.5. Ciliopathies.** ... 30
**1.6. Autophagy and primary cilium crosstalk.** ... 30
**2. Aim of the work** ... 33
**3. Materials and Methods** ... 34
**3.1. Cell Culture and transfection.** ... 34
**3.2. Preparation of Mouse Embryonic Fibroblasts (MEFs).** ... 34
**3.3. Immunofluorescence experiments.** ... 36
**3.3.1. Confocal imaging.** ... 36
**3.4. SDS-PAGE and Western-blot.** ... 36
**3.5. Primary cilia measurements and percentage of ciliated cells evaluation.** ... 37
**3.6. Statistical Analyses.** ... 37
**4. Results and Discussion** ... 39
**4.1. Ciliogenesis in ARPE-19 cells.** ... 39
**4.1.1. MID1 overexpression affects ciliogenesis in ARPE-19 cells.** ... 41
**4.1.2. MID1 E3 ubiquitin ligase activity is required to exert a role on primary cilium.** 42
**4.1.3. Dynamics of cilium elongation in the presence of exogenous MID1.** ... 44
**4.2. MID1 negatively regulates autophagy flux in ARPE-19 cells.** ... 48
**4.3. *Mid1*-depleted MEFs exhibit a longer primary cilium.** ... 57

**4.4. Autophagy flux regulation in MEFs.** ..... 62
**5. Conclusions** ..... 67
**6. Acknowledgements** ..... 70
**7. References** ..... 70

# 1. Introduction

The *MID1* gene, when mutated, is responsible of a form of the developmental disorder named Opitz G/BBB syndrome but the pathogenesis of the disease is still unravelled. In my thesis, I investigated cellular mechanisms that may help understanding the role of the *MID1* gene product in the onset of the disease.

## 1.1. Opitz G/BBB Syndrome.

Opitz G/BBB Syndrome (OS; OMIM: 300000) is a multiple congenital disease affecting midline structures development (Opitz et al., 1969a, 1969b). OS main features consist of facial anomalies (Figure 1), such as hypertelorism, prominent forehead, widow's peak, broad nasal bridge, anteverted nares, but also laryngotracheoesophageal defects (LTE) and genitourinary abnormalities, such as hypospadias, cryptorchidism and hypoplastic/bifid scrotum (Robin et al., 1996). There are two genetically forms of the disorder, an autosomal dominant and an X-linked form that are not distinguishable based on the clinical phenotype (Robin et al., 1996).

**Figure 1.** OS Patient frontal (left) and lateral (right) view (De Falco et al., 2003).

The autosomal dominant form (ADOS) is associated with a large region in chromosome 22 (22q11.2) that is frequently deleted in these patients. Recently, missense mutations in the *SPECC1L* gene on 22q11.2 have been reported to segregate with the phenotype in patients with autosomal dominant OS (Kruszka et al., 2015). SPECC1L is a cytoskeletal crosslinking protein, characterised by the presence of eight coiled-coil domains (CCDs) and a calponin homology domain (CHD), and it is involved in microtubule stability and actin cytoskeletal reorganization, playing a role in cell adhesion and migration (Saadi et al., 2011). SPECC1L is likely associated with the negative ends of the mitotic spindle microtubule, suggesting its involvement in spindle orientation and cell polarity. In addition, SPECC1L is involved in the response to stimuli acting during facial morphogenesis and requiring actin cytoskeleton reorganization: in fact, its knockdown leads to an impairment in the

reorganization of actin, in response to stimuli like increase of $Ca^{2+}$ and Wnt5a (Saadi et al., 2011). Although the phenotype of individuals harbouring *SPECC1L* mutations is indistinguishable from that of OS patients presenting no mutations in this gene, recent data suggest that the canonical LTE defects and male genital anomalies might not be observed in association with *SPECC1L* alterations (Bhoj et al., 2019). Therefore, it is possible that *SPECC1L* is not the only causative gene of the autosomal dominant form of OS in this region of human genome. Indeed, patients presenting the OS phenotype and 22q11.2 deletions that do not contain *SPECC1L* have been reported (Lacassie and Arriaza, 1996).

On the other hand, the X-linked form (XLOS) of the disease is caused by Loss-of-Function mutations in the *MID1/TRIM18* gene (hereafter *MID1*), localised on the short arm of the X chromosome at the level of band p22.3 in the proximity of the pseudoautosomal region (Quaderi et al., 1997). The prevalence of XLOS, hereafter OS, ranges from 1:50,000 to 1:100,000 in males. The females are usually carriers of the mutation on one allele and they present minor manifestations, usually ocular hypertelorism (Fontanella et al., 2008), likely as effect of X-inactivation mosaicism, although the reasons why only this feature is shown by carrier females has not been completely understood. The pathogenesis of the disease, despite several biochemical and cellular studies, is still not known. Defective fusion of midline tissues and reduced migration of Neural Crest cells during early development have been proposed but not substantiated yet by solid experimental data.

To start understanding the developmental mechanisms at the basis of OS, a mouse line carrying a non-functional *MID1* gene orthologue has been generated by disruption of the mouse *Mid1* first ATG-containing exon (Lancioni et al., 2010). Like in human, the *Mid1* gene is transcribed from the X chromosome-specific region although in mouse the 3' of the gene is located in the pseudoautosomal region thus spanning the boundary (Palmer et al., 1997). Whole mount and histological analyses of the $Mid1^{-/Y}$ show the presence of a malformed anterior cerebellum and sagittal sections through the vermis show hypoplasia and abnormalities of the most anterior lobes (I, II and III) (Lancioni et al., 2010): lobe I is totally missing, lobe II is not completely formed and lobe III is in many cases abnormal in shape (Figure 2). These defects originate during embryonic development as abnormalities in the anterior developing cerebellum are detectable since mid-gestation. Anterior cerebellar hypoplasia is also the brain anatomical abnormality present in approximately 35% of OS patients. This mouse line also displays behavioural defects that can correlate with intellectual disabilities and developmental delay observed in patients. Thus, the animal model recapitulates the neurological aspects of the disorder. However, craniofacial, tracheoesophageal, cardiac and urogenital abnormalities, that are shown by OS patients, are not present in $Mid1^{-/Y}$ mice: LTE region and the palate develop normally, there are no signs of

hypospadias, and ventricular and atrial septal defects are not observed (Lancioni et al., 2010). This discrepancy between the human and the murine phenotype might be due to either the genetic background or the evolutionary developmental differences between the two species that may translate in different expressivity of the clinical signs.

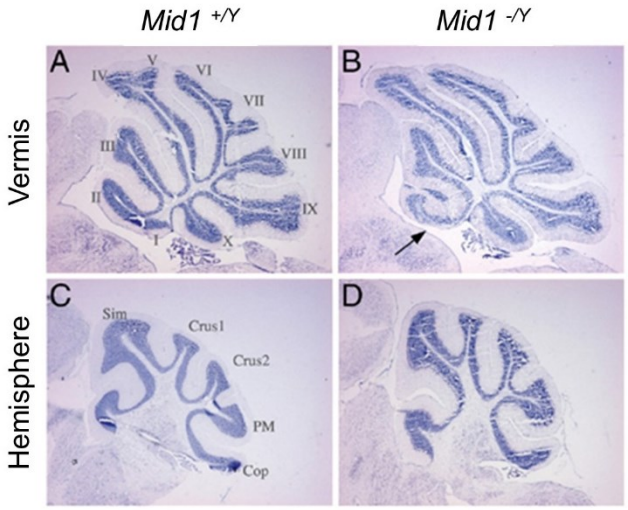


**Figure 2.** Abnormal cerebellum in *Mid1*$^{-/Y}$ mice. Sagittal sections through the cerebellar vermis (A, B) and hemisphere (C, D) of adult wild type and null mice stained with Nissl. Anterior is to the left. The numbers of the vermal and names of lateral lobes are indicated. The arrow in B indicates the anterobasal defect in *Mid1*$^{-/Y}$ mice (Lancioni et al., 2010).

## 1.2. *MID1* gene and protein.

The *MID1* gene encodes a member of the TRIpartite Motif (TRIM) family, hence also the name *TRIM18* for this gene (Reymond et al., 2001) and spans approximately 400 kb of genomic region (Quaderi et al., 1997; Perry et al., 1998; Van der Veyver et al., 1998). The gene consists of 9 coding exons (Figure 3A) and upstream to the first one the *MID1* gene presents alternative 5' untranslated exons and its transcription is driven by at least 5 alternative promoters (Landry and Mager, 2002). This results in several *MID1* transcript isoforms that involve not only the 5' of the gene and several polyadenylation signals but also the coding region and whose functions are not unravelled yet (Landry and Mager, 2002; Winter et al., 2004; Winter et al., 2007).

Like the other TRIM family members, MID1 is characterised by the presence of an N-terminal module composed of 3 domains (Figure 3B): a RING domain, two B-box domains (B-box 1 and B-box 2) and a coiled-coil region (Reymond et al., 2001). This tripartite motif is followed, in the MID1 protein, by a COS domain, a Fibronectin type III repeat (FN3), and a PRY-SPRY domain (Quaderi et al., 1997; Reymond et al., 2001; Short and Cox, 2006). The RING domain contains 8 residues that coordinate 2 atoms of zinc: seven conserved cysteine residues and a single conserved

histidine. The B-boxes assume a three-dimensional structure that is similar to the RING domain although their role is not yet clarified: B-box1 consists of one zinc atom coordinated by cysteine residues 119, 122, 142 and 145 and another one coordinated by cysteine residues 134 and 137 together with histidine residues 150 and 159 (Massiah et al., 2006); while B-box2 zinc atoms are coordinated with a so-called "cross-brace" pattern: one is coordinated by cysteine 175, histidine 178 and cysteine 195 and 198, the second one is coordinated by cysteine 187, aspartate 190 and histidine 204 and 207 (Massiah et al., 2007). The two B-box sequences are followed by a leucine-rich coiled-coil domain (Quaderi et al., 1997), implicated in homo- and hetero-interactions, and by a COS domain involved in MID1 association with microtubules (Cainarca et al., 1999; Schweiger et al., 1999; Short and Cox, 2006). MID1, like the other members of the TRIM family, belongs to the class of RING-containing E3 ubiquitin ligases (Meroni and Diez-Roux, 2005). Ubiquitin is a small 8-kDa peptide that is post-translationally bound to many, if not all, proteins to regulate their half-life, localisation or activity. In the Ubiquitination cascade, E3 ubiquitin ligases are responsible for substrate recognition favouring specific ubiquitin transfer and thus proper post-translational modification (Komander and Rape, 2012). Ubiquitin contains 7 lysine residues (Lys6, Lys11, Lys29, Lys33, Lys48 and Lys 63) that can be employed to build ubiquitin chains with different topology. In some cases, the N-terminal Met1 can also be employed to generate linear chains (Huang and Zhang, 2020). Mono- or poly-ubiquitination determines the fate of the substrates (Kulathu and Komander, 2012). Linkage through Lys48 leads to proteasomal degradation (Collins and Goldberg, 2017), Lys63 is involved in DNA repair, endocytosis and NF-κB (Nuclear Factor κ-light-chain-enhancer of activated B cells) signalling (Wu and Karin, 2015), whereas much less is known about the other linkages. It has been suggested that any linkage type may not be sufficient alone to fully address a substrate for proteasomal degradation (Lu et al, 2015). Ubiquitination cascade is carried out by three different enzymes: the E1 ubiquitin-activating enzyme transfers ubiquitin to an active cysteine of an E2 ubiquitin-conjugating enzymes, that transfers ubiquitin to the substrate with the help of a RING-containing E3 ubiquitin ligase (Shulman et al., 2009)

Despite more than 20 years of research on MID1 function, the pathogenesis of OS remains unresolved. In addition, the involvement of MID1 in clinically relevant conditions also in adulthood has further highlighted the need of better understanding its biological function.

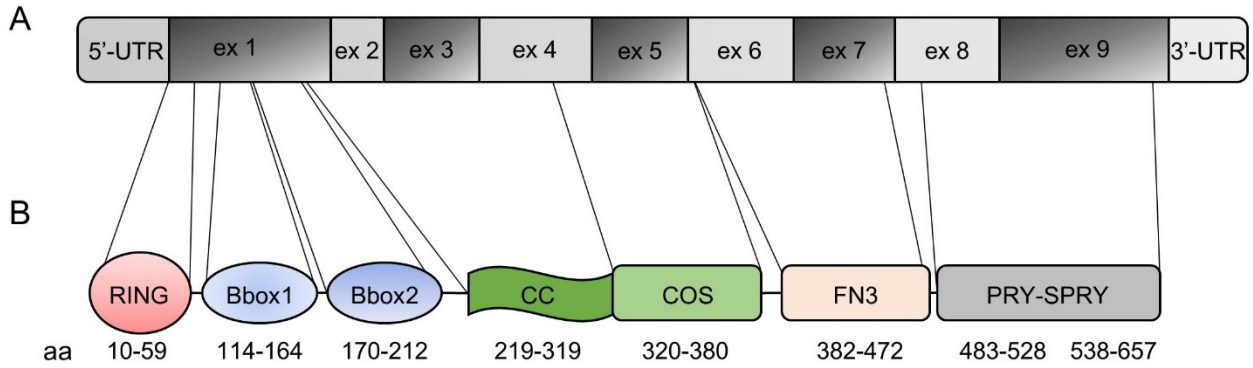


**Figure 3.** A) *MID1* gene mRNA structure. B) MID1 protein domain structure. The MID1 protein is 667 amino acid-long and the limits of the single domains are following in brackets: RING (10-59), Really Interesting New Gene domain; B-Box (B1, 114-164; B2, 170-212), B-Box domain; CC (219-319), Coiled-coil; COS (320-380), C-terminal subgroup one signature; FN3 (382-472), Fibronectin type III repeat; PRY (483-528), domain associated with SPRY domains; SPRY (538-657), SPla and the RYanodine Receptor (adapted from Baldini et al., 2020).

### 1.2.1. MID1 binds microtubules.

MID1 associates with microtubules during all cell cycle phases (Figure 4). It decorates the interphase microtubule apparatus but also the mitotic spindle during mitosis and the cytokinetic midbody microtubules (Cainarca et al., 1999; Schweiger et al., 1999; Gholkar et al., 2016; Zanchetta et al., 2017; Zanchetta and Meroni, 2019). MID1 is a phosphoprotein, and its phosphorylation status regulates microtubule binding dynamics (Liu et al., 2001; Aranda-Orgilles et al., 2008a) as well as its own bi-directional transport on microtubules (Aranda-Orgilles et al., 2008a).

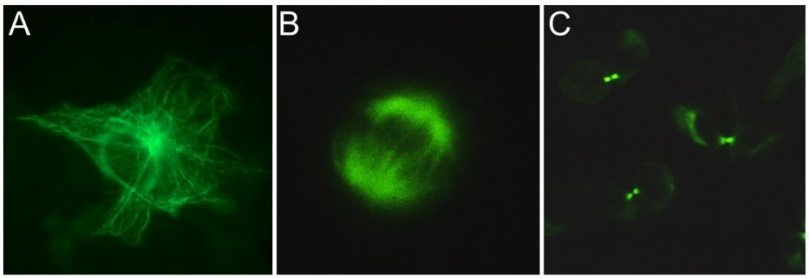


**Figure 4.** Immunofluorescence showing anti-MID1 antibody labelling in COS7 cells, followed by FITC-conjugated anti-rabbit antibody. A) Subcellular localization of endogenous MID1 protein in interphase, B) MID1 localisation in the mitotic spindle, C) MID1 labelled midbodies (Cainarca et al., 1999)

Whether MID1 association with microtubules affects their stability and dynamics is still not clear. What is known is that microtubule localisation is lost when MID1 harbours mutations found in OS patients, and this condition does not lead to microtubules disruption and/or dynamics impairment (Cainarca et al., 1999; Schweiger et al., 1999). On the contrary, in some instances, exogenous MID1 expression has a protective effect on microtubules from depolymerising drugs action (Schweiger et al., 1999), although in this case MID1 stabilising effect might be due to its sustained and strong expression. In addition, it has been observed that the cooperation of MID1 with one of its partners, MIG12 (MID1 interacting G-12 like protein, or MID1IP1), may contribute to microtubule stabilisation (Berti et al., 2004). MIG12 is detected on microtubules when co-transfected with MID1 and this interaction protects microtubules from depolymerisation. From a physiological point of view, it is possible that microtubule stabilisation might occur transiently in specific phases of cell life. Interestingly, MID1-deprived cells display division defects, such as cytokinetic arrest and delayed or aborted abscission, which induce cell binucleation or death (Gholkar et al., 2016). Moreover, a recently discovered partner of MID1, BRAF35 (BRCA2-Associated Factor 35), is involved in cytokinesis and both localise at the midbody where stable microtubules are present (Zanchetta and Meroni, 2019; Zanchetta et al., 2017). These data support the idea that MID1 might regulate microtubule dynamics in defined cell cycle phases. It is possible that MID1-dependent control of microtubule dynamics may also regulate other cellular processes in which these structures are involved.

### 1.2.2. MID1 binds α4 and downregulates PP2Ac.

As said above, MID1 is an E3 ubiquitin ligase implicated in ubiquitin post-translational modification. One of the first discovered MID1 interactor is Alpha4 (hereafter α4), the mammalian homologue of the yeast protein TAP42 and a non-canonical subunit of protein phosphatase 2A (PP2A) (Di Como and Arndt, 1996; LeNoue-Newton et al., 2016). MID1 interacts with α4 C-terminal domain through its B-box1 domain (Liu et al., 2001; Trockenbacher et al., 2001): through this interaction, MID1 tethers α4 to microtubules (Short et al., 2002) and indeed α4 assumes a typical microtubular pattern in MID1-overexpressing cells (Liu et al., 2001). In contrast, high levels of α4 displace MID1 from microtubules, without affecting microtubular structure and dynamics (Liu et al., 2001). Early analyses showed that α4 was not a proper target as it was not ubiquitinated upon MID1 overexpression. On the contrary, the catalytic subunit of PP2A (PP2Ac) level decreases when MID1 is overexpressed in cells (Trockenbacher et al., 2001). Therefore, α4 might serve as an adaptor protein promoting the formation of a ternary MID1/α4/PP2Ac complex and α4 promotes poly-ubiquitination of PP2Ac by scaffolding it to MID1 (Trockenbacher et al., 2001). However, at

the same time, α4 might act as a protective factor for PP2Ac degradation, through its ubiquitin interacting motif (UIM). It was shown that MID1 mono-ubiquitinates α4 leading to its calpain-mediated cleavage thus switching α4 activity from protective to degradative. In particular, the cleavage involves the C-terminal domain, implicated in MID1 interaction (Watkins et al., 2012). Consequently, MID1 loss-of-function leads to a reduction of the calpain-mediated cleavage of α4, thus increasing the protection of PP2Ac from proteasomal degradation. This can also explain the hypo-phosphorylated status of several microtubule-associated proteins (MAPs) observed in OS patients' fibroblasts (Trockenbacher et al., 2001). It is therefore possible that the MID1 E3 ligase activity is exerted on α4 and that PP2Ac poly-ubiquitination might be performed by another E3 ubiquitin ligase(s), since the calpain-mediated cleavage of α4 makes MID1 detach from the ternary MID1/α4/PP2Ac complex, leading to the hypothesis that cleaved α4 might redirect PP2Ac localisation promoting its polyubiquitination. In this way, only the microtubule pool of PP2Ac would be subjected to proteasomal degradation.

Since PP2A is involved in the regulation of several biological processes (Sontag, 2001), the MID1/α4/PP2Ac complex can modulate these activities mainly on microtubules. Indeed, this complex has been demonstrated to regulate the mechanistic Target Of Rapamycin Complex 1 (mTORC1) signalling in OS fibroblasts and in tumour cells. MID1-lacking cells having increased levels of PP2Ac show a reduced association between mTOR and Raptor, leading to a downregulation of mTORC1 complex formation and signalling (Liu et al., 2011). The mTORC1 signalling is involved in several processes, e.g. autophagy, protein synthesis, cell metabolism and proliferation (Jhanwar-Uniyal et al., 2019), to name some, and dysfunction of these in OS might contribute to the observed patients' phenotype.

### 1.2.3. MID1 crosstalk with Sonic Hedgehog pathway.

The data above suggest that a tight link exists between MID1 and the mTORC1 signalling. Among the several networks in which mTORC1 is involved, it has been reported that inhibition of mTORC1 activity upon rapamycin treatment reduces the translocation of the Sonic Hedgehog (Shh) pathway transcription factor GLI3 from the cytoplasm to the nucleus. In HeLa cells, activation of PP2A via inhibition of its catalytic subunit degradation, mediated by the MID1/α4 complex, leads to cytosolic retention of GLI3 and, as a consequence, a reduction of its function as a transcription activator (Krauss et al., 2008; Krauss et al., 2009). Moreover, MID1 could interact with Fu, a component of the Shh pathway, promoting its ubiquitination (Schweiger et al., 2014). Whether this process is a direct consequence of MID1 E3 ubiquitin ligase activity is not demonstrated yet. In addition, if this modification leads to the proteasome-mediated cleavage of Fu that produces a

90kDa ΔN-terminal fragment is presently unclear. A mimic of this putative ΔN-terminal fragment increases GLI3 nuclear localisation and, when the cleavage of Fu is reduced, e.g. due to MID1 silencing, nuclear translocation of GLI3 decreases leading to a consequent reduction of the expression of SHH target genes (Schweiger et al., 2014). Indeed, several data indicate that MID1 is involved in a reciprocal crosstalk with the Shh pathway. Although this phenomenon has been studied in cancer cell lines, the crosstalk between MID1 and the Shh pathway can be highly relevant in development given the strong implication of the Shh pathway in ventral midline definition as also observed in the phenotypic signs of OS. During development in *Xenopus*, ectopic Shh induces *mid1* expression in the entire developing optic vesicle, but also in the prospective forebrain (Pfirmann et al., 2016). Moreover, in the chicken Hensen's node, Shh can suppress *mid1* expression and mid1 can act upstream of Shh, due to the induction of *bmp4* expression (Granata and Quaderi, 2003). In this way, a feedback loop may exist, regulating the balance between *mid1* expression with medium levels of Shh inducing *mid1* expression, and lower levels suppressing *mid1* expression.

### 1.2.4. MID1 regulation of protein translation.

MID1 acts not only on proteic substrates but is also part of ribonucleoprotein (RNP) complexes (Aranda-Orgilles et al., 2008b). The MID1/α4 complex is able to bind several mRNAs carrying purine-rich region and forming hairpin structures, also named MID1 association sequence (MIDAS) (Aranda-Orgilles et al., 2011; Aranda-Orgilles et al., 2008b; Hettich et al., 2014). Through this association, MID1 tethers the transcripts to the ribosome- and translation-associated factors, namely elongation factor 1α (EF-1α), receptor of activated protein kinase C1 (RACK1), Nucleophosmin (NPM), Annexin A2 (ANXA2) and several 40S ribosomal proteins, thus promoting protein translation (Aranda-Orgilles et al., 2008b; Hettich et al., 2014; Kohler et al., 2014; Krauss et al., 2013; Matthes et al., 2018b). The disruption of the MID1/α4 binding is sufficient to abrogate the enhancing effect on the translation of mRNAs that are bound to the mRNP complex (Monteiro et al., 2018).

Among the MIDAS-harbouring transcripts, the 3-phosphoinositide dependent protein kinase-1 (PDPK-1) has been identified in association with the MID1-containing complex. PDPK-1 is a serine/threonine kinase involved in many cellular processes that plays a pivotal role, among others, in the mTOR signalling (Carneiro et al., 2015). Mutations in the *MID1* gene have been demonstrated to reduce PDPK-1 protein translation efficiency, since a functional *MID1* gene is able to rescue its synthesis (Aranda-Orgilles et al., 2011). Another example is represented by the β-secretase 1 (BACE1) sequence that encompasses several sites that fold like a MIDAS motif

enabling the BACE1 transcript to bind the MID1-complex promoting its translation (Aranda-Orgilles et al., 2011).

Neither the MID1 protein nor the other components of the multiprotein complex seem to contain any known RNA-binding domain (Aranda-Orgilles et al., 2008b). However, other members of the TRIM protein family have recently emerged as direct RNA binding partners through their C-terminal domains (i.e. NHL or PRY/SPRY domains) (Williams et al., 2019) and this can represent a novel role to explore for the members of this family.

## 1.3. Autophagy

### 1.3.1. Cellular quality control by the ubiquitin-proteasome system and autophagy.

As reported above, MID1 is an E3 ubiquitin ligase, involved in the ubiquitination of proteins mainly heading them to proteasome-mediated degradation. Actually, within the cells two proteolitic systems are implicated in protein degradation: the Ubiquitin-Proteasome System (UPS) and autophagy, the other mechanism by which cells control the quality of proteins and organelles to maintain proper cell homeostasis. A common feature between these two processes is ubiquitination: ubiquitination modifies substrates that can be destined to both proteasome- and lysosome-dependent degradation (Ohtake and Tsuchiya, 2017). Autophagy is a sort of backup system for protein substrates that cells cannot degrade through the proteasome. In the case of autophagy, the cargoes are collected by autophagic receptors such as p62/ SQSTM1 or NBR1, neighbour of BRCA1 gene 1 (Zaffagnini and Martens, 2016; Lamark et al., 2017). These cargo receptors recognise ubiquitin chains on substrates and at the same time interact with ATG8s proteins on autophagosomes through their LIR (LC3 interacting region) sequence (Cha-Molstad et al., 2015; Lamark et al., 2017). If protein aggregates cannot be degraded, the cargoes are collected by HDAC6 (histone deacetylase 6) through its ubiquitin binding domain (Ciechanover and Kwon, 2017), to be then degraded partially in the lysosome (Hyttinen et al., 2014). The cargo receptors seen above preferentially bind Lys63 chain linkages (Kirkin et al., 2009): parkin, TRIM13 and CHIP are some of the E3-ubiquitin ligases assembling Lys63 linkages on protein substrates destined to autophagy-mediated degradation (McKeon et al., 2015; Tomar et al., 2013; Ferreira et al., 2015). Some works show examples in which autophagy is activated when ubiquitinated proteins are not properly processed by proteasomes: proteasome inhibitors have been found to induce compensatory autophagy (Cha-Molstad et al., 2015), as well as rapamycin, a TOR inhibitor, that relieves the proteolytic load and cellular proteotoxicity from proteasomal inhibition (Ji and Kwon, 2017; Pan et al., 2008). On the opposite way, autophagy can impair proteasomal flux and result in the accumulation of ubiquitinated substrates (Matsumoto et al., 2011; Munch et al., 2014). Although it is clear that the

two systems are mutually regulated, many aspects regarding the mechanisms of selectivity and crosstalk remain to be clarified.

Recent works have shown how some TRIM proteins act as autophagy cargo receptors: an example is TRIM5α, targeting HIV-1 for autophagy destruction (Mandell et al., 2014), or TRIM16, targeting damaged lysosomes and phagosomes through the help of galectin 3 (Chauhan et al., 2017). Other TRIM E3 ligases are reported to regulate other steps of the autophagy pathway: for instance, TRIM21 has been reported to inhibit p62 polymerisation by ubiquitinating its Lys7 (Pan et al., 2016), or TRIM13 is involved in the autophagy induction during ER stress, maybe playing a role in autophagosome formation in the ER (Tomar et al., 2012). Several are the examples of TRIM proteins found to be involved in the autophagy pathway, and likely several mechanisms that are still not completely understood in autophagy induction and suppression may be regulated by TRIM proteins activity.

None of the screenings performed to date to assess TRIM proteins role in autophagic process identified MID1 as a regulator of this pathway (Mandell et al., 2014). However, a MID1 role in autophagy cannot be excluded in specific conditions and stimuli. For example, being a microtubule-associated protein, it might regulate autophagosome movement along microtubules (Kimura et al., 2008; Mackeh et al., 2013). Moreover, MID1-dependent degradation of a pool of PP2A catalytic subunit with the effect described above of regulating mTOR/Raptor association (Liu et al., 2011), can suggest that MID1 can work as a negative regulator of autophagy induction. Indeed, mTOR/Raptor phosphorylation status depends also on PP2A activity and the degradation of PP2Ac can lead to hyperphosphorylation of the mTORC1 complex, activating its signalling pathway that in turn blocks autophagy induction (see also below).

### 1.3.2. Autophagy pathway.

Autophagy is a “self-eating” process by which damaged and/or dysfunctional cellular organelles and proteins are degraded through lysosomes. However, this is not the only purpose of autophagy, since this process consists in a dynamic recycling system producing new materials and energy for cellular homeostasis (Mizushima and Komatsu, 2011). In this way, autophagy is needed to make morphological and functional changes to occur, for instance, during development and differentiation processes, that are always accompanied by drastic cellular and tissue remodelling, which require the elimination of pre-existing materials, thus supporting the building of new structures (Mizushima and Levine, 2010; Tsukamoto et al., 2008; Kuma et al., 2004). Moreover, other vital roles of autophagy are the maintenance of amino acids pool during stress conditions, the clearance of microbes and, consequently, the regulation of innate and adaptive immunity (Levine

and Deretic, 2007; Mizushima and Klionsky, 2007; Levine and Kroemer, 2008). Cancer, metabolic and neurodegenerative disorders, cardiovascular and pulmonary diseases, as well as several developmental diseases are caused by deregulations in the autophagy process (Levine and Kroemer, 2008; Mizushima et al., 2008; Perrotta et al., 2020).

In the last two decades, several genetic studies in yeast identified the so-called autophagy-related (*ATG*) genes (Klionsky et al., 2003; Nakatogawa et al., 2009), thus initiating the analyses of autophagy-defective organisms to better understand both how the pathway works and its physio-pathological role, in cells and *in vivo*, not only in yeast but also in vertebrates.

There are three main types of autophagy:

- Chaperone-mediated autophagy (CMA): this highly specific type of autophagy is a mechanism that makes the cells degrade proteins that directly translocate across the lysosomal membrane. HSPA8/HSC70 (Heat Shock 70 kDa protein 8) recognises a KFERQ pentapeptide motif on target proteins (Chiang et al., 1989). HSPA8 delivers the protein substrate to the lysosomal membrane, where the target is unfolded (Agarraberes and Dice, 2001) and then recognised by LAMP2A (lysosomal-associated membrane protein 2A) that multimerises making the substrate translocate into the lysosomal lumen (Bandyopadhyay et al., 2008; Orenstein and Cuervo, 2010; Parzych and Klionsky, 2014). Glycolytic enzymes, some transcription factors, proteasome subunits and proteins involved in vesicular trafficking are some of the substrate proteins degraded through this process (Arias and Cuervo, 2011).
- Microautophagy: in this case the lysosome engulfs small components present in the cytoplasm by forming invaginations of the lysosomal membrane. Microautophagy is involved in the maintenance of organelle size, membrane homeostasis and cell survival under nitrogen restriction (Marzella et al., 1981; Li et al., 2012). Relatively little is known about this process, including its regulation.
- Macroautophagy: this is the main autophagic pathway, characterised by the formation of a double-membrane vesicle, the autophagosome, in which cytoplasmic cargoes are delivered. Autophagosomes do not bud from a pre-existing organelle but form by expansion (Yang and Klionsky, 2009). In mammals, autophagosome formation starts at multiple sites within the cytoplasm: several studies suggest the endoplasmic reticulum (ER) structures, called omegasomes, as the initiation sites for autophagosome formation (Hayashi-Nishino et al., 2009). Following this initiation step, the membrane expands, forming the so-called phagophore, which is the double-membrane structure-sequestering compartment (He and Klionsky, 2009). Eventually, the phagophore double-membrane bends to generate a

spherical autophagosome (Parzych and Klionsky, 2014). At this point, the cargo must be delivered to the lysosome and the outer membrane of the autophagosome fuses with the lysosomal one, forming the autolysosome (Yang and Klionsky, 2009). Finally, lysosomal hydrolases digest the inner membrane of the autophagosome and the autophagic cargo (Figure 5). The degraded components are exported into the cytoplasm to be used by the cell in biosynthetic processes or to generate energy (Yorimitsu and Klionsky, 2011). There are two different types of macroautophagy: a nonselective process, by which the cell degrades a portion of cytoplasm material randomly sequestering it into autophagosomes, and a selective one, in which specific cargoes, such as specific proteins, organelles and invading bacteria, are embedded into autophagosomes (Mizushima et al., 2011; Parzych and Klionsky, 2014). Hereafter I will refer to macroautophagy as autophagy and I will discuss autophagy in mammals.

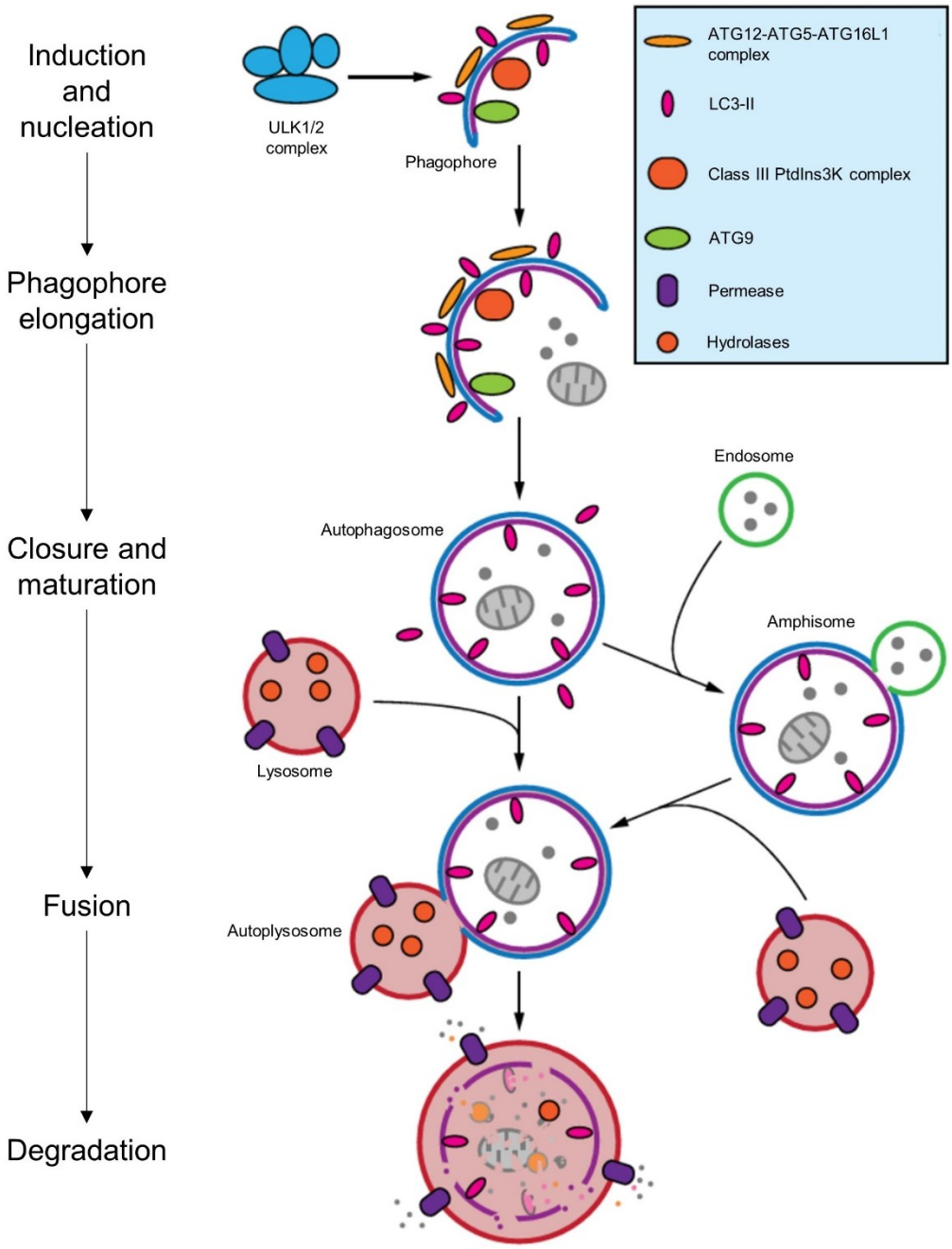


**Figure 5.** Nucleation of the phagophore occurs through the induction by the ULK1/2 complex. Elongation of the phagophore is aided by the ATG12-ATG5-ATG16L1 complex, the class III PtdIns3K complex, LC3-II, and ATG9. Eventually, the expanding membrane closes around its cargo to form an autophagosome. The outer membrane of the autophagosome will then fuse with the lysosomal membrane to form an autolysosome. In some instances, the autophagosome may fuse with an endosome, forming an amphisome, before fusing with the lysosome. The contents of the autolysosome are then degraded and exported back into the cytoplasm for reuse by the cell (adapted from Parzych and Klionsky, 2014)

### 1.3.3. Autophagy machinery.

In mammalian cells, induction of autophagosome formation starts with the assembly of an initiation complex, including either ULK1 or ULK2, ATG13, RB1-inducible coiled-coil1 (RB1CC1/FIP200), which are required for the induction of autophagy, and C12otf44/ATG101 (Hara et al., 2008; Ganley et al., 2009; Jung et al., 2009; Hosokawa et al., 2009).

At this initial point, another complex is recruited: the ATG14-containing class III phosphatidylinositol-3-kinase (PtdIns3K) complex (Itakura and Mizushima, 2010) that generates phosphatidylinositol-3-phosphate (PtdIns3P) essential for autophagy (Burman and Ktistakis, 2010). The PtdIns3K complex, consisting of PIK3C3/VSP34, PIK3R4/p150 and BECN1, is involved in the nucleation of the phagophore (Furuya et al., 2005; Itakura et al., 2008; Kihara et al., 2001; Liang et al., 1999; Yan et al.,2009). There are several proteins binding the PtdIns3K complex, i.e. WIPI1 and WIPI2, as well as the zinc-finger FYVE domain containing 1 (ZFYVE1/DFCP1), although their precise function in autophagy needs to be clarified (Jeffries et al., 2004; Polson et al., 2010; Proikas-Cezanne et al., 2004; Axe et al., 2008).

Two Ubiquitin-like (UBL) systems contribute to phagophore elongation (Weidberg et al., 2011), (Figure 6). The first system leads to the formation of a complex consisting of ATG12, ATG5 and ATG16L1: ATG12 is conjugated to ATG5 in an ATG7 (E1-like enzyme)- and ATG10 (E2-like enzyme)-dependent manner (Kim et al., 1999; Shintani et al., 1999; Ohsumi, 2001). ATG16L then noncovalently binds to ATG5 and dimerises, forming a larger complex (Mizushima et al., 2003). This complex associates with the phagophore but detaches after autophagosome maturation (Mizushima et al., 2003; Mizushima et al., 2001). The second UBL system consists of the LC3 (microtubule-associated protein 1 light chain 3) and GABARAP (gamma-aminobutyric acid receptor-associated protein) conjugating system, also called ATG8 conjugating system (Ichimura et al., 2000). Being LC3 the most studied ATG8 protein in mammals, hereafter I will indicate LC3 as representative of ATG8 proteins. ATG4, a cysteine protease, makes LC3 to expose a glycine residue at its C-terminus by proteolytic cleavage, named LC3-I (Kirisako et al.,2000; Geng and Klionsky, 2008). ATG7 then activates LC3-I and transfer it to ATG3 (E2-like enzyme) (Ichimura et al., 2000). ATG3-LC3-I complex is recognised by ATG12-ATG5-ATG16L1 that works as an E3-like enzyme, conjugating LC3-I to the lipid phosphatidylethanolamine (PE), forming LC3-II (Fujita et al., 2008; Hanada et al., 2007; Ichimura et al., 2000). LC3-II binds to both inner and outer autophagosome membranes (Kirisako et al., 2000; Geng and Klionsky, 2008). Lipidation process is accelerated under nutrient starvation or stress (Kabeya et al., 2000). On autophagic membranes, LC3-II plays a role in the expansion and closure of the autophagosome membrane and plays a role

in selecting cargoes for degradation: it has been demonstrated to act as a receptor for selective substrate p62/SQSTM1 (Bjørkøy et al., 2005).

Another protein involved in phagophore elongation is the transmembrane protein ATG9: under nutrient-rich conditions, ATG9 is localised in the *trans*-Golgi network and late endosomes, while under starvation or stress condition it concentrates to autophagosomes (Young et al., 2006). The exact function(s) of this protein is still unknown.

Phagophore maturation into a complete autophagosome is the least understood step of autophagy pathway. Once matured, autophagosomes traffic and fuse to the lysosome and/or endosomes, becoming an autolysosome (Parzych and Klionsky, 2014). Movement of autophagosomes towards lysosomes is dependent on microtubules (Monastyrska et al., 2009). In addition, components of the SNARE machinery are involved in the fusion process: syntaxin17 on autophagosomes is required for fusion, interacting with SNAP29 and lysosomal VAMP8 (Itakura et al., 2012).

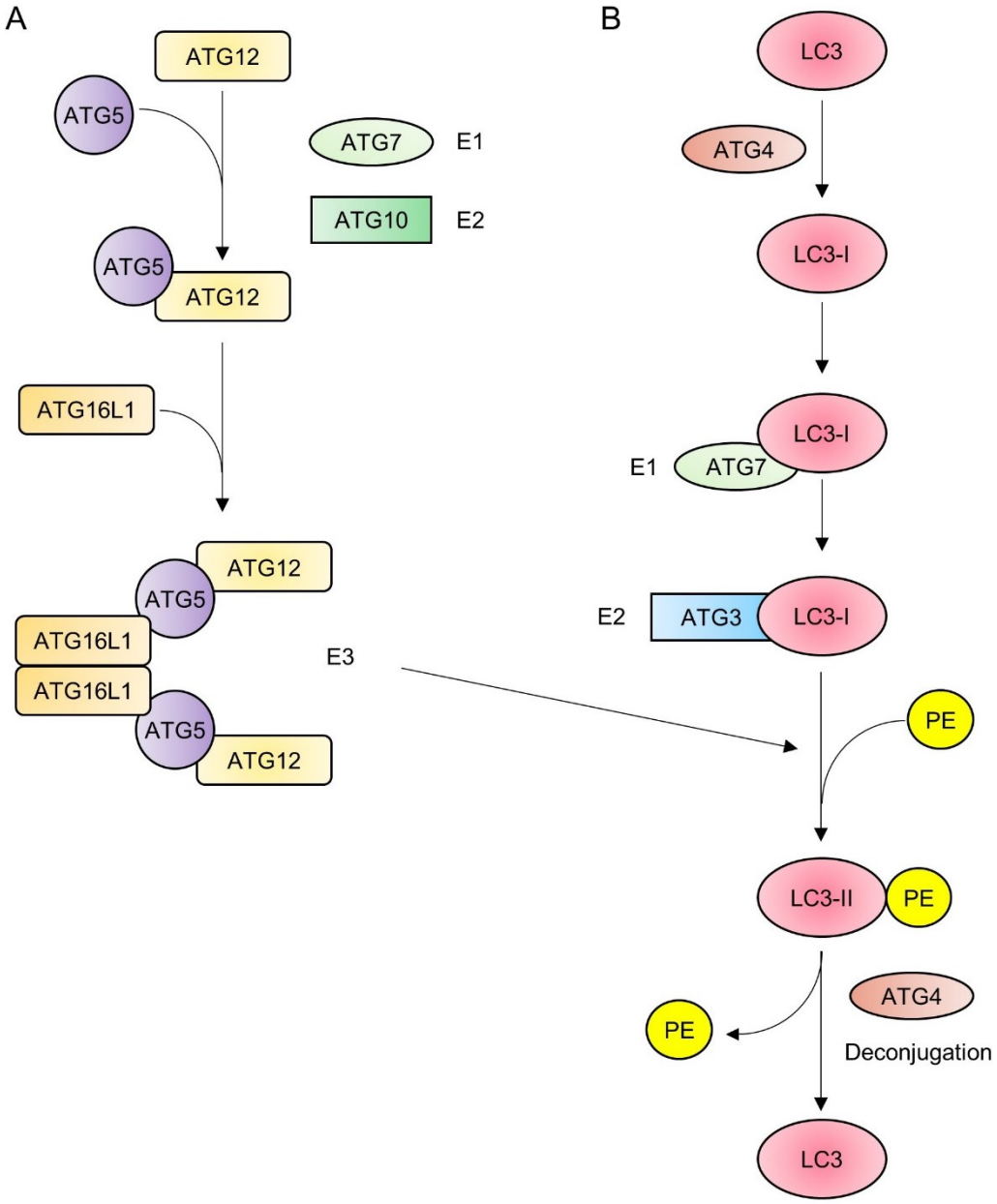


**Figure 6.** Autophagy conjugation systems. A) ATG12-ATG5-ATG16L1 conjugation complex. The ubiquitin-like protein ATG12 is irreversibly conjugated to ATG5 in an ATG7- and ATG10-dependent manner. ATG7 and ATG10 function as E1 activating and E2 conjugating enzymes, respectively. The ATG12–ATG5 conjugate binds ATG16L1 through ATG5. ATG16L1 dimerises and allows association with the phagophore, promoting membrane expansion. B) The LC3 conjugation system. LC3 is processed by ATG4 to reveal a C-terminal glycine (LC3-I). ATG7, an E1- like enzyme, activates LC3-I and transfers it to the E2-like enzyme ATG3. The ATG12–ATG5-ATG16L1 complex may participate as an E3 ligase in the conjugation of PE to LC3-I to create LC3-II, which can associate with the phagophore. LC3-II can subsequently be cleaved by ATG4 to release LC3 (deconjugation). PE: phosphatidylethanolamine (adapted from Parzych and Klionsky, 2014).

### 1.3.4. Autophagy regulation.

Autophagy process regulation is intricate and it took several years to understand the mechanisms involved in this process, although some steps have not been clarified yet. In nutrient-rich condition, a basal autophagy activity is present in some cell types and tissues, to maintain protein homeostasis. Autophagy is enhanced when cells are in a stress condition, including nutrient and/or growth factors starvation, hypoxia, and ER stress (He and Klionsky, 2009). c-AMP-dependent PKA (protein kinase A) and mTOR pathways are those mainly involved in the nutrient starvation response sensing carbon and nitrogen, respectively (Stephan et al., 2010). In mammals, PKA negatively regulates autophagy in the presence of nutrients, partially by phosphorylating LC3 (Cherra et al., 2010). mTORC1 is another major suppressor of autophagy induction; it is positively regulated by the presence of amino acids in lysosomes through RAG proteins, RAS-related small GTP-ases (Kim et al., 2008; Sancak et al., 2008; Shen et al., 2017). When amino acids are limiting, mTORC1 is distributed into the cytoplasm, but the presence of amino acids makes RAG GTPases to heterodimerise on lysosomes and switch from an inactive state (RAG A/B+GDP – RAG C/D+GTP) to an active state (RAG A/B+GTP – RAG C/D+GDP), thus making mTORC1 to translocate to the lysosome, in response to amino acids presence (Shen et al., 2017). Moreover, in the presence of nutrients, mTORC1 associates with the induction complex, but dissociates under nutrient-starvation: in association with the induction complex, mTORC1 phosphorylates ULK1/2 and ATG13, thus inactivating them, but, when cells are starving, mTORC1 detaches from the complex, leading to the dephosphorylation of the complex components and to the induction of autophagy (Jung et al., 2009; Hosokawa et al., 2009).

In addition, there are studies showing PKA- and mTORC1-dependent regulation mechanisms crosstalk. PKA phosphorylates mTORC1 (Mavrakis et al., 2006), but it can also indirectly activate mTORC1 through inactivation of AMP-activated protein kinase, AMPK (Djouder et al., 2010).

AMPK is another major energy-sensor in the cells responding to intracellular AMP and ATP levels to regulate several processes, autophagy included (Alers et al., 2012; Meley et al., 2006). When activated by low energy levels, AMPK either phosphorylates and activates the TSC1/2 complex that inhibits mTORC1 activity (Inoki et al., 2003) or directly inhibits mTORC1 (Gwinn et al., 2008; Yang and Klionsky, 2010). Moreover, AMPK activates ULK1 through phosphorylation (Egan et al., 2011; Kim et al., 2011; Lee et al., 2010; Shang et al., 2011), thus activating the initiation complex. AMPK can also be activated by calcium/calmodulin-dependent protein kinase kinase 2, $\beta$ (CAMKK2/CAMKKβ), induced by ER stress-dependent increase of intracellular $Ca^{2+}$ concentrations (Høyer-Hansen et al., 2007). Autophagy is also induced by ER stress through the

unfolded protein response (UPR) system (Ding et al, 2007; He and Klionsky, 2009; Qi and Chen, 2019).

Additionally, hypoxia and growth factors absence are known inducers of autophagy, even in the presence of nutrients (Alers et al., 2012; Arsham et al., 2003; Lum et al, 2005).

## 1.4. Ciliogenesis and primary cilium dynamics.

In the last 20 years autophagy related proteins and the mechanisms through which this process regulates cellular homeostasis and response to several stress conditions have been elucidated, although some features are still not completely understood. To date, one of the processes that is known to be regulated by the autophagy pathway is the primary cilium biogenesis and dynamics. Until 30 years ago, little was known about this organelle, now known to be the cellular "antenna", since one of its principal functions is to sense signals from the extracellular environment.

### 1.4.1. Primary cilium structure.

Primary cilia are complex and highly conserved organelles that protrude from the plasma membrane of almost all cell types (Goetz and Anderson, 2010; Satir and Christensen, 2007; Ishikawa and Marshall, 2011; Bernabé-Rubio and Alonso, 2017). They are structured around a cylindric microtubular skeleton, called axoneme surrounded by the ciliary membrane (Hu et al., 2001; Jana et al., 2014). Differently from motile cilia axoneme, that has a 9 + 2 structure consisting of 9 microtubule doublets and 2 central microtubules (Figure 7E), the primary cilium axoneme is lacking the 2 central microtubular structures (Figure 7F), as well as dynein arms involved in the movement of motile cilia (Ishikawa and Marshall, 2011; Bernabé-Rubio and Alonso, 2017; Wheway et al., 2018). In primary cilia, the 9 microtubule doublets are composed of a complete microtubule, called tubule A, connected to an incomplete one, the tubule B, consisting of 10 protofilaments instead of 13 (Ishikawa and Marshall, 2011; Jana et al., 2014; Bernabé-Rubio and Alonso, 2017). Tubulin present in these structures is post-translationally modified through acetylation, glutamylation and glycylation (Portran et al., 2017; Wloga et al., 2016; Gaertig and Wloga, 2008). Moreover, other proteins, such as tektins and the so-called protofilament ribbon proteins associate to the axoneme doublets, presumably to make the primary cilium not disassembling spontaneously (Steffen and Linck 1988; Linck and Norrander, 2003; Ishikawa and Marshall, 2011). The basal body from which the primary cilium axoneme is protruded originates from the mother centriole and consists of 9 microtubule triplets and its associated accessory structures (Figure 7B) (Malicki and Johnson, 2017).

The primary cilium might be divided in different compartments:

- the ciliary pocket, a depression located at the base of the cilium, where the basal body is docked to the plasma membrane. This invagination is present in cells of connective tissues, i.e. fibroblasts and chondrocytes, but not in other cell types where the cilium protrudes directly from the plasma membrane (Ghossoub et al., 2011; Molla-Herman et al., 2010). The basal body is connected to the plasma membrane through the so-called transition fibers (Figure 7C), that belong to the accessory structures of the basal body and emerge from the central microtubule of each triplet of the basal body (Wei et al., 2015; Wheway et al., 2018);
- distally, the transition zone is the region where the 9 microtubule triplets shift into doublets forming the axoneme (Figure 7D). Together with the transition fibers, the transition zone forms a sort of gate through which protein entrance in the cilium is regulated (Wheway et al., 2018; Garcia-Gonzalo and Reiter, 2017). Moreover, in this region the Y-linker proteins are involved in the connection of the plasma membrane to the outer doublet microtubules of the axoneme (Wei et al., 2015);
- the central part of the cilium consists of the axoneme doublets surrounded by the ciliary membrane (Jana et al., 2014; Ishikawa and Marshall, 2011). The axoneme elongates up to the ciliary tip, where the doublets become single microtubules (Figure 7G) that are gradually lost (Jana et al., 2014; Bernabé-Rubio and Alonso, 2017).

In addition, the composition of the ciliary membrane differs from the plasma membrane since it is enriched in receptors involved in the transduction of several signals and in GTPases regulating the ciliogenesis process and its reverse process, the disassembly of the organelle, such as ARF-like protein family factors (Hu et al., 2011).

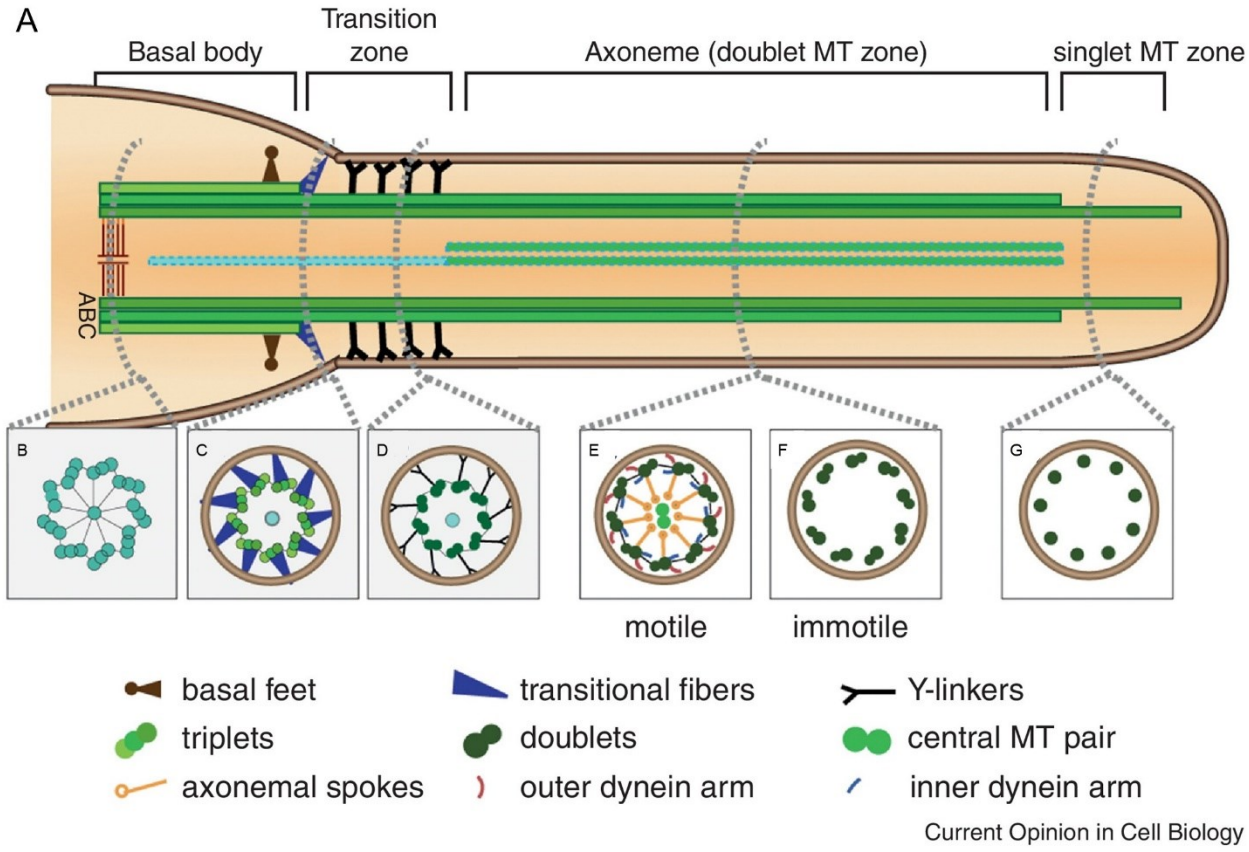


**Figure 7.** A) Schematic representation of primary cilium and basal body. B) Transversal section of the basal body, where 9 triplets are schematised. C) Transition fibres in the transition zone section. D) Y-linkers proteins anchoring the axoneme to the ciliary membrane. F) Axoneme of immotile primary cilium (in E the axoneme of motile cilia is schematised), with no central MT (microtubule) pair, axonemal spokes and dynein arms. G) Apical part, or ciliary tip, where doublets are converted in single microtubules (Jana et al., 2013)

### 1.4.2. Primary cilium assembly mechanism.

The mechanism by which the primary cilium is built, known as ciliogenesis, is a dynamic and highly regulated process and differs among the different cell types (Kim et al., 2011). Primary cilium is protruded by the cell during G0/G1 phase of the cell cycle, when the cell is in interphase or in a quiescent state (Malicki and Johnson, 2017; Paridaen et al., 2013). When the cell enters the cell cycle, the primary cilium is disassembled (Kim et al., 2011; Ishikawa and Marshall, 2011). Hence, cell cycle and primary cilium biogenesis are mutually exclusive events, likely because the mother centriole is needed in both processes, in the first as mitotic spindle organisation center and in the second as basal body (Kobayashi et al., 2011). These are finely regulated processes in which proliferative stimuli suppress ciliogenesis and, conversely, the primary cilium acts as a negative regulator of the cell cycle progression (Goto et al., 2016).

Two mechanisms of ciliogenesis are known: a canonical or intracellular pathway (Figure 8), that occurs in the cytoplasm and leads to the formation of the ciliary pocket, and an alternative pathway, that occurs at the plasma membrane with no ciliary pocket (Sorokin, 1968; Bernabé-Rubio et al., 2017). Which of the two pathways is occurring depends on the position of the centrosome within the cell: if it is near the nucleus, ciliogenesis starts intracellularly and a ciliary pocket is formed (Figure 8B), while if the centrosome is near the plasma membrane the cilium is built directly on it, without the formation of the pocket (Figure 8C) (Benmerah, 2013). In the intracellular pathway, cytoplasmic vesicles dock to the mother centriole and they fuse to form one ciliary vesicle. In this first step, Cep164, a distal appendage protein, and Talpid3, a distal centriolar protein, are necessary for the docking (Schmidt et al., 2012). In this way, the mother centriole matures to basal body and moves towards the plasma membrane. At the same time, the two internal microtubules of each triplet start to build the axoneme and the centriolar appendages mature into transition fibers. The extension of the axoneme is promoted by the removal of Cp110 from the mother centriole by MARK4 and the recruitment of Tau tubulin kinase 2, Ttbk2 (Spektor et al., 2007; Cajanek and Nigg, 2014; Kuhns et al., 2013). At this point, the shape of the ciliary vesicle is modified: it is extended and divided into an external and an internal membrane. Finally, when the basal body docks to the plasma membrane thanks to the transition fibers, the external membrane of the ciliary vesicle fuses with the plasma membrane, forming the ciliary pocket and exposing the new primary cilium outside the cell, with the internal membrane of the vesicle becoming the ciliary membrane. In this step, Rab8 is recruited to the mother centriole and activated by Rab11 and Rabin8 to enable primary cilium membrane assembly (Westlake et al., 2011). Finally, the axoneme continues to elongate to reach its definitive size, which is regulated by the balance between ciliary assembly and disassembly (Figure 8B) (Rohatgi and Snell, 2010; Bernabé-Rubio and Alonso 2017).

The alternative pathway is less studied and therefore not completely elucidated yet. Some hypotheses claim that it may involve both the docking of the basal body to the plasma membrane and the lateral diffusion of proteins and lipids from the plasma membrane (Garcia-Gonzalo et al., 2012). This pathway is typical of cells polarising the centrosome to the centre of the apical membrane (e.g. several, even not all, epithelial cells) that, consequently, do not have a ciliary pocket to the base of the primary cilium (Bernabé-Rubio et al., 2016; Reales et al., 2015; Zuo et al., 2009). In polarised cells an intercellular bridge forms at the apical cell surface during cytokinesis (Green et al., 2012) and several ciliary proteins are localised in the midbody remnant (Gromley et al., 2005; Delaval et al., 2011). When abscission occurs, one of the daughter cells inherits the midbody remnant (Green et al., 2012; Mullins et al., 1977; Mierzwa et al., 2014; Dionne et al., 2015) that localises near the tight junction. The remnant moves over the apical surface towards the

centrosome that is docked at the centre of the apical membrane and when the midbody remnant meets the centrosome the primary cilium building is enhanced (Figure 8 C) (Bernabé-Rubio et al., 2016).

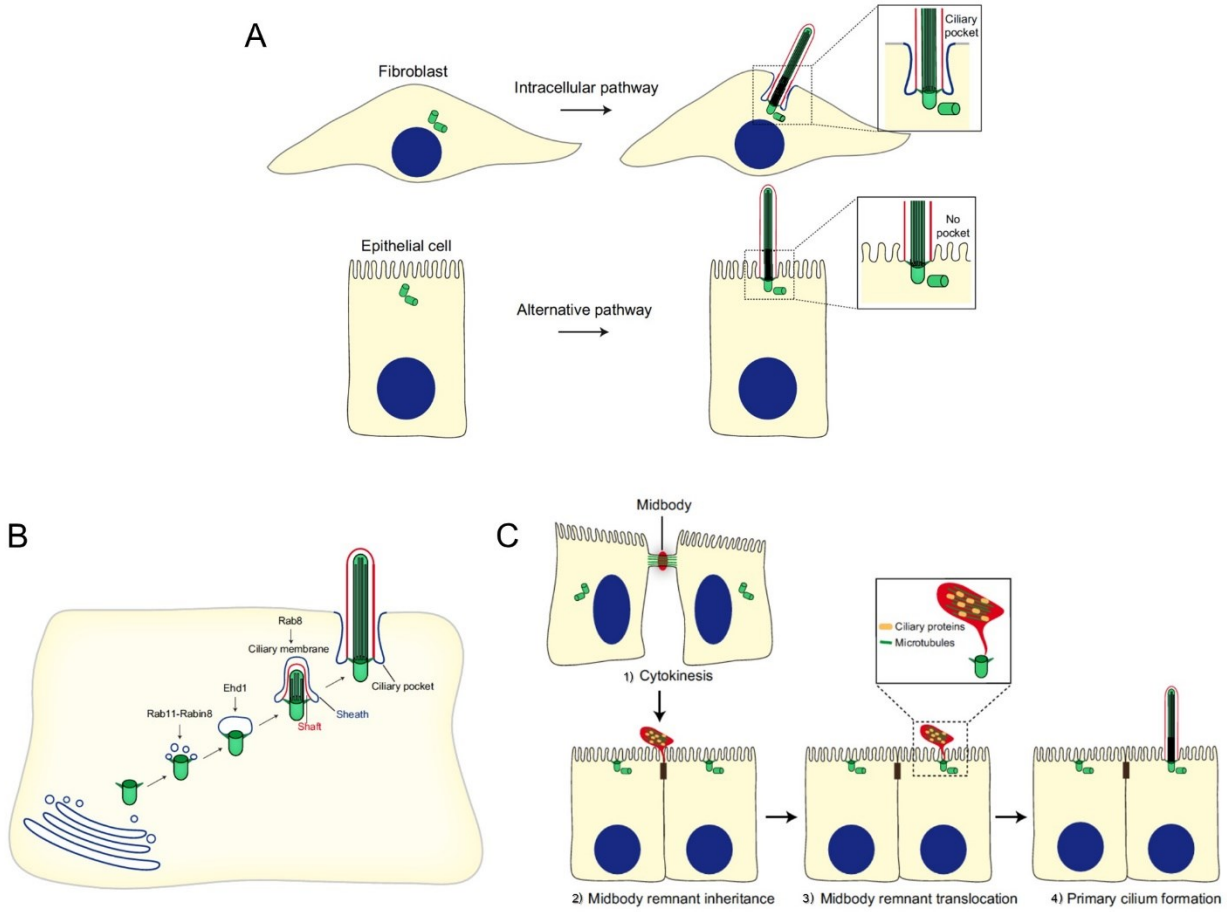


**Figure 8.** A) Primary ciliogenesis pathways schematic representations. The position of the centrosome, near the nucleus or close to the plasma membrane, and the presence or absence of a ciliary pocket predicts the type of pathway used for primary ciliogenesis. Fibroblasts and polarised epithelial cells are shown as examples of cells that use the intracellular and alternative routes, respectively. B) The intracellular pathway. Ciliogenesis initiates with the formation of a large ciliary vesicle at the distal end of the appendages of the mother centriole by fusion of smaller vesicles coming from the Golgi. The axoneme starts forming intracellularly and, as it grows, deforms the ciliary vesicle and establishes an inner membrane (shaft) and an outer membrane (sheath). The incipient cilium is finally exocytosed and the cilium becomes exposed in the plasma membrane. The sheath gives rise to the ciliary pocket, and the shaft forms the ciliary membrane. C) The alternative pathway. 1) In polarized epithelial cells, the intercellular bridge containing ciliary proteins forms at the apical cell surface during cytokinesis. 2) When abscission occurs, one of the two daughter cells inherits the midbody remnant, which localizes apically at the cell periphery, near the tight junctions. 3) The remnant subsequently moves over the apical surface towards the centrosome, which is docked at the centre of the apical membrane. 4) When the midbody meets the centrosome, the initiation of primary cilium

assembly is facilitated. The entire process of primary cilium formation takes place in the plasma membrane. (Bernabé-Rubio and Alonso, 2017)

### 1.4.3. Intraflagellar transport and ciliary trafficking.

Independently from the pathway utilised by the primary cilium to protrude, since the extension of the axoneme occurs on the cell surface and protein synthesis does not occur inside the primary cilium, a transport system is needed to make ciliary proteins entry the cilium: this system is the intraflagellar transport (IFT), that transfer proteins from the cytosol inside the cilium and vice versa and from the base of the cilium up to the tip and back (Rosenbaum and Witman, 2002; Taschner and Lorentzen, 2016; Ishikawa and Marshall, 2011; Bernabé-Rubio and Alonso, 2017). The IFT system is divided in two groups, one involved in the anterograde transport, called IFT-B complex, and one involved in the retrograde transport, the IFT-A complex, which move on tubule B and tubule A, respectively. These two complexes consist of several proteins that assemble at the base of the cilium and bind proteins that must be transported. When they reach the tip of the cilium, IFT-B complex is disassembled while the IFT-A complex is built, to return to the base of the cilium (Taschner and Lorentzen, 2016). IFT complexes form linear arrays, or "trains", that are transported along the axoneme by Kinesin-2 proteins and cytoplasmic dynein-2 (Cole et al., 1998; Pazour et al., 1998, 1999; Taschner and Lorentzen, 2016; Ishikawa and Marshall, 2011). The frequency of IFT trains entry, size and speed may influence ciliary length and shape (Marshall et al., 2005; Wren et al., 2013): indeed, mutations on both IFT-B and IFT-A complexes components lead to shortened cilia and cilia with bulbous distal tip, respectively (Perrault et al., 2015; Zhang et al., 2016; Takei et al., 2018; Botilde et al., 2013; Berbari et al., 2011; Follit et al., 2006; Liem et al., 2012; Fu et al., 2016; Hirano et al., 2017; Han et al., 2019).

Together with the transport of proteins along the cilium, the IFT system is involved also in the maintenance of the primary cilium, in its assembly and disassembly: once reached its optimal length, the axoneme is continuously polymerised and depolymerised at its extremities and its length is the result of the correct balance between anterograde and retrograde transport (Marshall et al., 2005; Liang et al., 2016), together with the release of extracellular vesicles through ectocytosis (Wood et al., 2013). Other accessory IFT proteins have been discovered over the years, among them, the Bardet-Biedl Syndrome (BBS) proteins that have been shown to undergo IFT-like movements along the axoneme and form the so-called BBSome. The BBSome acts as an adaptor that connect IFT complexes to signalling molecules and is required for the ciliary export of activated signalling receptors (Blaque et al., 2004; Nachury et al., 2007; Nachury et al., 2018). In several *Bbs*-knockout mice cells are still protruding the primary cilia, although their shape might be affected (Mykytyn et al., 2004; Davis et al., 2007; Ishikawa and Marshall, 2011). Only BBS1 and

BBS5 silencing in cells completely impaired ciliogenesis (Nachury et al., 2007; Loktev et al., 2008).

### 1.4.4. Primary cilium functions.

Primary cilia principal function is to sense and transduce signals coming from the extracellular environment, from light (Pearring et al., 2013) and mechanostimuli (Ferreira et al., 2019) to biochemical ones (Ishikawa and Marshall, 2011; Malicki and Johnson, 2017; Zimmerman and Yoder, 2015). Through this, the primary cilium can control several signalling pathways (Huangfu et al., 2003; Corbit et al., 2008; Wheway et al., 2018), cell cycle progression (Pan et al., 2013), cell differentiation (Ezratty et al., 2011; Forcioli-Conti et al., 2015) and autophagy (Pampliega et al., 2013; Ohron et al., 2016).

As a photoreceptor, the cilium is specialised in photon absorption by assuming a structure that makes it to concentrate visual pigments (Pearring et al., 2013). As a mechanosensor, the primary cilium can transduce stimuli like fluid flow, especially in renal epithelial cells (Ishikawa and Marshall, 2014; Wang et al., 2021), pressure and also vibrations. For what concerns biochemical stimuli, primary cilia transduce external stimuli through receptors locally enriched on its membrane and activate signalling pathways important for development, cell differentiation, cell proliferation, survival and migration. One of these pathways depends on Hedgehog ligands that regulate development stages of all metazoa as well as adult structures (Briscoe and Therond, 2013; Robbins et al., 2012). In vertebrates, Hh receptor Patched 1 (Ptch1) is localised in the primary cilium, whereas the seven transmembrane protein Smo is kept outside of cilium in the absence of Shh ligands. Only when Shh ligands bind to Ptch1, Smo inhibition is relieved and becomes activated by phosphorylation on specific residues in the carboxy-tail thus promoting a conformational change that alters intramolecular interactions (Sasai and Briscoe, 2012). After Ptch1 exits from the cilium, Smo can translocate to the tip of the primary cilium and the signaling pathway culminates in activation of the Glioma-associated oncogene family members (Gli) and induction of Hh target gene expression (Arensdorf et al., 2016). Indeed, Smo localisation to the primary cilium is essential for Shh signaling (Corbit et al., 2005).

Together with Hedgehog pathway, Platelet-derived growth factor a (PDGF-a) signalling, controlling cell migration, occurs in the primary cilium (Schneider et al., 2005), as well as canonical and noncanonical Wnt pathways, that regulates developmental and homeostatic processes (Wilcockson et al., 2016, May-Simera et al., 2014). Another pathway transduced by the primary cilium is the Hippo pathway, controlling organ size and proliferation (Zhao et al., 2010). In addition, G protein coupled receptors (GPCRs) of hormones, peptides, lipids and neurotransmitters,

including for instance those of dopamine, serotonin, neuropeptide Y and somatostatin, reside in primary cilia and use cilia for signalling transduction (Hilgendorf et al.,2016).

## 1.5. Ciliopathies.

A series of pathologies, called ciliopathies, have been linked to defects in primary cilium biogenesis and functions. Being the primary cilium present in almost all cell types, it is not surprising that ciliopathies are multi-organ pathologies and that several clinical signs are partially overlapping. More than 400 proteins have been found to be associated with the primary cilium, contributing to either its structure or its function, and almost half of them have been found mutated in ciliopathies (Reiter and Leroix, 2017). Importantly, ciliopathies study has helped to discover principal ciliary functioning, from basal body docking to the membrane for the cilium biogenesis (Ghossoub et al., 2011; Molla-Herman et al., 2010), to the role of the transition zone in selecting proteins entering the cilium and connecting the axoneme to the membrane (Wheway et al., 2018; Garcia-Gonzalo and Reiter, 2017), to the importance of the presence of signalling receptors on the primary cilium membrane (Huangfu et al., 2003; Corbit et al., 2008; Wheway et al., 2018).

Within ciliopathies we can found Joubert syndrome (JBTS), Nephronophthisis (NPHP), Oro-Facial-Digital syndrome (OFD), Jeune syndrome, Polycystic kidney disease, both the dominant and the recessive autosomal forms (ADPKD and ARPKD), Meckel-Gruber syndrome (MKS), Bardet-Biedl syndrome (BBS) and many others (Reiter and Leroix, 2017; Novarino et al., 2011; Davis and Katsanis, 2012). Some of the clinical signs of these diseases are shared with OS: for instance, defects in craniofacial development are present in OFD syndrome (de Conciliis et al., 1998; Franco and Thauvin-Robinet, 2016), as well as in JBTS, that includes also prominent forehead, cerebellum defects and consequent developmental delay (Joubert et al., 1969; Valente et al., 2013), in Pallister-Hall syndrome (PHS) laryngotracheal defects and cleft of the lip are present (Brown et al., 2020). These observations suggest that OS might underscore a primary cilium defect.

## 1.6. Autophagy and primary cilium crosstalk.

Recently, the appropriate assembly and functioning of the primary cilium has been linked to autophagy: indeed, several works have been published in the last years showing how autophagy can both positively and negatively regulate ciliogenesis and ciliary length depending on the nutrient availability, and conversely how ciliary pathways are involved in autophagy activation, supporting the importance of having a functional primary cilium to activate autophagy in nutrient deprivation condition (Pampliega et al., 2013; Tang et al., 2013; Struchtrup et al 2018).

Autophagy induction requires the presence of a functional primary cilium. Downregulation or loss of ciliary structural proteins and/or IFT complexes components, that are known to impair

ciliogenesis, prevents autophagy activation upon serum starvation, leading to lower autophagosomes formation: depletion of IFT proteins leads to a loss of proper autophagy induction that is dependent on Hh signalling, which in turn depends on intact IFT and primary cilium (Pampliega et al., 2013). Moreover, IFT proteins are involved in the recruitment of some ATG proteins, especially ATG16L, to the primary cilium, in particular to the ciliary pocket, that has been proposed as a further putative site where autophagosomes might originate (Pampliega et al., 2013; Pampliega and Cuervo, 2016; Morleo and Franco, 2019). This reciprocal regulation is context-dependent: in some studies, the decrease of basal autophagy due to a block in ciliogenesis can be restored by mTOR inhibition (Wang et al., 2015), while in some other contests this kind of treatment is not restoring autophagy when a primary cilium is absent (Pampliega et al., 2013). These findings suggest that the crosstalk between the primary cilium dynamics and autophagy are dependent on the cell type, the type of stimulus as well as culture conditions. The same stimulus may lead to a different effect, for instance Hh signalling can stimulate autophagy when the stimulus starts in the cilium (Pampliega et al., 2013) but it does not in proliferating cells where the primary cilium is absent (Jimenez-Sanchez et al., 2012).

For what concern the primary cilium length, several works report opposite and contrasting effects upon autophagy blockage on primary cilium length. This is due to the fact that autophagy can regulate the half-life of both positive and negative regulators of ciliary length. For example, IFT20 is degraded through basal autophagy to prevent continuous cilium growth when nutrients are present, but serum-starvation induced autophagy does not target IFT20, since it is necessary for the building of the cilium, but OFD1, in particular the centriolar satellites pool of OFD1, that suppresses ciliogenesis (Pampliega et al., 2013; Tang et al., 2013).

To add complexity to this relationship between autophagy and primary cilium, in some cell types, when autophagy is inhibited by drugs to study the effect of the block on primary cilium dynamics usually cells engage proteasome degradation to overcome autophagy block, although proteins targeted for the proteasome in these conditions are not know yet (Wang et al., 2015; Morleo and Franco 2019).

To conclude, changes in the ratio between degradation of positive and negative regulators can determine the final ciliogenesis rate that will be different depending on the cell type and the stimulus nature. As a consequence, some clinical manifestations observed in ciliopathies might be due to impairments in the autophagy pathway and, conversely, pathologies associated to altered autophagy, as neurodegenerative diseases, metabolic diseases and cancer could present abnormal cilia biogenesis and functioning.

Many aspects of this crosstalk have to be completely understood yet, but some of the OS features are shared with ciliopathies, giving rise to the hypothesis that MID1 might have a role in this cross-regulation process in the OS context.

# 2. Aim of the work

Opitz G/BBB syndrome is a congenital malformation characterised by several clinical signs affecting the ventral midline. The X-linked form (XLOS, hereafter OS) is caused by mutations in *MID1* gene, whose protein product is a member of the TRIM protein family of E3 ubiquitin ligases. Several findings on the biochemical function of the MID1 product have been reported, however, the pathogenetic mechanisms underlying this disease have not been elucidated yet. However, several of the OS clinical phenotypes are found also in other pathologies caused by mutations in proteins involved in primary cilium dynamics, i.e. ciliopathies. This may suggest a putative role of MID1 in controlling the primary cilium biogenesis, as well as its maintenance. Defects in primary cilium in OS cells might explain several of the signs observed in patients that are shared with ciliopathies.

The goal of my PhD project is to investigate MID1 role in both primary cilium dynamics and autophagy, being these processes reciprocally regulated. Indeed, on one side, MID1 is involved in the control of the level of the microtubular pool of PP2Ac (Trockenbacher et al., 2001), thus indirectly controlling the regulation of mTORC1 phosphorylation status (Liu et al.,2011). On the other hand, preliminary data suggest that MID1 behaves as a negative regulator of primary cilium length (Kim et al., 2010). Towards this goal, the following aims have been addressed:

Aim 1: investigate the role of MID1 during the assembly of the primary cilium, i.e. ciliogenesis.

Aim 2: investigate the role of MID1 in the autophagy process and its involvement in the control of ciliogenesis.

# 3. Materials and Methods

## 3.1. Cell Culture and transfection.

Human arising retinal pigment epithelial cell line (ARPE-19), and mouse embryonic fibroblasts (MEFs) have been maintained in culture in DMEM (Euroclone, ECB7501L), with 10% foetal bovine serum (FBS, Gibco 10270), 4 mM L-glutamine (Euroclone, ECB3000D), 100 units penicillin/100 µg streptomicine (Gibco, 15104).

For ciliogenesis induction, culture medium has been replaced with serum-free DMEM when cells were 80% confluent, for different time points before fixation or cell harvesting for protein extraction. Time course experiments to check primary cilia dynamics have been performed with cells 80% confluent and serum-starved for 16, 20, 24, 40 hours in ARPE-19, up to 48 hours in MEFs.

Plasmid DNA harbouring MycGFP-pcDNA3, MycGFP-MID1, MycGFP-MID1ΔRING, already available in the lab have been transfected in ARPE-19 cells through Lipofectamine 3000 vector (L3000015, Invitrogen) following manufacturer's instructions.

In ARPE-19 cells and MEFs, autophagy flux has been analysed by treating the cells with 100 µM of Chloroquine (#tlrl-chq, InvivoGen) at different time points (see Results and Discussion section for the different experimental conditions). For the analysis of basal autophagy flux, cells have been seeded at 80% confluence, transfected the following day, medium has been changed 6 hours after transfection as suggests by lipofectamines manufaturer's instructions, and cells have been finally treated with chloroquine the day following transfection. For the analysis of serum-starvation induced autophagy, after transfection, the medium has been replaced with serum-free DMEM, for 20 hours, then chloroquine has been added to block the lysosome. After the treatment, LC3II and p62 protein levels have been analysed through Western Blot.

## 3.2. Preparation of Mouse Embryonic Fibroblasts (MEFs).

MEFs have been prepared from wild-type (WT) and *Mid1*$^{-/Y}$ Knock-out (KO) embryos as per the following protocol. Embryos from an E13.5-pregnant *Mid1*$^{+/-}$ heterozygous female mated to a WT male have been harvested and placed in 100 mm cell culture dish upon placental and other maternal tissues removing. From this mating we can obtain WT and KO male littermates. Tail of the embryos have been removed and saved for genotyping (see below). Embryos have been then minced with a razor blade, trypsin added, and the dish placed in 37°C incubator for 10 minutes. Trypsin has been then quenched by adding 9 mL of complete DMEM and the suspension has been pipetted 10-20

times to further break up tissues. MEFs have been used for the ciliogenesis and autophagy experiments from passage 3 to 6.

Genotyping has been performed upon lysing the tail tissues and extracting genomic DNA with PCR biosystem Mouse Genotyping Kit (PCR-Biosystems, Resnova). PCR has been then performed with the following primers (30 cycles, annealing at 58°C):

- Mid1 NullF (5'-GCTCCCAGTAAAGACAGAC-3') and Mid1 NullR (5'-GAGCCCGTCTAGACCTCGC-3') to identify the presence of the WT locus (400 bp);
- Mid1 NullF and NEO1 (5'-CCAGAGGCCACTTGTGTAG-3') to identify the presence of the KO locus (320 bp).

To define the sex of the embryo, PCR (40 cycles, annealing at 54°C) to detect the Y chromosome specific *Sry* band (250 bp) has been performed using the following primers:

- mSryF: 5'-GAGAGCATGGAGGGCCAT-3'
- mSryR: 5'-CCACTCCTCTGTGACACT-3'

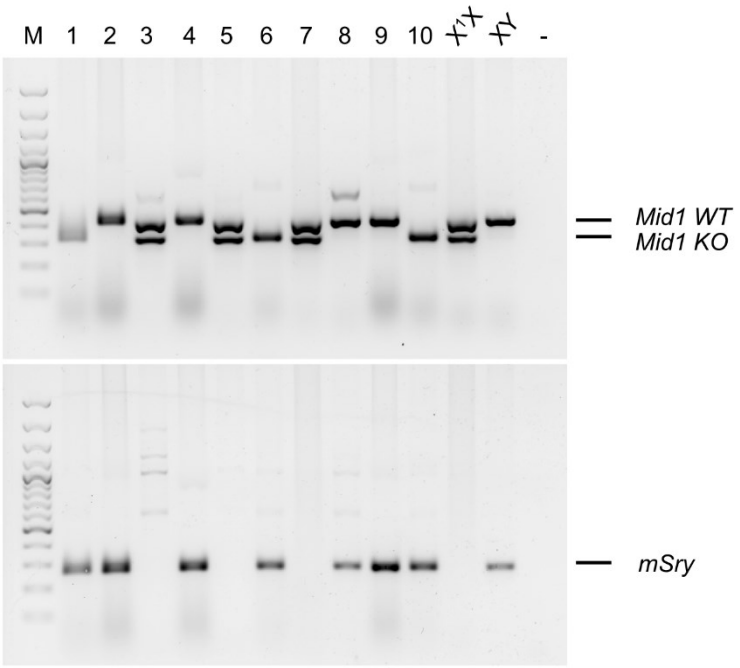


**Figure 9.** Embryos genotyping. Top gel, MID1 WT and KO amplified fragments as indicated; bottom gel, Sry amplification for sex determination. M: 100 bp molecular weight marker (Gene Ruler 100bp DNA ladder SM0322 (Thermo Scientific); Lane 3, 5, 7: heterozygote females; Lane 2, 4, 8, 9: WT males; Lane 1, 6, 10: KO males.

## 3.3. Immunofluorescence experiments.

ARPE-19 and MEFs cells have been seeded on glass coverslips to 80% confluence. ARPE-19 have been transfected with plasmid DNA as described above. After serum starvation, coverslips have been washed twice in PBS 1X (137mM NaCl, 2.7 mM KCl, 10 mM $Na_2HPO_4$, 1.8 mM $KH_2PO_4$, pH 7.4) and fixed in 4% paraformaldehyde (PFA) for 10 minutes at room temperature. Cells have been then washed again in PBS 1X and permeabilised with 0.1% Triton X-100 in PBS (PBST) for 5 minutes at room temperature, blocked with 5% BSA in PBST for 1 hour at room temperature. Coverslips have been then incubated with primary antibodies, diluted in 1% BSA in PBST, for 2 hours at room temperature. Anti-ARL13B antibody (17711-1-AP Proteintech) has been used at 1:400 dilution. Staining has been obtained after incubation for 1 hour at room temperature with a Cy3-conjugated anti-rabbit antibody (1:200 dilution, AP132C, Millipore). Coverslips have been mounted with Vectashield mounting medium plus DAPI (Vector Laboratories) and cells have been analysed with epifluorescence microscopy. 20X magnification images have been used to calculate ciliated cells percentage, through ImageJ (NIH, Bethesda, USA), while high-resolution 60X or 63X magnification images have been used to measure primary cilia length, through ImageJ software. Merges have been obtained with Photoshop Adobe.

### 3.3.1. Confocal imaging.

ARPE-19 cells transfected with MycGFP-MID1 together with mCherry-LC3 (gift from Carmine Settembre, TIGEM) were evaluated with a Nikon C1si. Confocal microscope Nikon C1si contains 457,477, 488, 514 nm argon laser lines and 408, 561, 640 nm diode lasers. Light was delivered to the sample with an 408/488/561/640 dichromatic reflector and 60X Plan Apo objectives were used. The system was operated with a pinhole size of one Airy disk. Electronic zoom was kept at minimum values for measurements to reduce potential bleaching. The confocal microscope and the acquisition protocols were inserted using the company proprietary software, NIS Elements C, version 5.0. Optical sections were obtained under a 60X oil-immersion objective at a definition of 1,024 × 1,024 pixels. Images were processed for z-projection and for illustration purposes by using ImageJ (NIH, Bethesda, USA).

## 3.4. SDS-PAGE and Western-blot.

ARPE-19 cells and MEFs have been lysed in RIPA buffer (50 mM Tris-HCl pH 8, 0.1% SDS, 150 mM NaCl, 0.5% NaDOC, 1% NP-40). Samples have been then sonicated 2 times, for 10 seconds. The insoluble fraction has been removed by centrifugation at 14,000 rpm at 4°C for 10 minutes. Protein quantification has been measured through a Bradford assay (BioRad, Cat.#500-0006) following the manufacturer's instructions. Proteins have been boiled at 95°C for 5 minutes in

sample buffer (250 mM Tris-HCl pH 6.8, 40% glycerol, 8% SDS, 5% β-mercaptoethanol, 0.04% bromophenol blue) and then loaded on 7.5%, 10%, 13% or 15% acrylamide gels, depending on the resolution required for each protein detected, and blotted on PVDF membranes (Immobilon-P, IPVH-00010, Millipore) over night at 4°C. Membranes have been then blocked in 5% Milk in TBS 1X (150 mM NaCl, 10 mM Tris, 0.065% HCl, pH 7.4) with 0.1% Tween (TBST), for 1 hour at room temperature. Primary antibodies have been diluted in 5% Milk in TBST and incubated for 2 hours at room temperature:

- Anti-c-myc 9e10 (M4439, Sigma Aldrich) 1:5000
- Anti-p62 (#39749, Cell Signaling) 1:1000
- Anti-LC3B (L7543, Sigma Aldrich) 1:3000
- Anti-GAPDH (G8795, Sigma Aldrich) 1:6000

Secondary antibodies have been incubated for 1 hour at room temperature, diluted in 5% Milk in TBST:

- Anti-Mouse HRP (AP308P, Millipore) 1:5000
- Anti-Rabbit HRP (A120-208P, Bethyl Laboratories) 1:5000

For bands detection, membranes have been incubated with HRP substrate (ECL Pierce, Invitrogen, 32106), for 1 minute, then the membranes have been placed between two plastic transparencies and exposed to an autoradiography film (GE Healthcare) for different time points depending on antibodies efficiency. For some immunoblots, after ECL incubation, detection has been performed with the ChemiDOC$^{TM}$ Touch Imaging System. GAPDH bands have been used as normaliser for protein band quantification, performed through ImageJ software.

### 3.5. Primary cilia measurements and percentage of ciliated cells evaluation.

Percentage of ciliated cells has been calculated as the ratio between the number of cells protruding a primary cilium and the total number of cells; the number of cells is indicated for each experiment in the relative text or caption (see Result and Discussion section). Primary cilia length has been measured upon Arl13B staining, through the ImageJ software relative to the resolution of the image (scale bar are indicated in Result and Discussion section for each immunofluorescence).

### 3.6. Statistical Analyses.

All the experiments in ARPE-19 cells have been performed at least three times, except for time course experiments for cilia dynamics analyses. Experiments in MEFs have been performed in biological triplicates (N=3 for both WT and KO MEFs). Statistical analyses performed to assess

differences between samples have been done using a two tail Student's t test or ANOVA test (JAMOVI software) when two variables should be considered, as indicated in each experiment.

# 4. Results and Discussion

## 4.1. Ciliogenesis in ARPE-19 cells.

MID1 is a cytoskeleton-associated protein that may be involved in the regulation of microtubular stability (Cainarca et al.,1999; Schweiger et al., 1999). Being the primary cilium a microtubule-based organelle (Ishikawa and Marshall, 2011; Bernabé-Rubio and Alonso, 2017) and sharing Opitz Syndrome (hereafter OS) some clinical signs with ciliopathies, our hypothesis is that MID1 might regulate primary cilium biogenesis and dynamics.

ARPE-19, a spontaneously arising retinal pigment epithelium cell line from a male donor, has been used to address this issue. Before starting to test whether MID1 might have a role in ciliogenesis in this cell line, the capacity of these cells to protrude a primary cilium has been tested. ARPE-19 cells have been seeded on glass coverslips and, at 80% of confluence, one coverslip has been fixed with 4% PFA for 10 minutes at room temperature and considered as $t_0$. The cells on the remaining coverslips have been serum-starved for 16, 20, 24, 40 and 48 hours, to follow the protrusion of the primary cilium during time and to detect the time point of its maximum length (Figure 10A). All coverslips have been fixed in 4% PFA for 10 minutes at room temperature, and immunofluorescence has been performed with an anti-ARL13B antibody that detects a small GTPase that localises to cilia as a marker for the primary cilium. For each time point, images at 20X magnifications (data not shown) have been taken to calculate the percentage of ciliated cells, whereas high-resolution 63X magnification images have been used to measure the primary cilium length (Figure 10B). As regards to the percentage of ciliated cell, these cells assemble a cilium with a high frequency already in normal growth condition, however there was a significant increase from t = 0h to t = 24h, a stabilisation between t = 24h and t = 40h followed by a further increase up to t = 48h when more than 50% of cells present a primary cilium (Figure 10C). For what concern the primary cilium length, 30 primary cilia have been measured from 63X magnification images for each time point. As shown in the graph in Figure 10D, these cells can protrude a quite long primary cilium also in the presence of the serum ($t_0$ cilium length average = 3.55 μm ± 0.95 μm), but its length reaches the maximum after 24 hours of serum-starvation (cilium length average = 4.43 μm ± 2.18 μm). Given these results, all the experiments involving the use of this cell line have been performed following this time line, namely serum-starving ARPE-19 cells for 24 hours, unless stated otherwise.

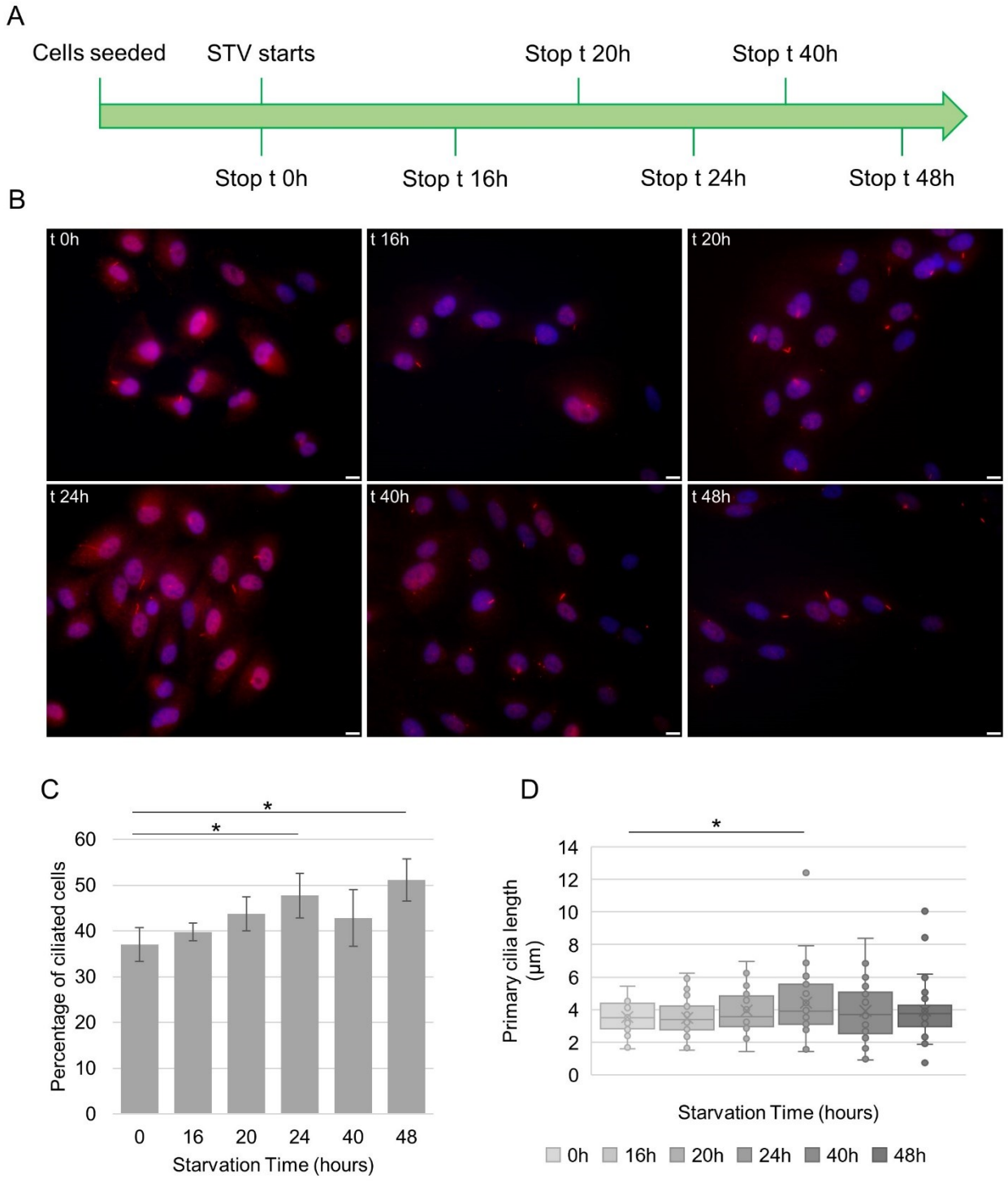


**Figure 10.** Time-course in ARPE-19 cells for ciliogenesis and primary cilium length analyses. A) Experimental scheme where starvation (STV) time points are indicated. B) Immunofluorescence images (63X magnification; scale bar = 10 µm) showing wild-type ARPE-19 cells serum starved for different times. C) Histogram indicating the percentage of ciliated cells, calculated as the ratio between the number of ciliated cells and the total number of the cells for each field (20X images used for this calculation are not shown). Data are indicated as MEAN±SD and significance has been assessed through the Student's t-test (*: $p<0.05$). D) Box plot graph indicating primary cilia length measurements for each time point (N = 30 cells for each time point). Significance has been assessed through the Student's t-test (*: $p<0.05$)

### 4.1.1. MID1 overexpression affects ciliogenesis in ARPE-19 cells.

In order to investigate whether the primary cilium can be affected by the presence of the exogenous MID1 protein, ARPE-19 cells have been transfected with either MycGFP-MID1 or empty vector (MycGFP-pcDNA3) as negative control. Due to a still unexplained drop in the number of detectable MycGFP-MID1 transfected cells after 48 hours of starvation, only the point at 24 hours of starvation has been analysed (Figure 11A). This time point is also in accordance with the analyses described above in ARPE-19 cells.

For our purpose in investigating the role of MID1 in ciliogenesis, ARPE-19 cells have been seeded on glass coverslips up to 80% of confluence. At this point, two coverslips have been transfected with the MycGFP-MID1 plasmid and other two with the empty vector. Six hours after lipofectamine-mediated transfection, medium has been changed: one coverslip for each plasmid has been maintained in a serum-containing medium (normal growth condition), while a serum-free medium for 24 hours (serum starvation) has been used for the other one. After this, coverslips have been fixed and immunofluorescence has been performed with the anti-ARL13B antibody. Percentage of transfected ciliated cells has been calculated for the GFP- and for the GFP-MID1-transfected cells, both in normal growth condition and upon serum starvation. Representative images are shown in top and middle panels in Figure 11B with MID1 expressing cells showing the expected microtubular distribution. In normal growth condition, the percentage of ciliated GFP-MID1-overexpressing cells was 34% on average (34 ± 5.3 %) in contrast to the percentage of ciliated GFP-overexpressing cells, that was 54% on average (54 ± 8.7 %) (Figure 11C). In the absence of serum, consistent with the experiments with untransfected ARPE-19 cells, 58.7% of GFP-transfected cells was ciliated (58.7 ± 7 %) whereas only 31.3% of GFP-MID1-transfected cells protruded the cilium (31.3 ± 6.1 %). From these results it is clear how MID1 overexpression limits the protrusion of ARPE-19 primary cilium in normal growth conditions and this effect is further increased upon starvation. Indeed, while GFP-positive cells ciliation increases in the absence of serum as expected, MID1 overexpressing cells do not increase and if possible, they even reduce ciliogenesis efficiency compared to normal growth condition (Figure 11C).

From the same samples, 50 primary cilia have been measured in transfected cells from high-resolution 63X magnification images. GFP-MID1-positive cells grown in serum-containing medium protruded a primary cilium that was on average 2.08 μm long (2.08 μm ± 0.1 μm), in contrast to GFP-positive cells that protruded on average a 2.66 μm long primary cilium (2.66 μm ± 0.23 μm) (Figure 11D). In contrast to this significant difference ($p<0.05$) in normal growth conditions, when the serum was removed from the culture medium, no significant difference could be appreciated between the two samples ($p>0.05$): GFP-transfected cells protruded a cilium that

reached 2.83 µm on average (2.83 µm ± 0.65 µm), while primary cilium in GFP-MID1-transfected cells was 2.64 µm long (2.64 µm ± 0.23 µm).

These results confirm that MID1 has a role in regulating primary cilium dynamics in ARPE-19 cells and that this effect depends on the cell culture conditions. In general, MID1 behaves as a negative regulator of the primary cilium assembly and elongation. However, while the formation of the cilium is reduced in both serum-containing and serum-starved conditions, its elongation is affected by MID1 mainly in the presence of the serum in the culture medium.

### 4.1.2. MID1 E3 ubiquitin ligase activity is required to exert a role on primary cilium.

MID1 is an E3 ubiquitin ligase acting in the last step of the ubiquitination process favouring the specific recognition of the substrate to be modified and allowing the correct transfer of the ubiquitin moiety to the target. One can hypothesise that its catalytic activity may be involved in the regulation of primary cilium protrusion and/or extension. To test if this is the case, in parallel to the experiments described above, ARPE-19 have been transfected also with a catalytically inactive form of MID1 lacking the RING domain (MycGFP-MID1ΔRING) and also in these cells the percentage of ciliated cells and the primary cilia length have been measured and compared to the GFP- and GFP-MID1-overexpressing cells. Representative images are shown in the bottom panels in Figure 11B showing a decoration of the microtubular cytoskeleton by MID1-ΔRING different from the MID1 full-length and presenting ribbon-like structures.

In both normal conditions and upon serum-starvation, no differences have been observed between GFP- and GFP-MID1ΔRING-positive cells for both the percentage of transfected ciliated cells and the primary cilia length (Figures 11C and D). In fact, in serum-containing medium, the percentage of ciliated GFP-MID1ΔRING-overexpressing cells was 44.7% on average (44.7 ± 11.4%), protruding a cilium on average 2.98 µm long (2.98 µm ± 0.32 µm). Upon serum-starvation, a 3.37 µm long primary cilium (3.37 µm ± 0.26 µm) is visible in the 54% ciliated cells (54 ± 8.7%).

Together, these data indicate that the effect of MID1 on ciliogenesis and primary cilium elongation is fully due to its catalytic activity. Indeed, most of the differences observed between the GFP-MID1- and GFP-MID1ΔRING-positive cells are statistically significant and the values of GFP-MID1ΔRING-positive cells are comparable with the values observed in the GFP-transfected cells. The effect on the length of the cilium in serum-starved cells is overcoming that of the control cells, possibly due to a dominant negative effect of MID1 lacking the RING domain on the endogenous wild-type protein: as reported in the Introduction section, MID1ΔRING protein may homodimerise with the wild-type protein through their coiled-coil domains, thus interfering with endogenous protein function.

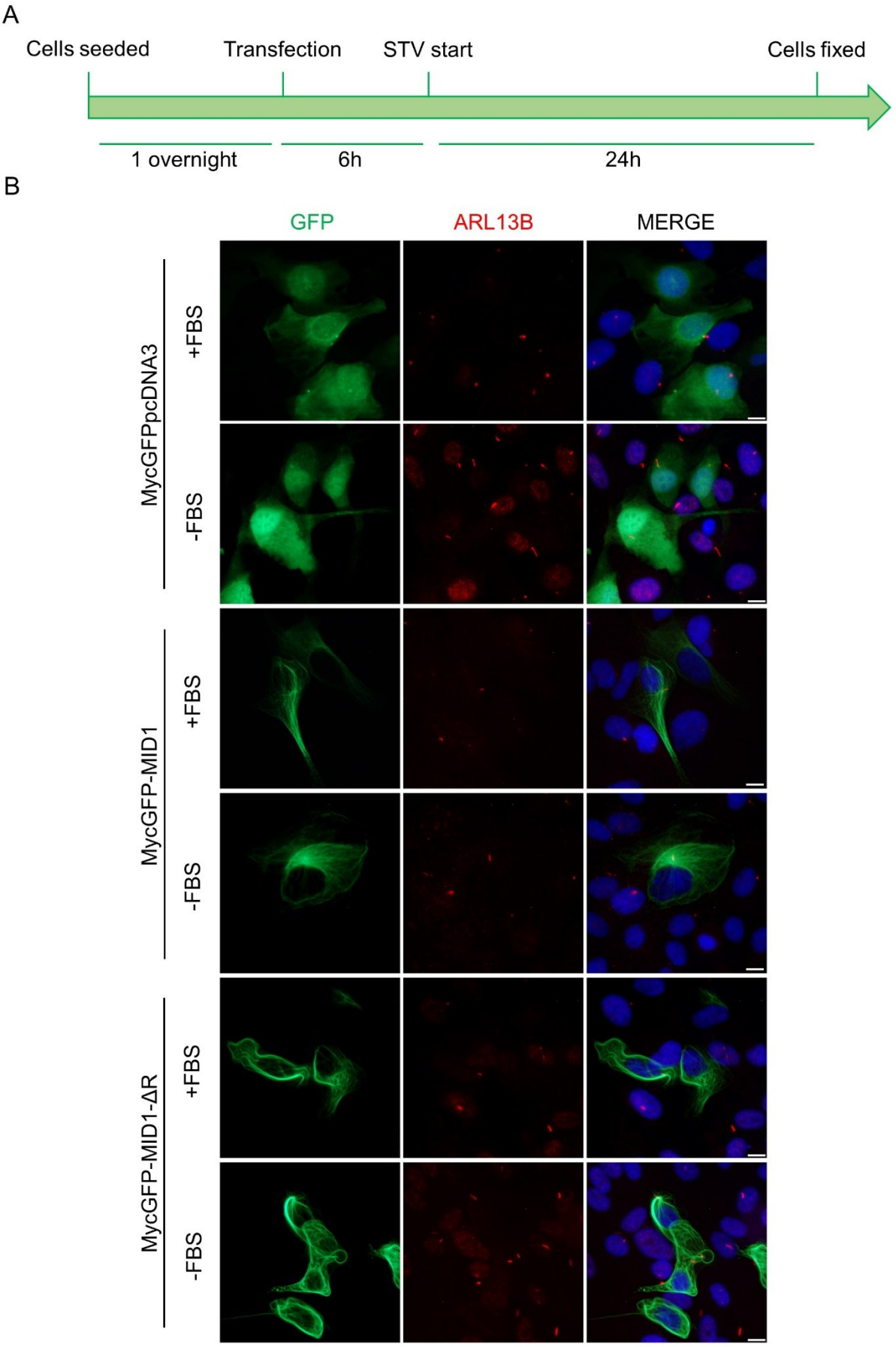


Figure legend on the next page

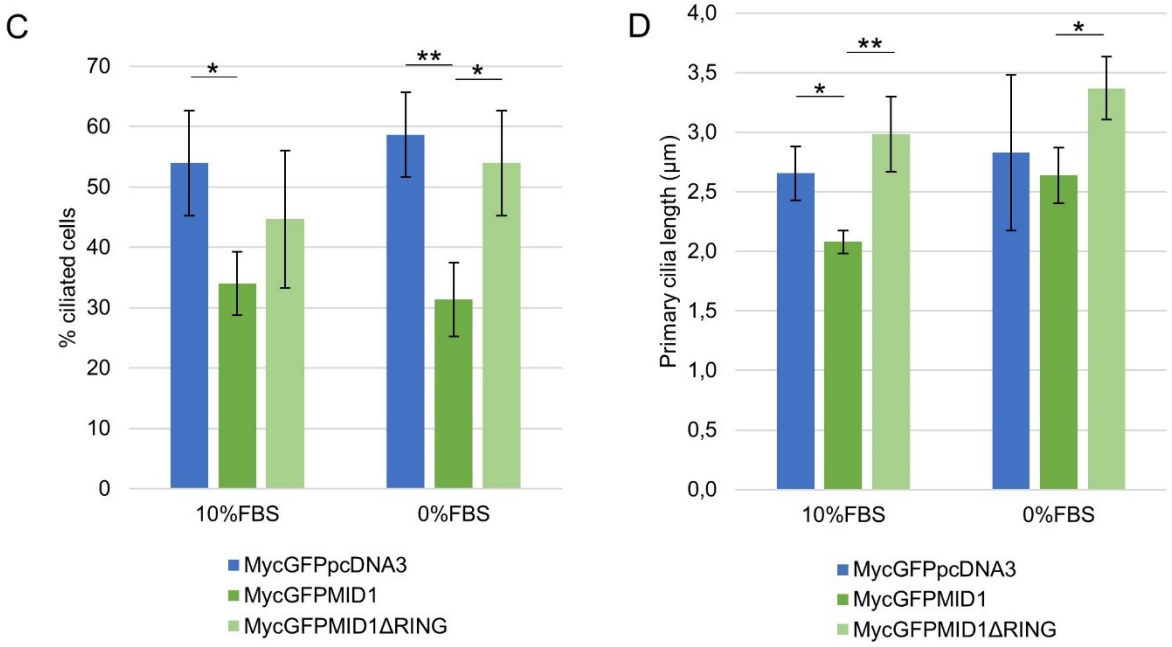


**Figure 11.** Cilia dynamics under serum starvation upon MID1 and MID1ΔRING overexpression in ARPE-19 cells. A) Representative scheme of the experiment repeated three times (STV, starvation). B) Immunofluorescence images (63X magnification; scale bar = 10 µm) showing ARPE-19 transfected with MycGFPpcDNA3, MycGFPMID1 and MycGFPMID1ΔRING maintained either in FBS-containing medium (+FBS) or serum-free medium (-FBS) as indicated. Primary cilia are marked with anti-ARL13B (red signal). C) Histogram indicating the percentage of transfected ciliated cells, calculated as the ratio between the number of transfected ciliated cells and the total number of transfected cells (n=50 for each condition). Data are indicated as MEAN±SD and significance has been assessed through the Student's t-test (*: $p<0.05$). D) Bar blot indicating primary cilia length measurements (MEAN±SD). Significance has been assessed through the Student's t-test (*: $p<0.05$; **: $p<0.01$)

### 4.1.3. Dynamics of cilium elongation in the presence of exogenous MID1.

Similar to the experiment performed in non-transfected ARPE-19 cells, a time-course experiment was also done in the presence of exogenous MID1. The goal was to appreciate the differences in the rate of primary cilium growth in the presence of exogenous MID1 and possibly to identify the elongation phase most affected. Cells have been seeded on coverslips and transfected with MycGFP-MID1 and MycGFP-MID1ΔRING and, serum starved for different time points and the cilium measured at each time point. The MycGFP-pcDNA3 plasmid has been used as a negative control (Figures 12A and B). Both GFP- and GFP-MID1ΔRING-positive cells protruded a cilium that grew until 20 hours and then started a stationary phase showing a cilium stable length (Figure 12C). The maximum length is reached few hours earlier than in non-transfected cells likely due to a

transfection effect. MID1-overexpressing cells cilium, although always shorter than the one protruded by control- and MID1ΔRING-positive cells, grew up to 16 hours then its length was found decreased by the 20-hour-time point to finally stabilise its length (Figure 12C).

From the ANOVA test performed in this experiment, there is a significant difference in the behaviour of the different transfected cells during time ($p<0,01$). Indeed, a difference in the rate of the primary cilium grow can be observed: while the GFP- and GFP-MID1ΔRING-expressing cells primary cilia slowly constantly grew up to 20 hours, GFP-MID1-positive cilia grow more rapidly within the first 16 hours but started to decrease and stabilise after that time point, as MID1 overexpression impaired primary cilium elongation.

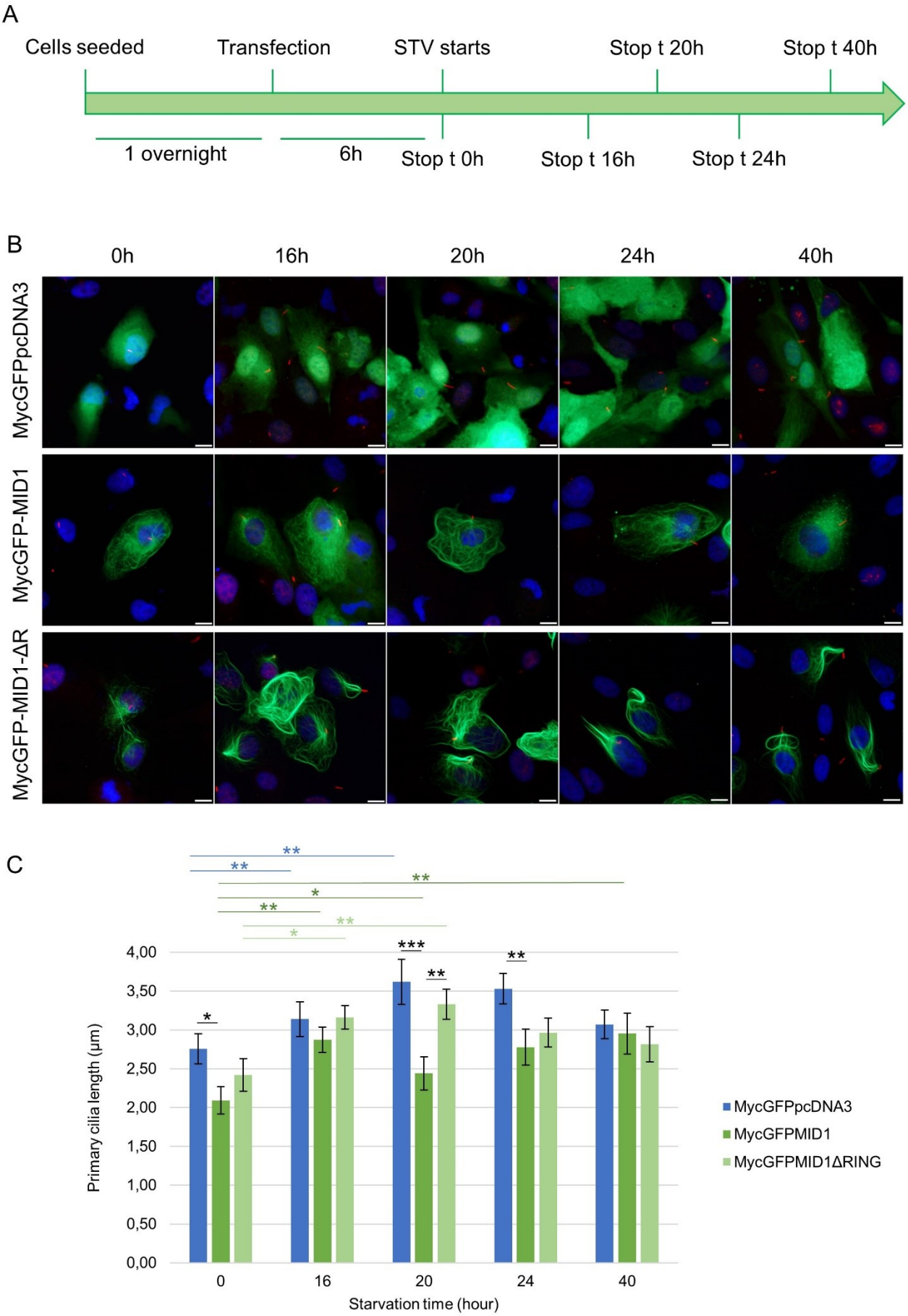


Figure legend on the next page

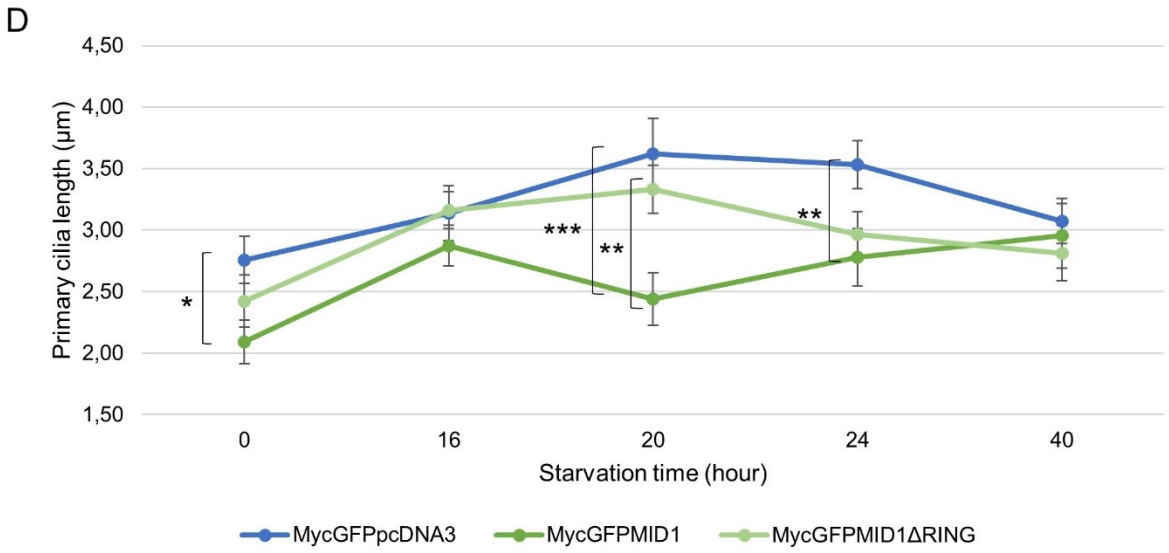


**Figure 12.** Time-course in ARPE-19 cells overexpressing GFP-MID1, GFP-MID1ΔRING and GFP as a negative control. A) Experimental scheme where starvation (STV) time points are indicated. B) Representative immunofluorescence images (63X magnification; scale bar = 10 µm) taken at the different time points. The primary cilia are marked through an anti-ARL13B (red signal). C) Histogram showing primary cilia measurements (N = 30 cilia) for each sample at each time point (MEAN±SEM). Statistical significance has been assessed through the ANOVA test (*: $p<0.05$; **: $p<0.01$; ***: $p<0.001$). D) The linear graph is a representation of primary cilium growth rate (MEAN±SEM). Significance has been assessed through the ANOVA test (*: $p<0.05$; **: $p<0.01$; ***: $p<0.001$).

At 24 hours of starvation in this experiment a statistically significant difference can be appreciated between GFP-MID1-expressing cells and the control. This difference has not been observed in the previous experiment, maybe due to a higher variability in the control samples.

We can conclude that in this human cell line MID1 overexpression impairs ciliogenesis in both normal- and serum-starved conditions. When the cilium is built, exogenous MID1 leads to the protrusion of shorter primary cilia: this effect is clear in normal growth conditions while in serum-free growth conditions this effect is observed mainly at specific times upon starvation due also to a different growth kinetics in the presence of MID1. It is worth pointing out that cell culture conditions play a pivotal role in highlighting the differences between the samples analysed. The data presented have been achieved in presence or absence of foetal bovine serum. It will be interesting to test the same upon depletion of other medium components, e.g. amino acids, to better understand the pathways implicating MID1 and primary cilium protrusion. Moreover, the data showed that MID1 catalytic activity is involved in the control of these processes, since the

introduction of a catalytically inactive form of MID1 makes the cells protruding primary cilia as numerous and long as the controls.

## 4.2. MID1 negatively regulates autophagy flux in ARPE-19 cells.

As mentioned in the Introduction section, MID1 might be indirectly involved in the control of the autophagy pathway. On microtubules, MID1 controls the stability of the catalytic subunit of Protein Phosphatase 2A (PP2Ac) (Trockenbacher et al., 2001) that in turn regulates the activity of mTOR, a key nutrient sensor that negatively regulates autophagy mainly through the control of the mTOR/Raptor complex (mTORC1) formation (Liu et al., 2011). Moreover, a series of recent studies have shown how primary cilium-associated pathways activate autophagy and conversely how autophagy participates in the control of ciliogenesis (Pampliega et al., 2013; Tang et al., 2013). Further, several TRIM proteins are directly involved in the regulation of different steps of the autophagy pathway (Mandell et al., 2014; Kumar et al., 2017; Hatakeyama 2017; van Gent et al., 2018; Di Rienzo et al., 2020). We reasoned that MID1-dependent regulation of ciliogenesis process and of primary cilium length might be explained by alterations in the autophagy process. Therefore, we started investigating a possible role of MID1 in the autophagic process in ARPE-19 cells.

There are several methods to study and monitor the autophagy process and dynamics. The detection of LC3-II protein levels, together with autophagy receptors, e.g. p62, through Western Blot analyses and detection of autophagosomes abundance and destiny through LC3 immunofluorescence are two of the most used methods. Cells experience both a physiological level of autophagy in non-stressed conditions, basal autophagy, and further stress-induced autophagy in response to several stimuli (see Introduction). To maintain the same stress conditions that induce ciliogenesis, we analysed autophagy in normal growth (basal) and upon serum starvation (induced).

GFP- and GFP-MID1-transfected cells have been serum-starved for 3, 6 and 9 hours, one over-night after the medium change upon transfection. Cells collected immediately before the starvation to start have been considered as time 0 (Figure 13A). Western blot analyses have been then performed by loading 5 μg of protein extract for each sample, and both LC3 and p62 protein levels have been analysed by immunoblot together with detection of transfected MID1 using anti-tag (cMyc) antibody (Figure 13B). The detected bands were quantified and normalised against the GAPDH-detected protein and the results are shown in the graphs of Figure 4.

At t = 0h, LC3-II protein levels (lower band in LC3 immunoblot) are higher in MID1 overexpressing cells than in the control (Figure 13C). As expected for starvation-induced autophagy activation, after 3 hours of serum-free growth, LC3-II levels strongly increased in the control while in GFP-MID1-expressing samples the basal high level is maintained stable with no further increase

in LC3-II protein levels. After 6 and 9 hours of serum-starvation, LC3-II levels decreased with similar dynamics in both sets of samples (Figure 13C). A similar trend is observed for what concerns p62 that it is basically behaving as LC3-II: at the starting point, although not significant, p62 protein levels are higher in GFP-MID1-positive cells than in control samples. Upon starvation, p62 protein levels increase in MID1-overexpressing samples is slower, if not absent, than in the control cells where p62 increased up to 6 hours and then started to decrease at 9 hours of serum-starvation (Figure 13D).

In the same experiments, we also noted a different behaviour of the non-lipidated form of LC3, LC3-I, in MID1-overexpressing cells and therefore also this form has been considered. Total levels of LC3 (LC3-I + LC3-II) have been analysed, together with the ratio LC3-II/LC3-I that is an indicator of autophagy activation. For what concern total LC3 levels (Figure 13E), the observed trend is very similar to what seen with LC3-II (Figure 13C) but with an even stronger difference between GFP-MID1-overexpressing cells and the controls at the starting point when considering both forms. As for LC3-II, then no differences can be observed at 3, 6 and 9 hours of starvation between the two samples. Further, as seen for LC3-II alone, there is a significant increase in LC3 levels in the first 3 hours of starvation in the GFP-positive samples than in GFP-MID1-transfected cells. By calculating instead LC3-II/LC3-I ratio, in GFP-MID1-positive cells this value is lower than GFP controls at time 0, due to the high levels of LC3I in the former, and then maintained lower or comparable at the beginning of starvation (3 and 6 hours) (Figure 13F). This can suggest that LC3 is either synthesised at higher level or not degraded as in the control cells. Whether this degradation is autophagy- or proteasome-mediated in these cells is still under investigation. These results can also suggest that the autophagy pathway might be somehow slowed down and LC3 tend to be accumulated when exogenous MID1 is expressed.

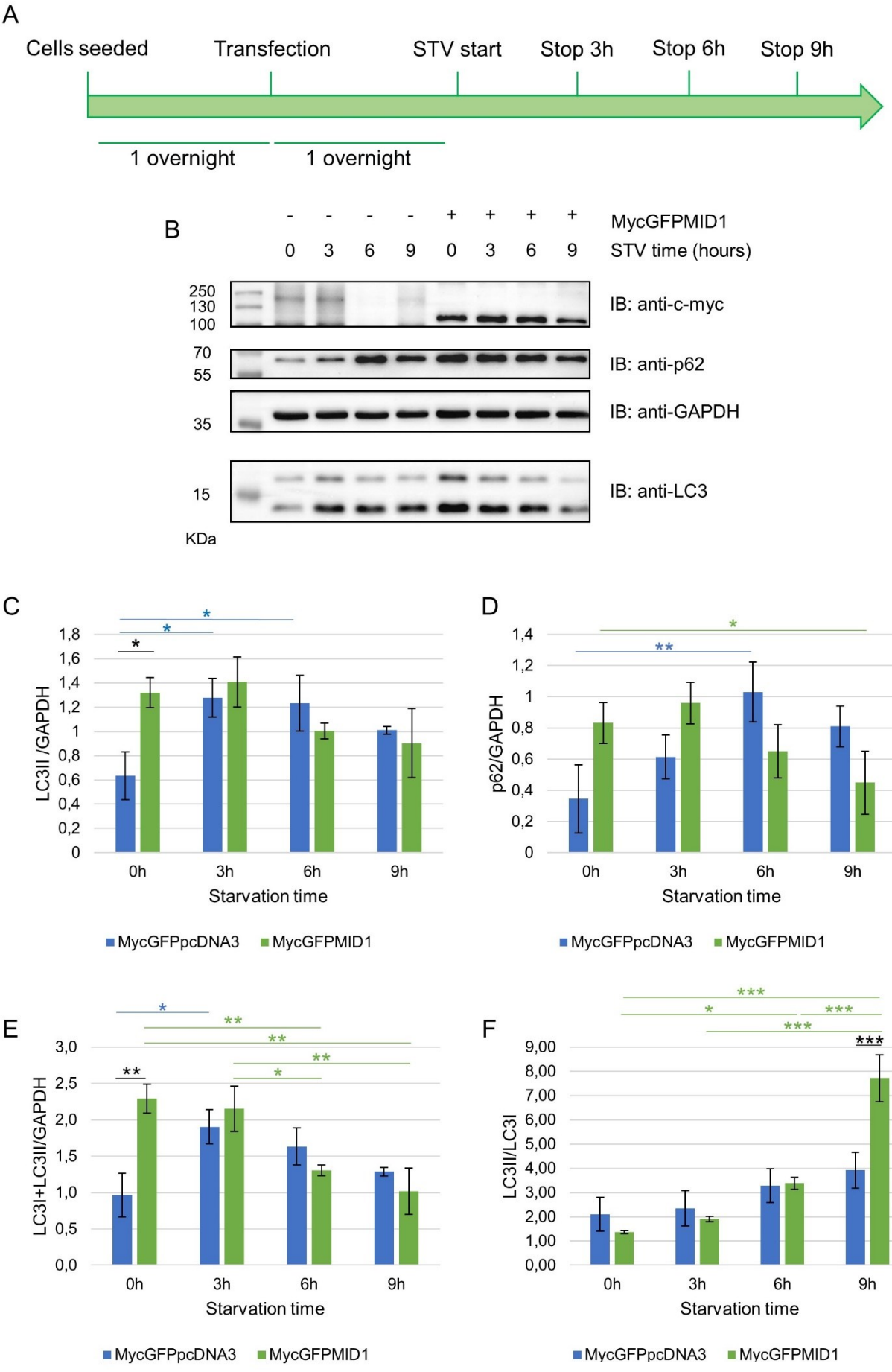


Figure legend on the next page

**Figure 13.** MID1 role in autophagy in ARPE-19 cells. A) Experimental scheme where starvation (STV) time points are indicated. B) Representative Western Blot analyses for p62 and LC3 protein levels detection; 5 μg of protein extract have been loaded and GAPDH has been used as loading control. Anti-c-Myc has been used to assess proper MID1 exogenous expression. C) Histogram of LC3-II protein levels normalised on GAPDH intensity. D) Histogram of p62 protein levels normalised on GAPDH. E) Total LC3 protein levels calculated as the sum of LC3-II and LC3-I intensities, both normalised on GAPDH. F) LC3-II/LC3-I ratio normalised against GAPDH signal. This experiment has been performed three times, data are represented as MEAN±SEM, and significance has been assessed through ANOVA test (*: $p<0.05$; **: $p<0.01$; ***: $p<0.001$)

The notion according to which an increased amount of autophagosomes number, observed through increased LC3-II protein levels, corresponds to an increased autophagy induction is not totally correct. Autophagosomes accumulation may correspond either to autophagy activity enhancement or to the suppression of steps downstream autophagosomes formation that leads to their turnover, i.e. lysosome-dependent degradation blockage. To understand this point, concomitant analysis of the autophagy flux is usually performed. One of the approaches entails the treatment with lysosomes inhibitors, such as chloroquine, that blocks lysosome acidification, or bafilomycin that blocks autophagosomes fusion to the lysosomes. By blocking the lysosome activity, LC3-II levels are increased due to accumulation in the cells (Tanida et al., 2005). LC3-II levels are increased also in basal conditions upon the treatment, but the difference in its levels in the presence or absence of the drug is larger under starvation, due to the fact that autophagy flux is usually increased upon starvation.

To better address this issue, ARPE-19 have been cultured in serum-containing medium and transfected with MycGFP-MID1 and MycGFP-pcDNA3 as a negative control in triplicate. Six hours after transfection, at the medium change, half of dishes for each plasmid have been maintained in serum-containing medium while in the remaining dishes have been shifted to a serum-free medium. After further 20 hours, chloroquine (100 μM) was added and kept for 4 hours (Figure 14A). At the end of the treatment, cells were lysed and protein extracts analysed by immunoblot (Figure 14B). In normal growth conditions, as expected, chloroquine treatment led to the accumulation of LC3-II protein levels in both GFP-MID1-overexpressing sample and in the control (Figure 14B), although LC3-II-accumulation was significantly lower in GFP-MID1-overexpressing cells than in GFP-overexpressing ones, suggesting a slower autophagy flux if exogenous MID1 is expressed (Figure 14C). In the absence of serum, results are inverted: LC3-II accumulates more in GFP-MID1-transfected cells than in the controls although this difference is not statistically significant (Figure 14D-E).

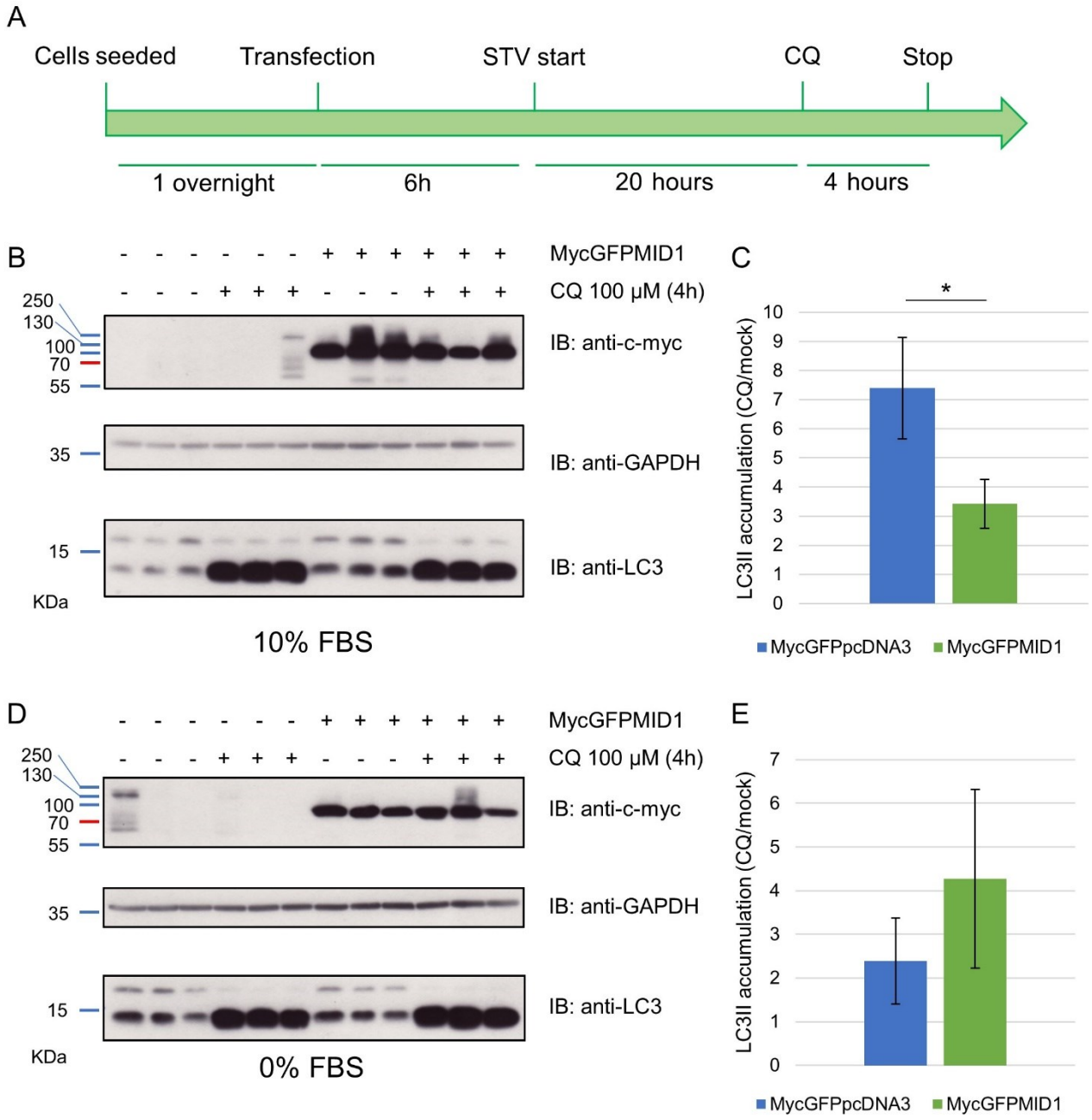


**Figure 14.** Autophagy flux analysis in ARPE-19 expressing exogenous MID1. A) Experimental scheme where starvation (STV) and Chloroquine (CQ) treatment time points are indicated. B) Western Blot analysis of samples from normal growth conditions (10% FBS). LC3 proteins (I and II) were detected and GAPDH has been used as loading control. Anti-c-Myc has been used to assess proper MID1 exogenous expression. In the blot, the three technical replicates are present. C) Quantification of LC3-II accumulation from the immunoblot in B, calculated as the ratio between CQ and mock, normalised against GAPDH. Statistical significance has been assessed with Student's t test (*: $p<0.05$). D) Western Blot analysis of serum-starved samples (0% FBS). Description as in B. In the blot, all the three technical replicates are present. E) Quantification of LC3-II accumulation from the immunoblot in D, calculated as the ratio between CQ and mock, normalised against GAPDH. Statistical significance has been assessed with Student's t test (data not statistically significant).

To further confirm these data, a time-course has been performed where cells have been treated for shorter time with chloroquine. The same experiment has been performed as above but treating cells for 30 minutes and 1 hour, always using a final concentration of 100 μM of chloroquine (Figure 15A). In basal conditions, as expected, LC3-II levels increased over time in GFP-overexpressing cells, but in MID1-transfected samples LC3-II levels increase was not as marked (Figure 15B-C). In the same experiment, p62 protein levels have also been analysed: although not statistically significant, in MID1-overexpressing cells p62 levels increased with the time of the treatment (Figure 15D-E) in contrast to the empty vector-transfected cells where the missed accumulation of p62 in the controls is not consistent. By blocking the lysosome, an increase in p62 protein levels was expected over time upon chloroquine treatment, but not occurring in GFP controls. Further experiments are needed to better understand this unexpected behaviour. Another inconsistent aspect is that p62 is accumulating in MID1-overexpressing cells, not expected if there is a delayed autophagy flux.

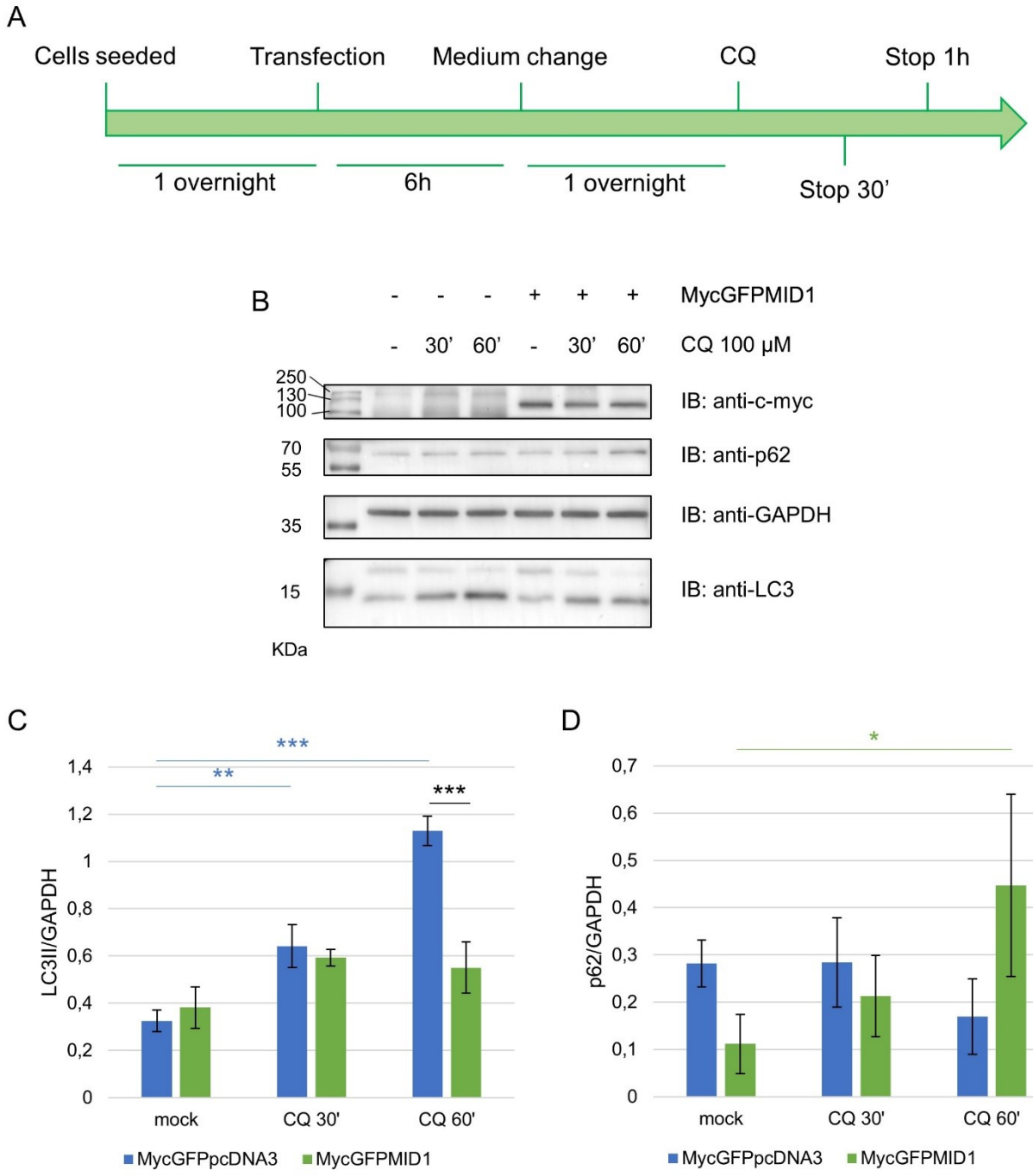


**Figure 15.** Basal autophagy flux analysis in ARPE-19 expressing exogenous MID1. A) Experimental scheme where CQ treatment starting point and stop points are indicated. B) Representative Western Blot of LC3 and p62 protein levels. This experiment has been repeated three times. C) Quantification of LC3-II protein levels normalised against GAPDH. Significance has been assessed with ANOVA test (**: $p<0.01$, ***: $p<0.001$). D) Quantification of p62 protein levels normalised against GAPDH. Statistical significance has been assessed with ANOVA test (*: $p<0.05$)

In the absence of serum, LC3-II behaviour is identical in the two transfected samples showing a time-dependent increase (Figure 16B-C). For what concerns p62 protein levels, it shows accumulation with time of treatment, but its levels are always lower in MID1-overexpressing cells

than in GFP-positive cells (Figure 16B-D), thus probably suggesting an induced autophagy in MID1-positive samples. All together, these experiments are showing how MID1 overexpression leads to a block of the autophagy pathway, slowing the flux down in basal conditions, but not upon serum-starvation.

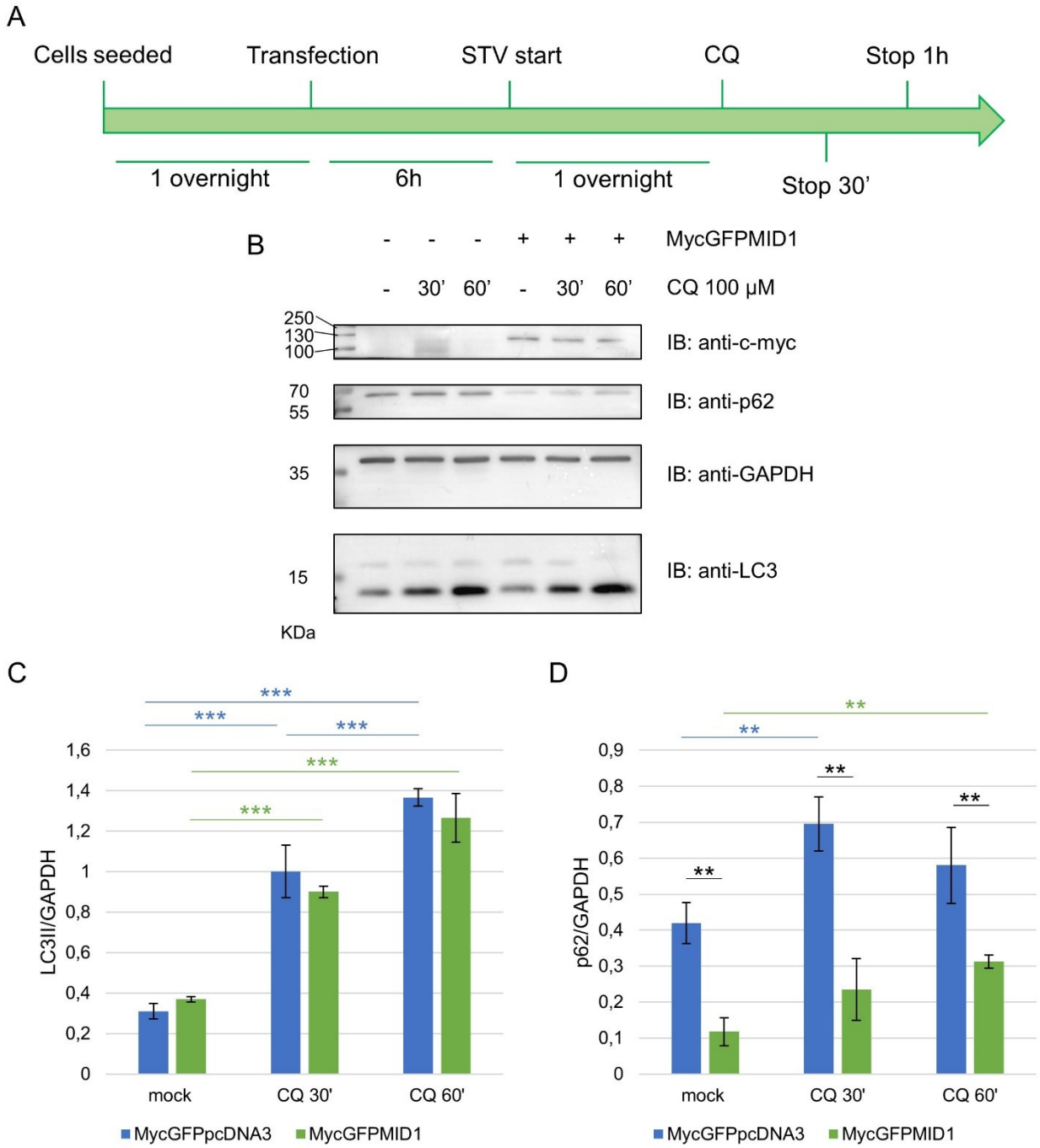


**Figure 16.** Serum starvation-induced autophagy flux analysis in ARPE-19 expressing exogenous MID1. A) Experimental scheme where CQ treatment starting point and stop points, as well as serum starvation (STV) are indicated. B) Representative Western Blot of LC3 and p62 protein levels. This experiment has been repeated three times. C) Quantification of LC3-II protein levels normalised against GAPDH. Statistical significance has been assessed with ANOVA test (**: $p<0.01$, ***: $p<0.001$). D) Quantification of p62

protein levels normalised against GAPDH. Statistical significance has been assessed with ANOVA test (*: $p<0.05$)

Confocal images from preliminary experiments performed in ARPE-19 overexpressing MycGFP-MID1 together with mCherry-LC3 plasmid, both in normal growth conditions and in serum starvation, show that some LC3-positive puncta are also GFP-positive, indicating a co-localisation of MID1 and LC3 on autophagosomes (Figure 17A). Additional experiments are definitely needed to better investigate this point; however, these data suggest that MID1 might localise to autophagosomes and be degraded through autophagy, thus hypothetically creating a feedback loop between autophagy process and MID1. This relationship between MID1 and LC3 is reinforced by the fact that *in silico* analyses with iLIR tool (Jacomin et al., 2016) showed that MID1 protein sequence contains a putative LIR (LC3 Interacting Region) sequence in its FN3 domain (Figure 17B). The fact that MID1 contains a LIR is indicative that it might be degraded through autophagy being embedded into the autophagosomes via LC3-II interaction, although when the lysosome has been blocked in the previous experiments, no differences in exogenous MID1 protein levels have been observed. Another possibility is that MID1 might interact with LC3-II in the outer side of the autophagosome membrane, thus regulating, for instance, autophagosomes movement on microtubules (Xie et al., 2010). This last hypothesis might explain why MID1 overexpression slows autophagy down, since its positioning on microtubules might regulate the movement of autophagosomes towards the lysosomes.

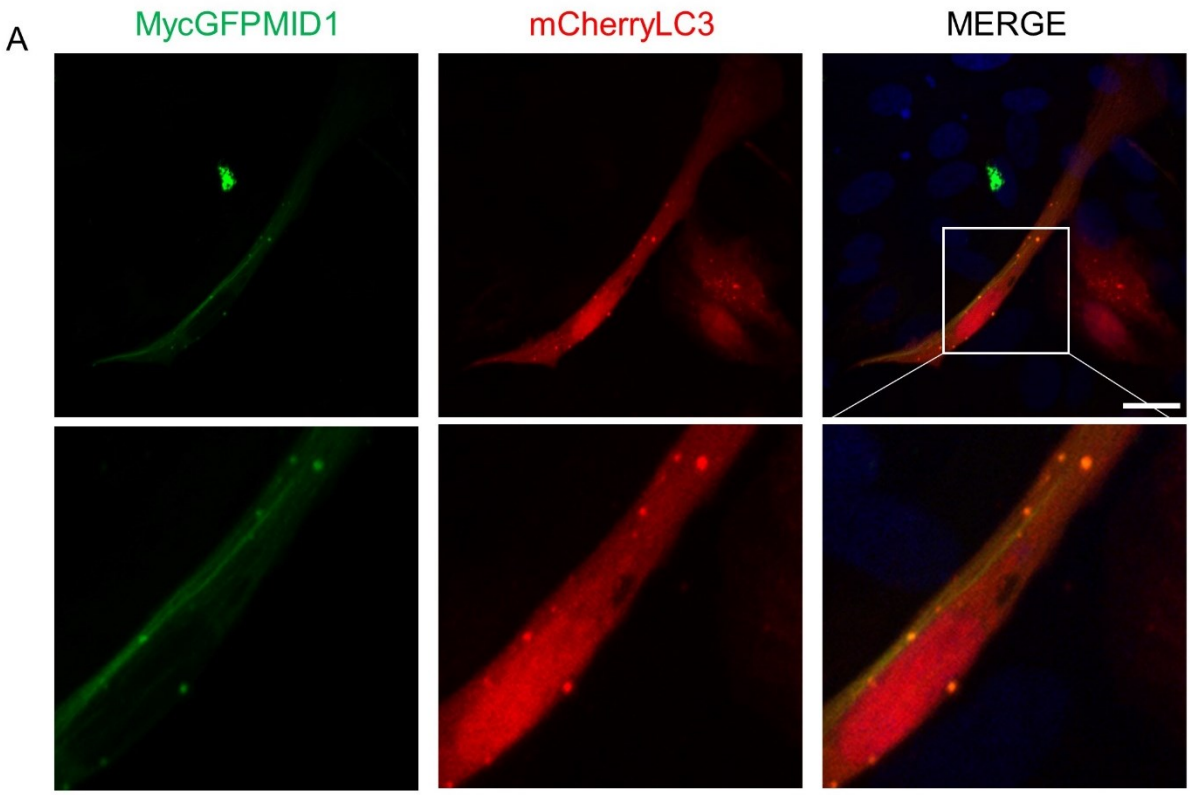


B

FN3

```
pattern                                  ******
Query     361  TFALDFSREKKLLECLDYLTAPNPPTIREELCTASYDTITVHWTSDDEFSVVSYELQYTI  420
               TFALDFSREKKLLECLDYLTAPNPPTIREELCTASYDTITVHWTSDDEFSVVSYELQYTI
Sbjct     361  TFALDFSREKKLLECLDYLTAPNPPTIREELCTASYDTITVHWTSDDEFSVVSYELQYTI  420
```

**Figure 17.** MID1 partially colocalises with LC3. A) Confocal images (60X magnification, 1024 x 1024 pixels, scale bar = 10µm) of ARPE19 cells co-transfected with MycGFPMID1 and mCherryLC3. B) LIR sequence indicated with the asterisks above the MID1 FN3 domain

Additional experiments are needed to clarify the role of MID1 in ciliogenesis and autophagy in ARPE-19 cell: the use of different version of overexpressed MID1, e.g. HA-tagged MID1; performing more detailed time course both for autophagy and ciliogenesis; the use of additional autophagy inhibitors; and test the knock-down or knock-out of MID1 to test these processes in the absence of MID1. Moreover, it should be of interest to mutagenise the LIR sequence to see whether the colocalisation between MID1 and LC3 is disrupted, and autophagy flux rate restored, as well as investigate whether MID1 catalytic activity is involved also in autophagy regulation.

## 4.3. *Mid1*-depleted MEFs exhibit a longer primary cilium.

Taking advantage of the availability of a mouse model lacking the *Mid1* gene (Lancioni et al., 2010), we decided to investigate whether *Mid1* absence impairs ciliogenesis and/or primary cilia

length also in mouse fibroblasts. Seven MEF primary cell lines established from 4 wild type (WT) and 3 knock-out (KO) littermates have been used for the following experiment. MEFs have been seeded on glass coverslips and, after reaching 80% confluence, they have been either maintained in medium with serum or starved in a serum-free medium for 24 hours (Figure 18A). Coverslips have been then fixed in 4% PFA for 10 minutes at room temperature and anti-ARL13B antibody has been used to mark the primary cilium by immunofluorescence (Figure 18B). As for ARPE-19 cells, 20X magnification images have been used to calculate the percentage of ciliated cells and 60X magnification images at higher resolution have been used to measure primary cilia. The percentage of ciliated fibroblasts was not affected by the absence of Mid1: WT MEFs protruding a cilium were 3.55% on average (3.55 ± 2.18%) in normal growth condition and 31.3% on average (31.3 ± 14.9%) after 24 hours of serum starvation, while KO MEFs protruding a cilium were 3.21 % on average (3.21 ± 1.39%) in the presence of the serum and 29.9% on average (29.9 ± 8.87%) in the absence of the serum (Figure 18C). Differently from ARPE-19 cells, only a very small percentage of MEFs are ciliated in normal conditions (see above). Therefore, primary cilium length has been measured only upon serum starvation. KO MEFs were able to protrude a longer cilium than the one protruded by WT cells upon serum starvation: WT MEFs primary cilia were2.64 μm long on average (2.64 μm ± 0.112 μm), while KO MEFs primary cilia were 2.85 μm long on average (2.85 μm ± 0.061 μm). Although this difference is small in value, in the 7 MEFs lines little variability was observed in these experiments leading to a statistically significant difference in cilium length (Figure 18D).

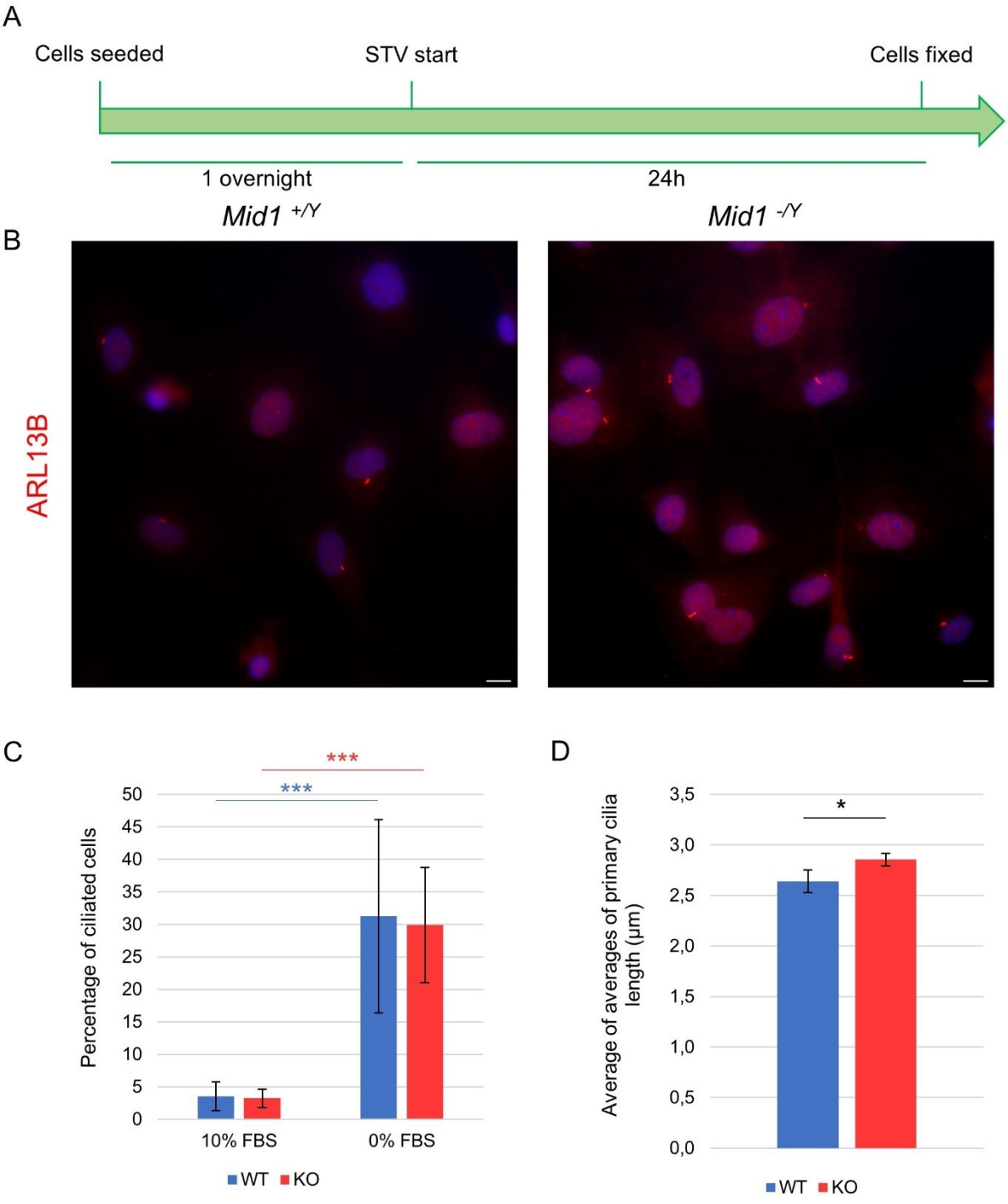


**Figure 18.** Mid1 depletion enhances primary cilium elongation. A) Representative scheme of the experiment, performed with N=4 WT MEFs and N=3 KO MEFs. B) Immunofluorescence images (60X magnification; scale bar = 10 µm) showing both WT and KO MEFs maintained in serum-free medium (STV, 24h). Primary cilia are marked with anti-ARL13B (red signal). C) Histogram indicating the percentage of ciliated cells, calculated as the ratio between the number of ciliated cells and the total number of cells. Data are indicated as MEAN±SD and statistical significance has been assessed through the Student's t-test (***:

p<0.001). D) Histogram indicating primary cilia length measurements (MEAN±SD). Statistical significance has been assessed through the Student's t-test (*: p<0.05)

As seen in human cells, also in this case the difference in primary cilium length between WT and KO MEFs might be due to a faster rate of primary cilium growth in the KO MEFs. To further confirm this issue, a time course experiment has been performed, where KO and WT MEFs have been starved at different time points (16, 20, 24, 40 and 48 hours) to see whether KO MEFs primary cilia reached the maximum length before the WT ones (Figure 19A). In these samples, primary cilia have been marked through immunofluorescence with an anti-ARL13B antibody. Thirty primary cilia have been analysed for each sample and each condition through epifluorescence microscopy and their length has been measured through ImageJ software from 60X magnification images (Figure 19B). From this analysis, it is evident how KO primary cilia reached their maximum length (3.01 μm ± 0.38 μm) upon 24 hours of starvation, while WT primary cilia need 48 hours to reach their maximum length (2.9 μm ± 0.5 μm). Moreover, especially in the first 24 hours, the primary cilia growth curve showed a more inclined slope in the KO than in the WT (Figure 19C), suggesting a faster ciliary growth rate in KO cells despite statistical analyses showed no significant differences between the two samples, except for the 20 hours time-point, where the Student's t-test shows a significant difference between WT and KO samples (not shown in Figure 19C).

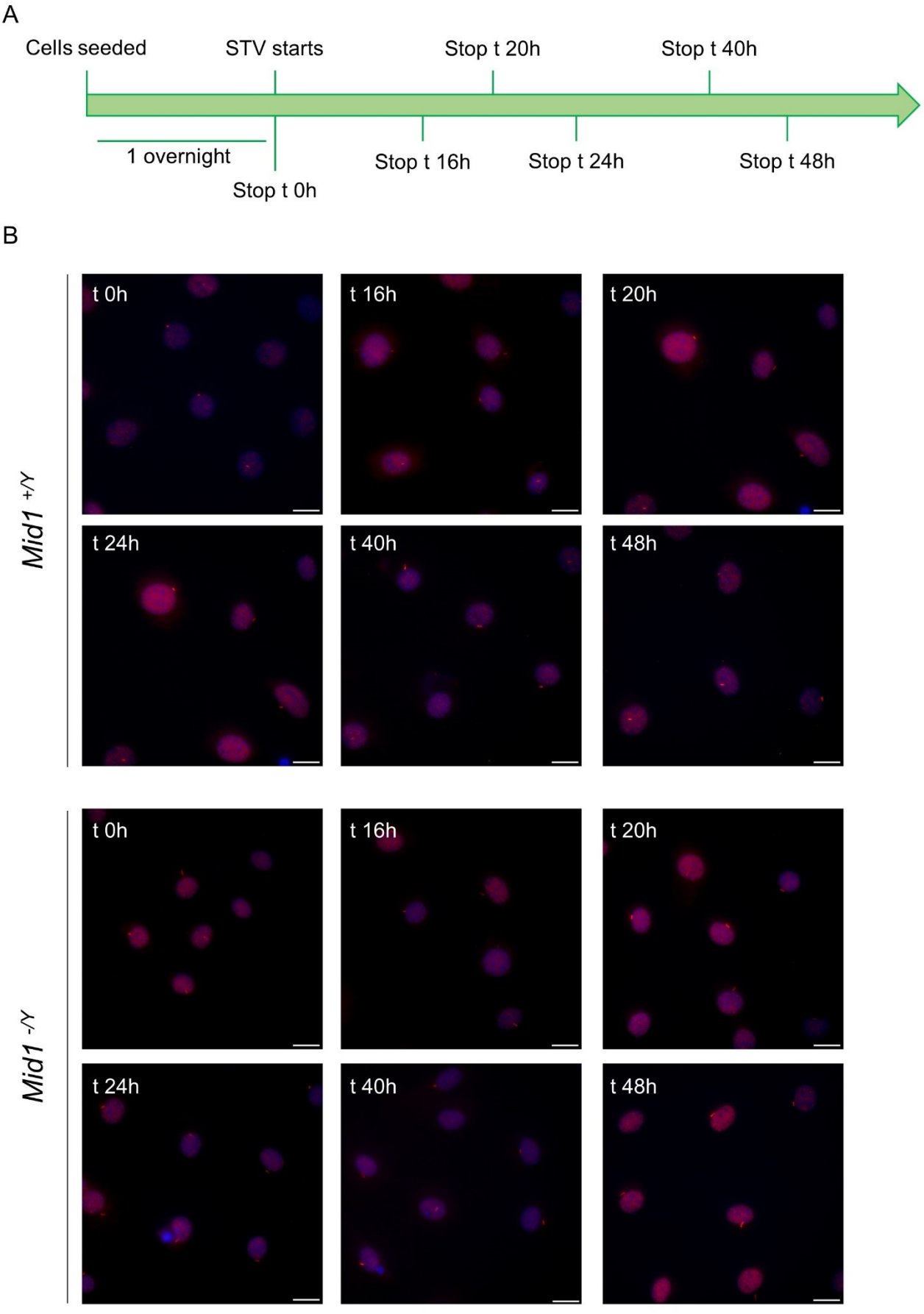


Figure legend on the next page

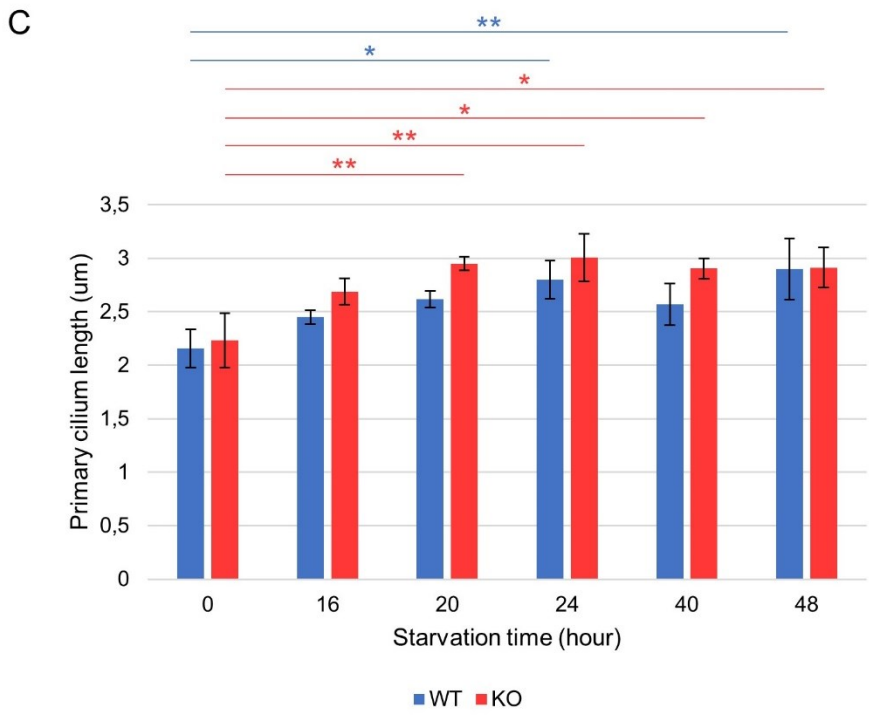


**Figure 19.** Time-course in WT and KO MEFs ciliogenesis. A) Experimental scheme where starvation (STV) time points are indicated. B) Immunofluorescence images (60X magnification; scale bar = 20 µm) taken at the different time points. The primary cilia are marked with anti-ARL13B (red signal). C) Histogram showing primary cilia measurements (N = 30 cilia for 3 WT and 3 KO samples) at each time point (MEAN±SEM). Statistical significance has been assessed through the ANOVA test (*: $p<0.05$; **: $p<0.01$)

These results are consistent with ARPE-19 time-course experiments, indeed, in both experiments cells expressing MID1 (exogenous protein in ARPE-19 and WT MEFs for the mouse model) show shorter cilia at 20 hours of serum-starvation.

## 4.4. Autophagy flux regulation in MEFs.

Given the results of the effect of MID1 in the ARPE-19 human cell line in an overexpression system, we reasoned that in MEFs lacking *Mid1* autophagy flux rate might be faster than WT littermates. Both WT and KO MEFs (N = 3 for each genotype) have been serum-starved for 3, 6 and 9 hours, to detect by western blot analyses both p62 and LC3-II levels (Figure 20A-B). In general, MEFs are characterised by high levels of LC3-II, therefore, to distinguish LC3-II and I a small protein amount has been loaded on gels for Western blot analyses. As it was performed in ARPE-19, the "time 0h" correspond to cells harvested immediately before starting the starvation in the other dishes. As regards p62 protein levels, no differences are detected among WT and KO cells at time 0 hours, while after 9 hours of starvation its levels start to significantly increase in KO cells, maybe indicating that its synthesis has been enhanced in response to autophagy induction through serum starvation or that its lysosomal-dependent degradation is blocked (Figure 20D). For what

concerns LC3-II protein levels, there are no detectable changes upon the different starvation times and no differences are observed among WT and KO although a huge variability has been observed among the different samples (Figure 20C).

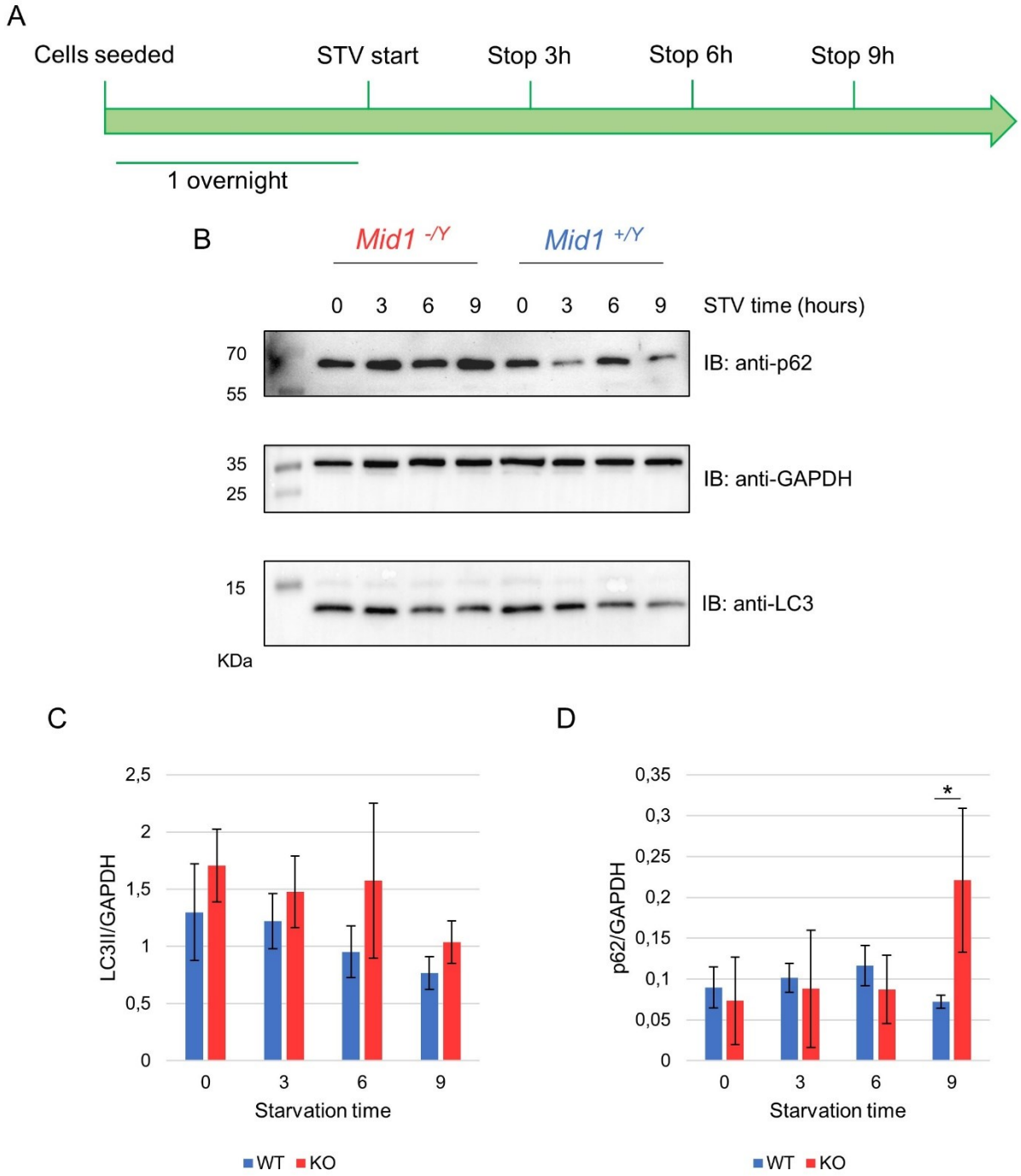


**Figure 20.** Autophagy induction upon serum-starvation (STV) in WT and KO MEFs. A) Experimental scheme where starvation (STV) time points are indicated. B) Western Blot analyses for p62 and LC3 protein levels detection. 3 µg of protein have been loaded and GAPDH has been used as normaliser. C) Histogram of LC3-II protein levels (lower band in LC3 WB) normalised against GAPDH. D) Histogram of p62 protein levels normalised against GAPDH. This experiment has been performed with 3 biological replicates for each

genotype, data are represented as MEAN±SEM, and significance has been assessed through ANOVA test (*: $p<0.05$)

Also, the autophagy flux has been analysed in MEFs. The same samples described above have been treated with 100 μM of chloroquine for 4 and 8 hours after they were serum starved for 24 hours (Figure 21A). Both p62 and LC3-II protein levels have been detected and analysed (Figure 21B). Although not statistically significant, likely due to the high variability in the samples, both p62 and LC3-II accumulation over time is higher in the KO samples than in WT ones, suggesting a faster autophagy flux in KO MEFs (Figure 21 C-D). This suggest that the increased p62 protein levels after 9 hours of starvation in KO cells is a response to autophagy induction and not due to a block of the autophagy flux.

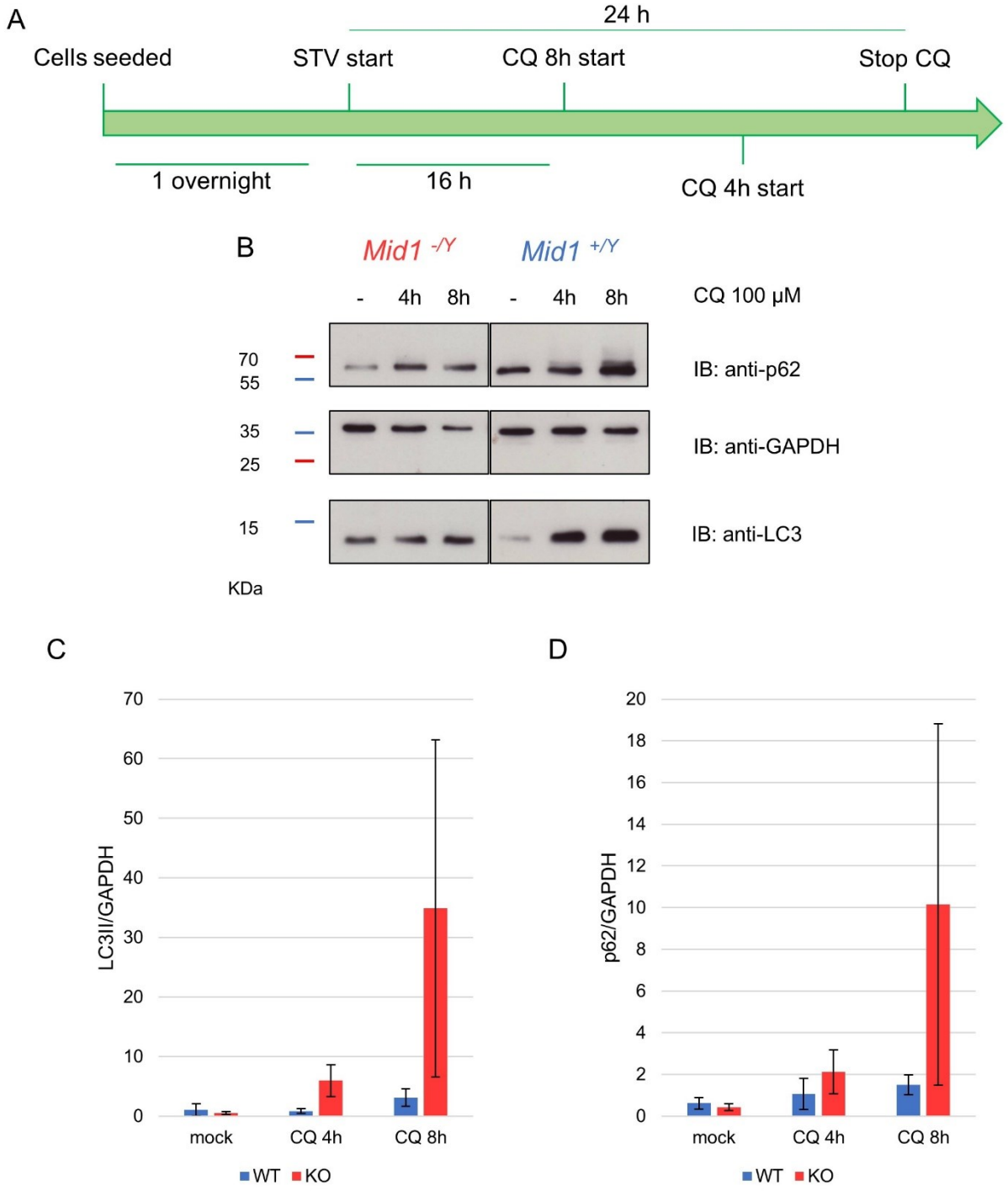


**Figure 21.** Serum starvation induced autophagy flux analysis in WT (N=3) and KO (N=3) MEFs. A) Experimental scheme where CQ treatment starting point and stop points are indicated. B) Representative Western Blot of LC3 and p62 protein levels. C) Quantification of LC3-II protein levels normalised against GAPDH. Significance has been assessed with ANOVA test (no statistically significant data). D) Quantification of p62 protein levels normalised against GAPDH. Significance has been assessed with ANOVA test (no statistically significant data).

The same experiments must be performed in a nutrient-rich condition, to evaluate basal autophagy levels in both WT and KO MEFs, and, further, other mice families must be analysed to better appreciate the differences between the two genotypes.

Taken all together, these data suggest that MID1 overexpression in human cells and *Mid1* depletion in the mouse model regulate the autophagy pathway, by slowing it down or by accelerating it, depending on the cell culture condition. It has to be taken in account that the response to chloroquine treatment might be different in fibroblasts and in epithelial cells, as well as autophagy flux regulation. It will be of interest to reintroduce Mid1 in KO cells or to slow autophagy down to see if a rescue occurs and, at the same time, verify the primary cilia length decrease.

# 5. Conclusions

Loss-of-function mutations in the *MID1* gene are responsible for the X-linked form of Opitz G/BBB Syndrome (OS), whose pathogenetic mechanisms are still under investigation. One of the hypotheses is that OS is a neurocristopathy, that is a pathology caused by defects in Neural Crest Cells (NCCs) migration, proliferation, and differentiation, being some features shared between these two pathologies, for instance hypertelorism, broad nasal bridge, cleft of lip and palate and heart defects (Winter et al., 2016). However, so far, no data demonstrate this hypothesis, since the mouse and OS patients do not show other typical aspects of neurocristopathies, for instance OS patients do not show hypoplasia of facial bones, and besides NCCs aberrant migration would not explain the major clinical sign observed in OS, i.e. hypospadias.

Several OS clinical features are also shared with ciliopathies, a class of pathologies caused by impairments in primary cilium assembly and/or dynamics, an organelle that functions as an antenna for the cell, making it to sense different stimuli mainly from the extracellular environment. Starting from the hypothesis that MID1 might be involved in the regulation of the processes that lead the cells to build the primary cilium, we found that exogenous MID1 expression in a human epithelial cell line (ARPE-19) impairs primary cilium protrusion, by limiting its growth. Both in the presence and in the absence of serum, which usually leads to the induction of ciliogenesis, the percentage of ciliated cells in the presence of exogenous MID1 is reduced. Moreover, when cilia manage to grow, they are shorter in the presence of exogenous MID1 if compared to a GFP-expressing control, especially in the presence of serum. This suggests that MID1 is a negative regulator of both primary cilium biogenesis and elongation and that this effect may depend on cell culture conditions. Moreover, MID1 role in this contest depends also on its E3 ubiquitin ligase activity, since its effect is totally abolished when exogenous catalytically dead MID1-ΔRING is expressed and the latter show comparable cilia percentage and length to the control. The fact that cilia length in MID1-ΔRING expressing cells is even longer that in the control, suggests a dominant negative effect of MID1-ΔRING mutant on the endogenous MID1 protein, likely due to their homodimerisation property. Time course experiments showed that also the speed of cilium growth is different when exogenous MID1 protein is present: indeed 16 hours of serum starvation are required to reach the maximum length in MID1-expressing cells compared to 20-24 for GFP- and MID1ΔRING-expressing cells, maximum length that nevertheless still remains shorter than controls.

In mouse embryonic fibroblasts, the absence of Mid1 protein does not affect cells' ability to protrude the primary cilium; however, consistent with what observed in human ARPE-19 cells, primary cilia are longer in KO cells upon starvation, reaching their maximum length in 24 hours,

while WT cells keep elongating for longer time. This confirms that MID1 is a negative regulator of primary cilium elongation.

The differences observed between epithelial cells and fibroblasts might be due to the fact that these cells follow the alternative pathway and the intracellular pathway, respectively, to build the primary cilium (Figure 8). Moreover, the two experimental models are different, since in the human cell line the role of MID1 has been assessed by exogenous protein overexpression while in MEFs Mid1 is depleted. Eliminating MID1 from ARPE-19 and re-introducing Mid1 in KO MEFs might be useful to confirm our data. In addition, as the MID1 E3 ubiquitin ligase activity is necessary to exert a role as primary cilium regulator, future experiments are needed to investigate which factors are targeted by this ubiquitin ligase activity. Being a negative regulator of ciliogenesis, MID1 may ubiquitinate positive regulators of cilia biogenesis, leading to their proteasome-dependent degradation, or can also ubiquitinate a negative regulator of ciliogenesis impairing its removal from the mother centriole appendices, thus preventing, for instance, its docking to the plasma membrane. Another hypothesis is that MID1, being a microtubule associated protein possibly involved in microtubule stabilisation (Schweiger et al., 1999), might be involved in the axoneme polymerisation and stabilisation, although MID1 has not been observed to localise at the primary cilium. Another aspect to consider is that the starvation experiments have been performed in DMEM without serum. Therefore, it will be of interest to eliminate other medium components from the culture medium, i.e. amino acids and/or glucose, to better highlight the differences seen between MID1-overexpressing cells and controls and to see whether mTORC1, that senses amino acids availability, is involved in this process by regulating autophagy.

Autophagy and primary cilium are reciprocally regulated (Pampliega et al., 2013; Tang et al., 2015), in a cell type-dependent manner as well as in a stimulus-dependent manner. My results indicate that MID1 regulates autophagy flux differently depending on the cell type and on the presence or absence of the serum in the culture medium. In nutrient-rich condition, only basal autophagy is active and, by analysing its flux in ARPE-19, MID1 is slowing down this process (Figure 14 and 15). When the serum is removed from the medium, no differences can be appreciated between cells expressing exogenous MID1 and the ones expressing the GFP (Figure 14 and 16). The only aspect that changes between the basal and the serum-removal induced autophagy in these samples is that in MID1 overexpressing samples, in serum starvation, p62 levels are always lower than GFP ones, although it is accumulating like in the GFP control upon chloroquine treatment. Therefore, in epithelial cells MID1 regulates only basal autophagy.

Basal autophagy has been found to negatively regulate ciliogenesis by targeting IFT20 that travels from the Golgi to the basal body carrying materials for the primary cilium construction. But

if MID1 is delaying basal autophagy, IFT20 should not be targeted for autophagy dependent degradation when MID1 is overexpressed, so I would expect a higher percentage of ciliated cells and longer cilia in these samples. This may suggest that the ciliary phenotype observed in ARPE-19 in serum-containing medium is not basal autophagy dependent or that other pathways may be involved. One alternative hypothesis might be that MID1 is targeting a positive regulator of ciliogenesis, targeting it by ubiquitination for proteasome-dependent degradation. It has been shown that in cells with impaired autophagy, the cilium can be built thank to the Hh signalling (Pampliega et al., 2013). Given MID1 role in the Hh pathway, where it targets Fu, I cannot exclude that the ciliary phenotype observed with exogenous MID1 might be due to an activation of this pathway (Krauss et al., 2008; Schweiger et al., 2014). However, another hypothesis can suggest that MID1 alters the autophagosomes "journey" on microtubules: autophagosomes have been found to localise to the base of the primary cilium (Pampliega et al., 2013) targeting proteins or protein complexes involved in several ciliary processes. MID1 might regulate proper movement of autophagosomes towards both the basal body, to target the cargo proteins, and to the lysosomes for degradation. In serum-free conditions, instead, induced autophagy seems not to be impaired, so also in this case, the explanation of the ciliary phenotype should be found elsewhere. It is important to highlight a limitation in many of the experiments reported: MID1-overexpressing cells do not show statistical significance when compared to the GFP controls. This may be a consequence of the low percentage of transfected cells and/or differences in the levels of the expression of the exogenous protein among the cells. Indeed, it would be of interest to obtain MID1-knockout ARPE-19 to confirm our results.

Moreover, the analysis of ciliogenesis in the presence or absence of MID1 upon the use of compounds that modulate autophagy (inducers and inhibitor) will be crucial to understand if a crosstalk between these two processes involves MID1.

Another important process to be investigated is primary cilium disassembly, usually occurring when cells re-enter the cell cycle, through depolymerisation of the axoneme and its consequent reabsorption, or through exocysts release from the ciliary tips.

In fibroblasts, only serum-starvation induced autophagy flux has been analysed; in these conditions Mid1 depletion tends to result in a faster autophagy flux, although no statistically significant differences can be observed between WT and KO samples. A limitation in this case is the high variability among the samples with the same genotype leading often to non-statistically significant results. This might be due to an intrinsic feature of the cellular/animal model; indeed, the different samples represent independent biological replicates.

A faster autophagy flux may lead to a faster degradation of any of the negative regulator of ciliary elongation, such as OFD1, thus leading to a longer cilium. Indeed, some of the phenotypic features characterising oro-facial-digital type I syndrome (OFD1 syndrome), caused by mutations in the *OFD1* gene, are also observed in OS, although with a milder phenotype. Further experiments are required to better study basal autophagy in WT and KO MEFs, as well as Hh pathway involvement in the regulation of all these processes. Hh pathway role in Opitz Syndrome might be of great importance, since mutations in Sonic Hedgehog are linked to another ciliopathy, holoprosencephaly, in which the midline structure phenotype is opposite to the one observed in OS patients.

To conclude, MID1 acts as a negative regulator of basal autophagy as well as a negative regulator of ciliogenesis. MID1 regulation of autophagy may occur in a PP2Ac-dependent manner, thus involving mTORC1 (Li et al., 2011), a question that needs to be addressed in future experiments. MID1 regulation of primary cilium dynamics is cell type dependent, influencing both ciliogenesis and cilia elongation in epithelia and only cilia elongation in fibroblasts. Cilia that elongate without proper control are pathological; in fact, in most of the ciliopathies, cilia are longer than they should be. Being almost all the phenotypes in OS overlapping with those found in ciliopathies, OS could be from now on considered as a ciliopathy.

# 6. Acknowledgements

The PhD fellowship has been supported by the “Fondo Sociale Europeo 2014/2020, Friuli Venezia Giulia”. Prof. Meroni’s Lab, Department of Life Sciences, hosted all research activities.

# 7. References

1. Agarraberes FA, Dice JF. A molecular chaperone complex at the lysosomal membrane is required for protein translocation. J Cell Sci (2001) 114,2491-2499.
2. Alers S, Loffler AS, Wesselborg S, Stork B. Role of AMPK-mTOR-Ulk1/2 in the regulation of autophagy: crosstalk, shortcuts, and feedbacks. Mol Cell Biol (2012) 32:2-11
3. Aranda-Orgilles B, Aigner J, Kunath M, Lurz R, Schneider R, Schweiger S. Active transport of the ubiquitin ligase MID1 along the microtubules is regulated by protein phosphatase 2A. PLoS One (2008a) 3, e3507.
4. Aranda-Orgilles B, Rutschow D, Zeller R, Karagiannidis AI, Kohler A, Chen C, Wilson T, Krause S, Roepcke S, Lilley D, Schneider R, Schweiger S. Protein Phosphatase 2A (PP2A)-

specific Ubiquitin Ligase MID1 Is a Sequence-dependent Regulator of Translation Efficiency Controlling 3-Phosphoinositide-dependent Protein Kinase-1 (PDPK-1). J Biol Chem (2011) 286, 39945-39957.

5. Aranda-Orgilles B, Trockenbacher A, Winter J, Aigner J, Kohler A, Jastrzebska E, Stahl J, Muller EC, Otto A, Wanker EE, Schneider R, Schweiger S. The Opitz syndrome gene product MID1 assembles a microtubule-associated ribonucleoprotein complex. Hum Genet (2008b)123, 163-176.
6. Arensdorf AM, Marada S, Ogden SK. Smoothenes Regulation: a tale of two signals. Trends Pharmacol Sci (2016) 37(1):62-72
7. Arias E, Cuervo AM. Chaperone-mediated autophagy in protein quality control. Curr Opin Cell Biol (2011) 23:184-189.
8. Arsham AM, Howell JJ, Simon MC. A novel hypoxia inducible factor-independent hypoxic response regulating mammalian target of rapamycin and its targets. J Biol Chem (2003) 278:29655-29660
9. Axe EL, Walker SA, Manifava M, Chandra P, Roderick HL, Habermann A, Griffiths G, Ktistakis NT. Autophagosome formation from membrane compartments enriched in phosphatidylinositol 3-phosphate and dynamically connected to the endoplasmic reticulum. J Cell Biol (2008) 182: 685–701
10. Berbari NF, Kin NW, Sharma N, Michaud EJ, Kesterson RA, Yoder BK. Mutations in Traf3ip1 reveal defects in ciliogenesis, embryonic development, and altered cell size regulation. Dev Biol (2011) 360:66-76
11. Bernabé-Rubio M, Alonso MA. Routes and machinery of primary cilium biogenesis. Cell Mol Life Sci (2017) 74:4077-4095
12. Bernabé-Rubio M, Andrés G, Casares-Arias J, Fernández-Barrera J, Rangel L, Reglero-Real N, Gershlick DC, Fernández JJ, Millán J, Correas I, Miguez DG, Alonso MA. Novel role for the midbody in primary ciliogenesis by polarized epithelial cells. J Cell Biol (2016) 214(3):259-273
13. Berti C, Fontanella B, Ferrentino R, Meroni G. Mig12, a novel Opitz syndrome gene product partner, is expressed in the embryonic ventral midline and co-operates with Mid1 to bundle and stabilize microtubules. BMC Cell Biol (2004) 5:9.
14. Bhoj EJ, Haye D, Toutain A, Bonneau D, Nielsen IK, Lund IB, Bogaard P, Leenskjold S, Karaer K, Wild KT, Grand KL, Astiazaran MC, Gonzalez-Nieto LA, Carvalho A, Lehalle D, Amudhavalli SM, Repnikova E, Saunders C, Thiffault I, Saadi I, Li D, Hakonarson H, Vial Y, Zackai E, Callier P, Drunat S, Verloes A. Phenotypic spectrum associated with SPECC1L

pathogenic variants: new families and critical reviwe of the nosology of Teebi, Opitz GBBB, and Baraitser-Winter syndrome. Eur J Med Genet. (2019) 62(12):103588.

15. Bjørkøy G, Lamark T, Brech A, Outzen H, Perander M, Øvervatn A, Stenmark H, Johansen T. p62/SQSTM1 forms protein aggregates degraded by autophagy and has a protective effect on huntingtin-induced cell death. J Cell Biol (2005) 171:603-614
16. Blacque OE, Reardon MJ, Li C, McCarthy J, Mahjoub MR, Ansley SJ, Badano JL, Mah AK, Beales PL, Davidson WS, Johnsen RC, Audeh M, Plasterk RHA, Baillie DL, Katsanis N, Quarmby LM, Wicks SR, Leroux MR. Loss of *C. elegans* BBS-7 and BBS-8 protein function results in cilia defects and compromised intraflagellar transport. Genes Dev (2004) 18:1630-1642
17. Botilde Y, Yoshiba S, Shinohara K, Hasegawa T, Nishimura H, Shiratori H, Hamada H. Cluap1 localizes preferentially to the base and tip of cilia and is required for ciliogenesis in the mouse embryo. Dev Biol (2013) 381:203-212
18. Briscoe J, Therond PP. The mechanisms of Hedgehog signalling and its roles in development and disease. Nat Rev Mol Cell Biol (2013) 14:416-429
19. Brown C, Moore SH, Nagy M. Pallister Hall Syndrome: laryngeal anomalies and failure to thrive. Ear Nose Throat J (2020) 145561319897428
20. Burman C and Ktistakis NT. Regulation of autophagy by phosphatidylinositol 3-phosphate. FEBS Lett (2010) 584: 1302-1312
21. Cainarca S, Messali S, Ballabio A, Meroni G. Functional characterization of the Opitz syndrome gene product (midin): evidence for homodimerization and association with microtubules throughout the cell cycle. Hum Mol Genet (1999) 8, 1387-1396.
22. Cajanek L, Nigg EA. Cep164 triggers ciliogenesis by recruiting Tau tubulin kinase 2 to the mother centriole. Proc Natl Acad Sci USA (2014) 111:E2841-E2850
23. Carneiro BA, Kaplan JB, Altman JK, Giles FJ, Platanias LC. Targeting mTOR signaling pathways and related negative feedback loops for the treatment of acute myeloid leukemia. Cancer Biol Ther (2015) 16, 648-656.
24. Cell (2008) 19: 2092-2100
25. Cha-Molstad H., Sung KS, Hwang J, Kim KA, Yu JE, Yoo YD, Jang JM, Han DH, Molstad M, Kim JG, Lee YJ, Zakrzewska A, Kim S-H, Kim ST, Kim SY, Lee HG, Soung NK, Ahn JS, Ciechanover A, Kim BY, Kwon YT. Amino-terminal arginylation targets endoplasmic reticulum chaperone BiP for autophagy through p62 binding. Nat. Cell Biol. (2015) 17, 917–929
26. Chauhan S, Kumar S, Jain A, Ponpuak M, Mudd MH, Kimura T, Choi SW, Peters R, Mandell M, Bruun J-A, Johansen T, Deretic V. TRIMs and galectins globally cooperate and TRIM16 and

galectin-3 co-direct autophagy in endomembrane damage homeostasis. Dev. Cell (2016) 39:13-27

27. Cherra SJ, III, Kulich SM, Uechi G, Balasubramani M, Mountzouris J, Day BW, Chu CT. Regulation of the autophagy protein LC3 by phosphorylation. J Cell Biol (2010) 190:533-539
28. Chiang HL, Terlecky SR, Plant CP, Dice JF. A role for a 70-kilodalton heat shock protein in lysosomal degradation of intracellular proteins. Science (1989) 246,382-385.
29. Ciechanover A, Kwon YT. Protein quality control by molecular chaperones in neurodegeneration. Front Neurosci (2017) 11:185
30. Cole DG, Diener DR, Himelblau AL, Beech PL, Fuster JC, Rosenbaum JL. Chlamydomonas kinesin-II-dependent intraflagellar transport (IFT): IFT particles contain proteins required for ciliary assembly in *Caenorhabditis elegans* sensory neurons. J Cell Biol (1998) 141:993-1008
31. Collins GA, Goldberg AL. The logic of the 26S Proteasome. Cell (2017) 169(5):792-806
32. Corbit KC, Aanstad P, Singla V, Norman AR, Stainier DYR, Reiter JF. Vertebrate Smoothened functions at the primary cilium. Nature (2005) 437:1018-1021
33. Corbit KC, Shyer AE, Dowdle WE, Gaulden J, Singla V, Chen M-H, Chuang P-T, Reiter JF. Kif3a constrains beta-catenin-dependent Wnt signalling through dual ciliary and non-ciliary mechanisms. Nat Cell Biol (2008) 10:70-76
34. Davis EE, Katsanis N. The ciliopathies: A translational model into systems biology of human genetic disease. Curr Opin Genet Dev (2012) 22(3):290-303
35. Davis RE, Swiderski RE, Rahmouni K, Nishimura DY, Mullins RF, Agassandian K, Philip AR, Searby CC, Andrews MP, Thompson S, Berry CJ, Thedens DR, Yang B, Weiss RM, Cassell MD, Stone EM, Sheffield VC. A knockin mouse model of the Bardet-Biedl syndrome 1 M390R mutation has cilia defects, ventriculomegaly, retinopathy, and obesity. Proc. Natl Acad. Sci. USA (2007) 104:19422-19427
36. de Conciliis L, Marchitiello A, Wapenaar M, Borsani G, Giglio S, Mariani M, Consalez G, Zuffardi O, Franco B, Ballabio A, Banfi S. Characterization of Cxorf5 (71-7A), a novel human cDNA mapping to Xp22 and encoding a protein containing coiled-coil a-helical domains. Genomics (1998) 51(2):243-250;
37. De Falco F, Cainarca S, Andolfi G, Ferrentino R, Berti C, Rodrìguez Criado G, Rittinger O, Dennis N, Odent S, Rastogi A, Liebelt J, Chitayat D, Winter R, Jawanda H, Ballabio A, Franco B, Meroni G. X-linked Opitz syndrome: novel mutations in the *MID1* gene and redefinition of the clinical spectrum. Am J Med Genet A (2003)120A(2):222-228
38. Delaval B, Bright A, Lawson ND, Doxsey S. The cilia protein IFT88 is required for spindle orientation in mitosis. Nat Cell Biol (2011) 13:461-468

39. Di Como CJ, Arndt KT. Nutrients, via the Tor proteins, stimulate the association of Tap42 with type 2A phosphatases. Genes Dev (1996) 10,1904-1916.
40. Di Rienzo M, Romagnoli A, Antonioli M, Piacentini M, Fimia GM. TRIM proteins in autophagy: selective sensors in cell damage and immune responses. Cell Death Differ (2020) 27(3):887-902
41. Ding WX, Ni HM, Gao W, Hou YF, Melan MA, Chen X, Stolz DB, Shao ZM, Yin XM. Differential effects of endoplasmic reticulum stress-induced autophagy on cell survival. J Biol Chem (2007) 282:4702-4710
42. Dionne LK, Wang X-J, Prekeris R Midbody: from cellular junk to regulator of cell polarity and cell fate. Curr Opin Cell Biol (2015) 35:51-58
43. Djouder N, Tuerk RD, Suter M, Salvioni P, Thali RF, Scholz R, Vaahtomeri K, Auchli Y, Rechsteiner H, Brunisholz RA, Viollet B, Ma ¨ kela ¨ TP, Wallimann T, Neumann D, Krek W. PKA phosphorylates and inactivates AMPKa to promote efficient lipolysis. EMBO J (2010) 29:469-481
44. Ezratty EJ, Stokes N, Chai S, Shah AS, Williams SE, Fuchs E. A role for the primary cilium in Notch signalling and epidermal differentiation during skin development. Cell (2011) 145:1129–1141
45. Ferreira JV, Soares AR, Ramalho JS, Pereira P, Girao H. K63 linked ubiquitin chain formation is a signal for HIF1A degradation by chaperone-mediated autophagy. Sci. Rep. (2015)5, 10210
46. Ferreira R, Fukui H, Chow R, Vilfan A, Vermot J. The cilium as a force sensor-myth versus reality. J Cell Sci (2019)132, jcs213496
47. Follit JA, Tuft RA, Fogarty KE, Pazour GJ. The intraflagellar transport protein IFT20 is associated with the Golgi complex and is required for cilia assembly. Mol Biol Cell (2006) 17:3781-3792
48. Fontanella B, Russolillo G, Meroni G. MID1 mutations in patients with X-linked Opitz G/BBB Syndrome. Hum Mutat (2008) 29(5):584-594.
49. Forcioli-Conti N, Lacas-Gervais S, Dani C, Peraldi P. The primary cilium undergoes dynamic size modifications during adipocyte differentiation of human adipose stem cells. Biochem Biophys Res Commun (2015) 458:117-122
50. Franco B, Thauvin-Robinet C. Update on oralfacial-digital syndromes (OFDS). Cilia (2016) 5:12
51. Fu W, Wang L, Kim S, Li J, Dynlacht BD. Role for the IFT-A complex in selective transport to the primary cilium. Cell Rep (2016) 17:1505-1517
52. Fujita N, Itoh T, Omori H, Fukuda M, Noda T, Yoshimori T. The Atg16L complex specifies the site of LC3 lipidation for membrane biogenesis in autophagy. Mol Biol

53. Furuya N, Yu J, Byfield M, Pattingre S, Levine B. The evolutionarily conserved domain of Beclin 1 is required for Vps34 binding, autophagy and tumor suppressor function. Autophagy (2005)1: 46–52
54. Gaertig J, Wloga D. Ciliary tubulin and its post-translational modifications. Curr Top Dev Biol (2008) 85:83-113
55. Ganley IG, Lam du H, Wang J, Ding X, Chen S, Jiang X. ULK1-ATG13-FIP200 complex mediates mTOR signaling and is essential for autophagy. J Biol Chem (2009) 284:12297-12305
56. Garcia-Gonzalo FR, Reiter JF. Open sesame: how transition fibers and the transition zone control ciliary composition. Cold Spring Harb Perspect Biol (2017) 9(2):a028134
57. Garcia-Gonzalo FR, Reiter JF. Scoring a backstage pass: mechanisms of ciliogenesis and ciliary access. J Cell Biol (2012) 197:697-709
58. Geng J and Klionsky DJ. The Atg8 and Atg12 ubiquitin-like conjugation systems in macroautophagy. EMBO (2008) Rep 9:859–864
59. Gholkar AA, Senese S, Lo YC, Vides E, Contreras E, Hodara E, Capri J, Whitelegge JP, Torres JZ. The X-Linked-Intellectual-Disability-Associated Ubiquitin Ligase Mid2 Interacts with Astrin and Regulates Astrin Levels to Promote Cell Division. Cell reports (2016) 14, 180-188.
60. Ghossoub R, Molla-Herman A, Bastin P, Benmerah A. The ciliary pocket: a once-forgotten membrane domain at the base of cilia. Biol Cell (2011) 103:131-144
61. Goetz SC, Anderson KV. The primary cilium: a signalling centre during vertebrate development. Nat Rev Genet (2010) 11:331-344
62. Goto H, Inaba H, Inagaki M. Mechanisms of ciliogenesis suppression in dividing cells. Cell Mol Life Sci (2016) 74:881-890
63. Granata A, Quaderi NA. The Opitz syndrome gene MID1 is essential for establishing asymmetric gene expression in Hensen's node. Dev Biol (2003) 258,397-405.
64. Green RA, Paluch E, Oegema K. Cytokinesis in animal cells. Annu Rev Cell Dev Biol (2012) 28:29-58
65. Gromley A, Yeaman C, Rosa J, Redick S, Chen C-T, Mirabelle S, Guha M, Sillibourne J, Doxsey SJ. Centriolin anchoring of exocyst and SNARE complexes at the midbody is required for secretory-vesicle-mediated abscission. Cell (2005) 123:75-87
66. Gwinn DM, Shackelford DB, Egan DF, Mihaylova MM, Mery A, Vasquez DS, Turk BE, Shaw RJ. AMPK phosphorylation of raptor mediates a metabolic checkpoint. Mol Cell (2008) 30:214-226

67. Han S, Miyoshi K, Shikada S, Amano G, Wang Y, Yoshimura T, Katayama T. TULP3 is required for localization of membrane-associated proteins ARL13B and INPP5E to primary cilia. Biochem Biophys Res Commun (2019) 509:227-234
68. Hanada T, Noda NN, Satomi Y, Ichimura Y, Fujioka Y, Takao T, Inagaki F, Ohsumi Y. The Atg12-Atg5 conjugate has a novel E3-like activity for protein lipidation in autophagy. J Biol Chem (2007) 282: 37298-37302
69. Hara T, Takamura A, Kishi C, Iemura S, Natsume T, Guan J-L, Mizushima N. FIP200, a ULK-interacting protein, is required for autophagosome formation in mammalian cells. J Cell Biol (2008) 181:497-510
70. Harada M, Hanada S, Toivola DM, Ghori N, Omary MB. Autophagy activation by rapamycin eliminates mouse MalloryDenk bodies and blocks their proteasome inhibitor-mediated formation. Hepatology (2008) 47, 2026-2035
71. Hayashi-Nishino M, Fujita N, Noda T, Yamaguchi A, Yoshimori T, Yamamoto A. A subdomain of the endoplasmic reticulum forms a crandle for autophagosomes formation. Nat Cell Biol (2009) 11:1433-1437.
72. He C, Klionsky DJ. Regulation mechanisms and signaling pathways of autophagy. Annu Rev Genet (2009) 43:67-93.
73. He C, Klionsky DJ. Regulation mechanisms and signalling pathways of autophagy. Annu Rev Genet (2009) 43:67-93
74. Hettich MM, Matthes F, Ryan DP, Griesche N, Schroder S, Dorn S, Kraubeta S, Ehninger D. The anti-diabetic drug metformin reduces BACE1 protein level by interfering with the MID1 complex. PLoS One (2014) 9, e102420.
75. Hilgendorf KI, Johnson CT, Jackson PK. The primary cilium as a cellular receiver: organizing ciliary GPCR signalling. Curr Opin Cell Biol (2016) 39:84-92
76. Hirano T, Katoh Y, Nakayama K. Intraflagellar transport-A complex mediates ciliary entry and retrograde trafficking of ciliary G protein-coupled receptors. Mol Biol Cell (2017) 28:429-439
77. Hosokawa N, Sasaki T, Iemura S, Natsume T, Hara T, Mizushima N. Atg101, a novel mammalian autophagy protein interacting with Atg13. Autophagy (2009) 5: 973-979
78. Høyer-Hansen M, Bastholm L, Szyniarowski P, Campanella M, Szabadkai G, Farkas T, Bianchi K, Fehrenbacher N, Elling F, Rizzuto R, Mathiasen IS, Jaättelä M. Control of macroautophagy by calcium, calmodulin-dependent kinase kinase-b, and Bcl-2. Mol Cell (2007) 25:193-205
79. Hu Q, Nelson WJ. The ciliary diffusion barrier: the gatekeeper for the primary cilium compartment. Cytoskeleton (2011) (Hoboken, NJ) 68:313-324
80. Huang Q, Zhang X. Emerging roles and research tools of atypical ubiquitination.

81. Huangfu D, Liu A, Rakeman AS, Murcia NS, Niswander L, Anderson KV. Hedgehog signalling in the mouse requires intraflagellar transport proteins. Nature (2003) 426:83-87
82. Hyttinen JM, Amadio M, Viiri J, Pascale A, Salminen A, Kaarniranta K. Clearance of misfolded and aggregated proteins by aggrephagy and implications for aggregation diseases. Ageing Res Rev (2014) 18:16-28
83. Ichimura Y, Kirisako T, Takao T, Satomi Y, Shimonishi Y, Ishihara N, Mizushima N, Tanida I, Kominami E, Ohsumi M, Noda T, Ohsumi Y. A ubiquitin-like system mediates protein lipidation. Nature (2000) 408:488-492
84. Inoki K, Zhu T, and Guan K-L. TSC2 mediates cellular energy response to control cell growth and survival. Cell (2003) 115:577-590
85. Ishikawa H, Marshall WF. Ciliogenesis: building the cell's antenna. Nat Rev Mol Cell Biol (2011) 12:222-234
86. Ishikawa H, Marshall WF. Mechanobiology of ciliogenesis. Bioscience (2014) 64:1084-1091
87. Itakura E and Mizushima N. Characterization of autophagosome formation site by a hierarchical analysis of mammalian Atg proteins. Autophagy (2010) 6:764-776
88. Itakura E, Kishi C, Inoue K, Mizushima N. Beclin 1 forms two distinct phosphatidylinositol 3-kinase complexes with mammalian Atg14 and UVRAG. Mol Biol Cell (2008) 19:5360–5372
89. Itakura E, Kishi-Itakura C, and Mizushima N. The hairpintype tail-anchored SNARE syntaxin 17 targets to autophagosomes for fusion with endosomes/lysosomes. Cell (2012) 151:1256-1269
90. Jacomin AC, Samavedam S, Promponas V, Nezis IP iLIR database: a web resource for LIR motif-containing proteins in eukaryotes. Autophagy (2016) 12:1945-1953
91. Jana SC, Marteil G, Bettencourt-Dias M. Mapping molecules to structure: unveiling secrets of centriole and cilia assembly with near-atomic resolution. Curr Opin Cell Biol (2014) 26:96-106
92. Jeffries TR, Dove SK, Michell RH, Parker PJ. PtdIns-specific MPR pathway association of a novel WD40 repeat protein, WIPI49. Mol Biol Cell (2004) 15: 2652–2663
93. Jhanwar-Uniyal M, Wainwright JV, Mohan AL, Tobias ME, Murali R, Gandhi CD, Schmidt MH. Diverse signaling mechanisms of mTOR complexes: mTORC1 and mTORC2 in forming a formidable relationship. Advances in biological regulation (2019) 72,51-62.
94. Jimenez-Sanchez M, Menzies FM, Chang YY, Simecek N, Neufeld TP, Rubinsztein DC. The Hedgehog signalling pathway regulates autophagy. Nat Commun (2012) 3:1200
95. Joubert M, Eisenring JJ, Robb JP, Andermann F. Familial agenesis of the cerebellar vermis. A syndrome of episodic hyperpnea, abnormal eye movements, ataxia, and retardation. Neurology (1969) 19:813-25

96. Jung CH, Jun CB, Ro SH, Kim YM, Otto NM, Cao J, Kundu M, and Kim DH. ULK-Atg13-FIP200 complexes mediate mTOR signaling to the autophagy machinery. Mol Biol Cell (2009) 20:1992–2003
97. Jung CH, Jun CB, Ro SH, Kim YM, Otto NM, Cao J, Kundu M, Kim DH. ULK-Atg13-FIP200 complexes mediate mTOR signalling to the autophagy machinery. Mol Biol Cell (2009) 20: 1992-2003
98. Kabeya Y, Mizushima N, Ueno T, Yamamoto A, Kirisako T, Noda T, Kominami E, Ohsumi Y, Yoshimori T. LC3, a mammalian homologue of yeast Apg8p, is localized in autophagosome membranes after processing. EMBO J (2000) 19:5720-5728
99. Kihara A, Noda T, Ishihara N, Ohsumi Y. Two distinct Vps34 phosphatidylinositol 3-kinase complexes function in autophagy and carboxypeptidase Y sorting in Saccharomyces cerevisiae. J Cell Biol (2001) 152: 519–530
100. Kim E, Goraksha-Hicks P, Li L, Neufeld TP, Guan K-L. Regulation of TORC1 by Rag GTPases in nutrient response. Nat Cell Biol (2008) 10: 935-945
101. Kim J, Dalton VM, Eggerton KP, Scott SV, Klionsky DJ. Apg7p/Cvt2p is required for the cytoplasm-to-vacuole targeting, macroautophagy, and peroxisome degradation pathways. Mol Biol Cell (1999) 10: 1337–1351
102. Kim J, Kundu M, Viollet B, Guan K-L. AMPK and mTOR regulate autophagy through direct phosphorylation of Ulk1. Nat Cell Biol (2011) 13:132-141
103. Kim J, Lee JE, Heynen-Genel S, Suyama E, Ono K, Lee KY, Ideker T, Aza-Blanc P, Gleeson JG. Functional genomic screen for modulators of ciliogenesis and cilium length. Nature (2010) 464:(7291):1048-51
104. Kim S, Tsiokas L. Cilia and cell cycle re-entry: more than a coincidence. Cell Cycle (2011) 10:2683-2690
105. Kimura S, Noda T, Yoshimori T. Dynein-dependent movement of autophagosomes mediates efficient encounters with lysosomes. Cell Struct Funct (2008) 33(1):109-122
106. Kirisako T, Ichimura Y, Okada H, Kabeya Y, Mizushima N, Yoshimori T, Ohsumi M, Takao T, Noda T, Ohsumi Y. The reversible modification regulates the membrane binding state of Apg8/Aut7 essential for autophagy and the cytoplasm to vacuole targeting pathway. J Cell Biol (2000) 151:263–276
107. Kirkin V, McEwan DG, Novak I, Dikic I. A role for ubiquitin in selective autophagy. Mol Cell (2009) 34(3):256-269

108. Klionsky DJ, Cregg JM, Dunn Jr WA, Emr SD, Sakai Y, Sandoval IV, Sibirny A, Subramani S, Thumm M, Veenhuis M, Ohsumi Y. A unified nomenclature for yeast autophagy-related genes. Dev Cell (2003) 5(4),539-545.
109. Kobayashi T, Dynlacht BD. Regulating the transition from centriole to basal body. J Cell Biol (2011) 193:435-444
110. Kohler A, Demir U, Kickstein E, Krauss S, Aigner J, Aranda-Orgilles B, Karagiannidis AI, Achmuller C, Bu H, Wunderlich A, Schweiger MR, Schaefer G, Schweiger S, Klocker H, Schneider R. A hormone-dependent feedback-loop controls androgen receptor levels by limiting MID1, a novel translation enhancer and promoter of oncogenic signaling. Molecular cancer (2014) 13, 146.
111. Komander D, Rape M. The ubiquitin code. Annu Rev Biochem (2012) 81,203-229.
112. Krauss S, Foerster J, Schneider R, Schweiger S. Protein phosphatase 2A and rapamycin regulate the nuclear localization and activity of the transcription factor GLI3. Cancer Res (2008) 68,4658-4665.
113. Krauss S, Griesche N, Jastrzebska E, Chen C, Rutschow D, Achmuller C, Dorn S, Boesch SM, Lalowski M, Wanker E, Schneider R, Schweiger S. Translation of HTT mRNA with expanded CAG repeats is regulated by the MID1-PP2A protein complex. Nature communications (2013) 4, 1511.
114. Krauss S, So J, Hambrock M, Kohler A, Kunath M, Scharff C, Wessling M, Grzeschik KH, Schneider R, Schweiger S. Point mutations in GLI3 lead to misregulation of its subcellular localization. PLoS One (2009) 4,e7471.
115. Kruszka P, Li D, Harr MH, Wilson NR, Swarr D, McCormick EM, Chiavacci RM, Li M, Martinez AF, Hart RA, McDonald-McGinn DM, Deardoff MA, Falk MJ, Allanson JE, Hudson C, Johnson JP, Saadi I. Mutations in *SPECC1L*, encoding sperm antigen with calponin homology and coiled-coil domains 1-like, are found in some cases of autosomal dominant Opitz G/BBB syndrome. J. Med. Genet. (2015) 52(2):104-110.
116. Kuhns S, Schmidt KN, Jr Reymann, Gilbert DF, Neuner A, Hub B, Carvalho R, Wiedemann P, Zentgraf H, Erfle H, KlingmüllerU, Boutros M, Pereira G. The microtubule affinity regulating kinase MARK4 promotes axoneme extension during early ciliogenesis. J Cell Biol (2013) 200:505-522
117. Kulathu Y, Komander D. Atypical ubiquitylation - the unexplored world of polyubiquitin beyond Lys48 and Lys63 linkages. Nat Rev Mol Cell Biol (2012) 13:508–523.

118. Kuma A, Hatano M, Matsui M, Yamamoto A, Nakaya H, Yoshimori T, Ohsumi Y, Tukuhisa T, Mizushima N. The role of autophagy during the early neonatal starvation period. Nature (2004) 432(7020),1032-1036.
119. Lacassie Y, Arriaza MJ. Opitz G/BBB syndrome and the 22q11.2 deletion. Am. J. Med. Genet. (1996) 62(3):318
120. Lamark T, Svenning S, Johansen T. Regulation of selective autophagy: the p62/SQSTM1 paradigm. Essays Biochem (2017) 61:609-624
121. Lancioni A, Pizzo M, Fontanella B, Ferrentino R, Napolitano LMR, De Leonibus E, Meroni G. Lack of *Mid1*, the mouse orthologue of the Opitz syndrome gene, causes abnormal development of the anterior cerebellar vermis. J. Neurosci. (2010) 30(8),2880-2887.
122. Lee JW, Park S, Takahashi Y, Wang HG. The association of AMPK with ULK1 regulates autophagy. PLoS One (2010) 5:e15394
123. LeNoue-Newton ML, Wadzinski BE, Spiller BW. The three types 2A protein phosphatases, PP2Ac, PP4c and PP6c, are differentially regulated by Alpha4. Biochem Biophys Res Commun (2016) 475,64-69.
124. Levine B, Deretic V. Unveiling the roles of autophagy in innate and adaptive immunity. Nat Rev Immunol (2007) 7(10),767-777.
125. Li WW, Li J, Bao J. Microautophagy: lesser-known self-eating. Cell Mol Life Sci (2012) 69(7):1125-1136.
126. Liang XH, Jackson S, Seaman M, Brown K, Kempkes B, Hibshoosh H, Levine B. Induction of autophagy and inhibition of tumorigenesis by beclin 1. Nature (1999) 402: 672–676
127. Liang Y, Meng D, Zhu B, Pan J. Mechanism of ciliary disassembly. Cell Mol Life Sci (2016) 73:1787-1802
128. Liem KF Jr, Ashe A, He M, Satir P, Moran J, Beier D, Wicking C, Anderson KV. The IFT-A complex regulates Shh signaling through cilia structure and membrane protein trafficking. J Cell Biol (2012) 197:789-800
129. Linck RW, Norrander JM. Protofilament ribbon compartments of ciliary and flagellar microtubules. Protist (2003) 154:299-311
130. Liu E, Knutzen CA, Krauss S, Schweiger S, Chiang GG. Control of mTORC1 signaling by the Opitz syndrome protein MID1. Proc Natl Acad Sci U S A (2011) 108,8680-8685.
131. Liu J, Prickett TD, Elliott E, Meroni G, Brautigan DL. Phosphorylation and microtubule association of the Opitz syndrome protein mid-1 is regulated by protein phosphatase 2A via binding to the regulatory subunit alpha 4. Proc Natl Acad Sci U S A (2001) 98, 6650-6655.

132. Loktev AV, Zhang Q, Beck JS, Searby CC, Scheetz TE, Bazan JF, Slusarski DC, Sheffield VC, Jackson PK, Nachury MV. A BBSome subunit links ciliogenesis, microtubule stability, and acetylation. Dev Cell (2008) 15:854-865
133. Lu Y, Lee BH, King RW, Finley D, Kirschner MW. Substrate degradation by the proteasome: a single-molecule kinetic analysis. Science (2015)348:1250834
134. Lum JJ, Bauer DE, Kong M, Harris MH, Li C, Lindsten T, Thompson CB. Growth factor regulation of autophagy and cell survival in the absence of apoptosis. Cell (2005) 120: 237-248
135. Mackeh R, Perdiz D, Lorin S, Codogno P, Poüs C. Autophagy and microtubules-new story, old players (2013) 126(Pt5):1071-1080
136. Malicki JJ, Johnson CA. The cilium: cellular antenna and central processing unit. Trends Cell Biol (2017) 27:126-140
137. Mandell MA, Kimura T, Jain A, Johansen T, Deretic V. TRIM proteins regulate autophagy: TRIM5 is a selective autophagy receptor mediating HIV-1 restriction. Autophagy (2014) 10:2387-2388
138. Marshall WF, Qin H, Rodrigo Brenni M, Rosenbaum JL. Flagellar length control system: testing a simple model based on intraflagellar transport and turnover. Mol Biol Cell (2005) 16, 270-278
139. Marzella L, Ahlberg J, Glaumann H. Autophagy, heterophagy, microautophagy and crinophagy as the means for intracellular degradation. Virchowa Arch B Cell Pathol Incl Mol Pathol (1981) 36(2-3):219-234.
140. Massiah MA, Matts JA, Short KM, Simmons BN, Singireddy S, Yi Z, Cox TC. Solution structure of the MID1 B-box2 CHC(D/C)C(2)H(2) zinc-binding domain: insights into an evolutionarily conserved RING fold. J Mol Biol (2007) 369:1-10
141. Massiah MA, Simmons BN, Short KM, Cox TC. Solution Structure of the RBCC/TRIM B-box1 domain of human MID1: B-box with a RING. J Mol Biol (2006) 358:532–545.
142. Matsumoto G, Wada K, Okuno M, Kurosawa M, Nukina N. Serine 403 phosphorylation of p62/SQSTM1 regulates selective autophagic clearance of ubiquitinated proteins. Mol. Cell (2011) 44, 279-289
143. Matthes F, Massari S, Bochicchio A, Schorpp K, Schilling J, Weber S, Offermann N, Desantis J, Wanker E, Carloni P, Hadian K, Tabarrini O, Rossetti G, Krauss S. Reducing Mutant Huntingtin Protein Expression in Living Cells by a Newly Identified RNA CAG Binder. ACS chemical neuroscience (2018b) 9, 1399-1408.
144. Mavrakis M, Lippincott-Schwartz J, Stratakis CA, Bossis I. Depletion of type IA regulatory subunit (RIa) of protein kinase A (PKA) in mammalian cells and tissues activates mTOR and causes autophagic deficiency. Hum Mol Genet (2006) 15:2962-2971

145. May-Simera HL, Kelley MW. Cilia, Wnt signalling, and the cytoskeleton. Cilia (2012) 1:7
146. McKeon JE, Sha D, Li L, Chin LS. Parkin-mediated K63-polyubiquitination targets ubiquitin C-terminal hydrolase L1 for degradation by the autophagy-lysosome system. Cell. Mol. Life Sci. (2015) 72, 1811-1824.
147. Meley D, Bauvy C, Houben-Weerts JH, Dubbelhuis PF, Helmond MT, Codogno P, Meijer AJ. AMP-activated protein kinase and the regulation of autophagic proteolysis. J Biol Chem (2006) 281:34870-34879
148. Meroni G, Diez-Roux G. TRIM/RBCC, a novel class of 'single protein RING finger' E3 ubiquitin ligase. Bioessays (2005) 27,1147-1157.
149. Mierzwa B, Gerlich DW. Cytokinetic abscission: molecular mechanisms and temporal control. Dev Cell (2014) 31:525-538
150. Mizushima N, Klionsky DJ. Protein turnover via autophagy: implications for metabolism. Annu Rev Nutr (2007) 27,19-40.
151. Mizushima N, Komatsu M. Autophagy: renovation of cells and tissues. Cell (2011) 147(4),728-741.
152. Mizushima N, Kuma A, Kobayashi Y, Yamamoto A, Matsubae M, Takao T, Natsume T, Ohsumi Y, Yoshimori T. Mouse Apg16L, a novel WD-repeat protein, targets to the autophagic isolation membrane with the Apg12-Apg5 conjugate. J Cell Sci (2003) 116: 1679–1688
153. Mizushima N, Levine B, Cuervo AM, Klionsky DJ. Autophagy fights disease through cellular self-digestion. Nature (2008) 451(7182),1069-1075.
154. Mizushima N, Levine B. Autophagy in mammalian development. Nat Cell Biol (2010) 12(9),823-830
155. Mizushima N, Yamamoto A, Hatano M, Kobayashi Y, Kabeya Y, Suzuki K, Tokuhisa T, Ohsumi Y, Yoshimori T. Dissection of autophagosome formation using Apg5-deficient mouse embryonic stem cells. J Cell Biol (2001) 152: 657–668
156. Mizushima N, Yoshimori T, Ohsumi Y. The role of atg proteins in autophagosome formation. Annu. Rev. Cell Dev. Biol. (2011) 27, 107-132
157. Molla-Herman A, Ghossoub R, Blisnick T, Meunier A, Serres C, Silbermann F, Emmerson C, Romeo K, Bourdoncle P, Schmitt A, Saunier S, Spassky N, Bastin P, Benmerah A. The ciliary pocket: an endocytic membrane domain at the base of
158. Monastyrska I, Rieter E, Klionsky DJ, Reggiori F. Multiple roles of the cytoskeleton in autophagy. Biol Rev Camb Philos Soc (2009) 84:431-448
159. Monteiro O, Chen C, Bingham R, Argyrou A, Buxton R, Pancevac Jonsson C, Jones E, Bridges A, Gatfield K, Krauss S, Lambert J, Langston R, Schweiger S, Uings I. Pharmacological

disruption of the MID1/alpha4 interaction reduces mutant Huntingtin levels in primary neuronal cultures. Neuroscience letters (2018) 673, 44-50.

160. Morleo M, Franco B. The autophagy-cilia axis: an intricate relationship. Cells (2019) 8(8):905
161. Mullins J, Biesele JJ. Terminal phase of cytokinesis in D-98S cells. J Cell Biol (1977) 73:672-684
162. Munch D, Rodriguez E, Bressendorff S, Park OK, Hofius D, Petersen M. Autophagy deficiency leads to accumulation of ubiquitinated proteins, ER stress, and cell death in Arabidopsis. Autophagy (2014) 10, 1579-1587
163. Mykytyn K, Mullins RF, Andrews M, Chiang AP, Swiderski RE, Yang B, Braun T, Casavant T, Stone EM, Sheffield VC. Bardet-Biedl syndrome type 4 (BBS4)-null mice implicate Bbs4 in flagella formation but not global cilia assembly. Proc. Natl Acad. Sci. USA (2004) 101:8664-8669
164. Nachury MV, Loktev AV, Zhang Q, Westlake CJ, Peränen J, Merdes A, Slusarski DC, Scheller RH, Bazan JF, Sheffield VC, Jackson PK. A core complex of BBS proteins cooperates with the GTPase Rab8 to promote ciliary membrane biogenesis. Cell (2007) 129:1201-1213
165. Nachury MV. The molecular machines that traffic signalling receptors into and out of cilia. Curr Opin Cell Biol (2018) 51:124-131
166. Nakatogawa H, Suzuki K, Kamada Y, Ohsumi Y. Dynamics and diversity in autophagy mechanisms: lessons from yeast. Nat Rev Mol Cell Biol (2009) 10(7),458-467.
167. Novarino G, Akizu N, Gleeson JG Modeling human disease in humans: the ciliopathies. Cell (2011) 147:70-79
168. Ohsumi Y. Molecular dissection of autophagy: two ubiquitin-like systems. Nat Rev Mol Cell Biol (2001) 2: 211–216
169. Ohtake F, Tsuchiya H. The emerging complexity of ubiquitin architecture. J Biochem (2017) 161(2):125-133
170. Opitz JM, Frias JL, Gutenberger JE, Pellet JR. The G syndrome of multiple congenital anomalies. BD:OAS (1969a) V(2):95-101.
171. Opitz JM, Summit RL, Smith DW. The BBB syndrome: familial telecanthus with associated congenital anomalies. BD:OAS (1969b) V(2):86-94.
172. Orenstein SJ, Cuervo AM. Chaperon-mediated autophagy:molecular mechanisms and physiological relevance. Semin Cell Dev Biol (2010) 21:719-726.
173. Orhon I, Dupont N, Zaidan M, Boitez V, Burtin M, Schmitt A, Capiod T, Viau A, Beau I, Kuehn EW, Friedlander G, Terzi F, Codogno P. Primary-cilium-dependent autophagy controls epithelial cell volume in response to fluid flow. Nat Cell Biol (2016) 18:657-667

174. Palmer S, Perry J, Kipling D, Ashworth A. A gene spans the pseudoautosomal boundary in mice. Proc Natl Acad Sci USA (1997) 94,12030-12035.
175. Pampliega O, Cuervo AM. Autophagy and primary cilia: dual interplay. Curr Opin Cell Biol (2016) 39:1-7
176. Pampliega O, Orhon I, Patel B, Sridhar S, Diaz-Carretero A, Beau I, Codogno P, Satir BH, Satir P, Cuervo AM. Functional interaction between autophagy and ciliogenesis. Nature (2013) 502:94-200
177. Pan J, Seeger-Nukpezah T, Golemis EA. The role of the cilium in normal and abnormal cell cycles: emphasis on renal cystic pathologies. Cell Mol Life Sci (2013) 70:1849-1874.
178. Pan J-A, Sun Y, Jiang Y-P, Bott AJ, Jaber N, Dou Z, Yang B, Chen J-S, Catanzaro JM, Du C, Ding W-X, Diaz-Meco MT, Moscat J, Ozato K, Lin RZ, Zong W-X. TRIM21 ubiquitylates SQSTM1/p62 ans suppresses protein sequestration to regulate redox homeostasis. Mol Cell (2016) 62(1):149-151
179. Pan T, Kondo S, Zhu W, Xie W, Jankovic J, Le W. Neuroprotection of rapamycin in lactacystin-induced neurodegeneration via autophagy enhancement. Neurobiol. Dis. (2008) 32, 16-25.
180. Paridaen JTML, Wilsch-Bräuninger M, Huttner WB. Asymmetric inheritance of centrosome-associated primary cilium membrane directs ciliogenesis after cell division. Cell (2013) 155:333–344
181. Parzych KR, Klionsky DJ. An overview of autophagy: Morphology, mechanism and regulation. Antioxi Redox Signal (2014) 20(3):460-473.
182. Pazour GJ, Dickert BL, Witman GB. The DHC1b (DHC2) isoform of cytoplasmic dynein is required for flagellar assembly. J Cell Biol (1999) 144, 473–481
183. Pazour GJ, Wilkerson CG, Witman GB. A dynein light chain is essential for the retrograde particle movement of intraflagellar transport (IFT). J Cell Biol (1998) 141, 979-992
184. Pearring JN, Salinas RY, Baker SA, Arshavsky VY. Protein sorting, targeting and trafficking in photoreceptor cells. Prog Retina Eye Res (2013) 36:24-51
185. Perrault I, Halbritter J, Porath JD, Gerard X, Braun DA, Gee HY,Fathy HM, Saunier S, Cormier-Daire V, Thomas S, Attié-Bitach T, Boddaert N, Taschner M, Schueler M, Lorentzen E, Lifton RP, Lawson JA, Garfa-Traore M, Otto EA, Bastin P, Caillaud C, Kaplan J, Rozet J-M, Hildebrandt F. IFT81, encoding an IFT-B core protein, as a very rare cause of a ciliopathy phenotype. J Med Genet (2015) 52:657-665
186. Pfirmann T, Jandt E, Ranft S, Lokapally A, Neuhaus H, Perron M, Hollemann T. Hedgehog-dependent E3-ligase Midline1 regulates ubiquitin-mediated proteasomal degradation of Pax6 during visual system development. Proc Natl Acad Sci U S A (2016) 113,10103-10108.

187. Polson HE, de Lartigue J, Rigden DJ, Reedijk M, Urbe S, Clague MJ, Tooze SA. Mammalian Atg18 (WIPI2) localizes to omegasome-anchored phagophores and positively regulates LC3 lipidation. Autophagy (2010) 6: 506–522
188. Portran D, Schaedel L, Xu Z, Thery M, Nachury MV. Tubulin acetylation protects long-lived microtubules against mechanical ageing. Nat Cell Biol (2017) 19:391-398
189. primary and motile cilia. J Cell Sci (2010) 123:1785-1795
190. Proikas-Cezanne T, Waddell S, Gaugel A, Frickey T, Lupas A, Nordheim A. WIPI-1a (WIPI49), a member of the novel 7-bladed WIPI protein family, is aberrantly expressed in human cancer and is linked to starvation-induced autophagy. Oncogene (2004) 23: 9314–9325
191. Proteomics (2020) e1900100.
192. Qi Z, Chen L. Endoplasmic Reticulum Stress and Autophagy. Adv Exp Med Biol (2019) 1206:167-177
193. Quaderi NA, Schweiger S, Gaudenz K, Franco B, Rugarli, EI, Berger W, Feldman GJ, Volta M, Andolfi G, Gilgenkrantz S, Marion RW, Hennekam RC, Opitz JM, Muenke M, Ropers HH, Ballabio A. Opitz G/BBB syndrome, a defect of midline development, is due to mutations in a new RING finger gene on Xp22. Nature Genetics (1997) *17*, 285-291.
194. Rasband, W.S., ImageJ, U. S. National Institutes of Health, Bethesda, Maryland, USA, https://imagej.nih.gov/ij/, 1997-2018.
195. Reales E, Bernabé-Rubio M, Casares-Arias J, Rentero C, Fernández-Barrera J, Rangel L, Correas I, Enrich C, Andrés G, Alonso MA. The MAL protein is crucial for proper membrane condensation at the ciliary base, which is required for primary cilium elongation. J Cell Sci (2015) 128:2261-2270
196. Reiter JF, Leroux MR. Genes and molecular pathways underpinning ciliopathies. Nat Rev Mol Cell Biol (2017) 18(9):533-547
197. Reymond A, Meroni G, Fantozzi A, Merla G, Cairo S, Luzi L, Riganelli D, Zanaria E, Messali S, Cainarca S, Guffanti A, Minucci S, Pelicci PG, Ballabio A. The tripartite motif family identifies cell compartments. Embo J (2001) 20, 2140-2151.
198. Robbins DJ, Fei DL, Riobo NA. The Hedgehog signal transduction network. Sci Signal (2012) 5:re6
199. Robin NH, Opitz JM, Muenke M. Opitz G/BBB syndrome: clinical comparison of families linked to Xp22 and 22q, and a review of the literature. Am. J. Med. Genet. (1996) 62:305-317.
200. Rohatgi R, Snell WJ. The ciliary membrane. Curr Opin Cell Biol (2010) 22:541-546
201. Rosenbaum JL, Witman GB. Intraflagellar transport. Nat Rev Mol Cell Biol (2002) 3:813-825

202. Saadi I, Alkuraya FS, Gisselbrecht SS, Goessling W, Cavallesco R, Turbe-Doan A, Petrin AL, Harris J, Siddiqui U, Grix AW Jr, Hove HD, Leboulch P, Glover TW, Morton CC, Richieri-Costa A, Murray JC, Erickson RP, Maas RL. Deficiency of the cytoskeletal protein SPEEC1L leads to oblique facial clefting. Am. J. Hum. Genet. (2011) 89(1):44-55
203. Sancak Y, Peterson TR, Shaul YD, Lindquist RA, Thoreen CC, Bar-Peled L, Sabatini DM. The Rag GTPases bind raptor and mediate amino acid signalling to mTORC1. Science (2008) 320:1496-1501
204. Sasai N, Briscoe J. Primary cilia and graded Sonic Hedgehog Signalling. Wiley Interdiscip Rev Dev Biol (2012) 1(5):753-772
205. Satir P, Christensen ST. Overview of structure and function of mammalian cilia. Annu Rev Physiol (2007) 69:377-400
206. Schmidt KN, Kuhns S, Neuner A, Hub B, Zentgraf H, Pereira G. Cep164 mediates vesicular docking to the mother centriole during early steps of ciliogenesis. J Cell Biol (2012) 199:1083-1101
207. Schneider L, Clement CA, Teilmann SC, Pazour GJ, Hoffmann EK, Satir P, Christensen ST. PDGFRa signaling is regulated through the primary cilium in fibroblasts. Curr Biol (2005) 15:1861–1866
208. Schulman BA, Harper JW. Ubiquitin-like protein activation by E1 enzymes: the apex for downstream signalling pathways. Nat Rev Mol Cell Biol (2009) 10:319-331
209. Schweiger S, Dorn S, Fuchs M, Kohler A, Matthes F, Muller EC, Wanker E, Schneider R, Krauss S. The E3 ubiquitin ligase MID1 catalyzes ubiquitination and cleavage of Fu. J Biol Chem (2014) 289, 31805-31817.
210. Schweiger S, Foerster J, Lehmann T, Suckow V, Muller YA, Walter G, Davies T, Porter H, van Bokhoven H, Lunt PW, Traub P, Ropers HH. The Opitz syndrome gene product, MID1, associates with microtubules. Proc Natl Acad Sci U S A (1999) 96, 2794-2799.
211. Shang L, Chen S, Du F, Li S, Zhao L, Wang X. Nutrient starvation elicits an acute autophagic response mediated by Ulk1 dephosphorylation and its subsequent dissociation from AMPK. Proc Natl Acad Sci U S A (2011) 108:4788-4793
212. Shen K, Choe A, Sabatini DM. Intersubunit crosstalk in the Rag GTPase heterodimer enables mTORC1 to respond rapidly to amino acid availability. Mol Cell (2017) 68(4):821
213. Shintani T, Mizushima N, Ogawa Y, Matsuura A, Noda T, Ohsumi Y. Apg10p, a novel protein-conjugating enzyme essential for autophagy in yeast. EMBO J (1999) 18: 5234–5241
214. Short KM, Cox TC. Sub-classification of the rbcc/trim superfamily reveals a novel motif necessary for microtubule binding. J Biol Chem (2006) 281, 8970-8980.

215. Short KM, Hopwood B, Yi Z, Cox TC. MID1 and MID2 homo- and heterodimerise to tether the rapamycin-sensitive PP2A regulatory subunit, Alpha4, to microtubules: implications for the clinical variability of X-linked Opitz G/BBB syndrome and other development disorders. BMC Cell Biol (2002) 3,1.
216. Sontag E. Protein phosphatase 2A: the Trojan Horse of cellular signaling. Cell Signal (2001) 13,7-16.
217. Sorokin SP. Reconstructions of centriole formation and ciliogenesis in mammalian lungs. J Cell Sci (1968) 3:207-230
218. Spektor A, Tsang WY, Khoo D, Dynlacht BD. Cep97 and CP110 suppress a cilia assembly program. Cell (2007) 130:678-690
219. Steffen W, Linck RW. Evidence for tektins in centrioles and axonemal microtubules. Proc. Natl Acad. Sci. USA (1988) 85:2643-2647
220. Stephan JS, Yeh YY, Ramachandran V, Deminoff SJ, Herman PK. The Tor and cAMP-dependent protein kinase signalling pathways coordinately control autophagy in *Saccharomyces cerevisiae*. Autophagy (2010) 6:294-295
221. Struchtrup A, Wiegering A, Stork B, Ruther U, Gerhardt C. The ciliary protein RPGRIP1L governs autophagy independently of its proteasome-regulating function at the ciliary base in mouse embryonic fibroblasts. Autophagy (2018) 14:567-583
222. Takei R, Katoh Y, Nakayama K. Robust interaction of IFT70 with IFT52-IFT88 in the IFT-B complex is required for ciliogenesis. Biol Open (2018) 7:bio033241
223. Tang Z, Lin MG, Stowe TR, Chen S, Zhu M, Stearns T, Franco B, Zhong Q. Autophagy promotes primary ciliogenesis by removing OFD1 from centriolar satellites. Nature (2013) 502(7470):254-257
224. Tanida I, Minematsu-Ikeguchi N, Ueno Takashi, Kominami E. Lysosomal turnover, but not a cellular level, of endogenous LC3 is a marker for autophagy. Autophagy (2005) 1(2):84-91
225. Taschner M, Lorentzen E. The intraflagellar transport machinery. Cold Spring Harb Perspect Biol (2016) 8(10):a028092
226. The jamovi project (2021). Jamovi. (Version 1.8). retrievered form https://www.jamovi.org.
227. Tomar D, Prajapati P, Sripada L, Singh K, Singh R, Singh AK, Singh R. TRIM13 regulates caspase-8 ubiquitination, translocation to autophagosomes and activation during ER stress induced cell death. Biochim. Biophys. Acta (2013) 1833, 3134-3144
228. Tomar D, Singh R, Singh AK, Pandya CD, Singh R. Trim13 regulates ER stress insuced autophagy and clonogenic ability of the cells. Biochim Biophys Acta (2012) 1823 (2):316-326

229. Trockenbacher A, Suckow V, Foester J, Winter J, Krauss S, Ropers HH, Schneider R, Schweiger S. MID1, mutated in Opitz Syndrome, encodes an ubiquitin ligase that targets phosphatase 2A for degradation. Nat Genet (2001) 29,287-294.
230. Tsukamoto S, Kuma A, Murakami M, Kishi C, Yamamoto A, Mizushima N. Autophagy is essential for preimplantation development of mouse embryos. Science (2008) 321(5885),117-120.
231. Valente EM, Dallapiccola B, Bertini E. Joubert syndrome and related disorders. Handb Clin Neurol (2013) 113:1879-1888
232. van Gent M, Sparrer KMJ, Gack MU. TRIM proteins and their roles in antiviral host defenses. Annu Rev Virol (2018) 5(1):385-405
233. Wang S, Livingston MJ, Su Y, Dong Z. Reciprocal regulation of cilia and autophagy via the mTOR and proteasome pathways. Autophagy (2015) 11:607-616
234. Wang W, Jack BM, Wang HH, Kavanaugh MA, Maser RL, Tran PV. Intraflagellar transport proteins as regulators of primary cilia length. Front Cell Dev Biol (2021) 9:661350
235. Watkins GR, Wang N, Mazalouskas MD, Gomez RJ, Guthrie CR, Kraemer BC, Schweiger S, Spiller BW and Wadzinski BE. Monoubiquitination promotes calpain cleavage of the protein phosphatase 2A (PP2A) regulatory subunit alpha4, altering PP2A stability and microtubule-associated protein phosphorylation. J Biol Chem (2012) 287,24207-24215.
236. Wei Q, Ling K, Hu J. The essential roles of transition fibers in the context of cilia. Curr Opin Cell Biol (2015) 35:98-105
237. Weidberg H, Shvets E, Elazar Z. Biogenesis and cargo selectivity of autophagosomes. Annu Rev Biochem (2011) 80: 125–156
238. Westlake CJ, Baye LM, Nachury MV, Wright KJ, Ervin KE, Phu L, Chalouni C, Beck JS, Kirkpatrick DS, Slusarski DC, Sheffield VC, Scheller RH, Jackson PK. Primary cilia membrane assembly is initiated by Rab11 and transport protein particle II (TRAPPII) complex-dependent trafficking of Rabin8 to the centrosome. Proc Nat Acad Sci USA (2011) 108:2759-2764
239. Wheway G, Nazlamova L, Hancock JT. Signalling through the primary cilium. Front.Cell Dev Biol (2018) 6:8
240. Wilcockson SG, Sutcliffe C, Ashe HL Control of signalling molecule range during developmental patterning. Cell Mol Life Sci (2016) 74(11):1937-1956
241. Williams FP, Haubrich K, Perez-Borrajero C, Hennig J. Emerging RNA-binding roles in the TRIM family of ubiquitin ligases. Biol Chem (2019) 400, 1443-1464.
242. Winter J, Basilicata MF, Stemmler MP, Krauss Sybille. The MID1 protein is a central player during development and in disease. Front Biosci (2016) 21:664-82

243. Winter J, Kunath M, Roepcke S, Krause S, Schneider R, and Schweiger S. Alternative polyadenylation signals and promoters act in concert to control tissue-specific expression of the Opitz Syndrome gene MID1. BMC Mol Biol (2007) 8, 105.
244. Winter J, Lehmann T, Krauss S, Trockenbacher A, Kijas Z, Foerster J, Suckow V, Yaspo ML, Kulozik A, Kalscheuer V, Schneider R, Schweiger S. Regulation of the MID1 protein function is fine-tuned by a complex pattern of alternative splicing. Hum Genet. (2004). 114, 541-552.
245. Wloga D, Joachimiak E, Louka P, Gaertig J. Posttranslational modifications of tubulin and cilia. Cold Spring Harb Perspect Biol. (2016) 9(6):a028159
246. Wood CR, Huang K, Diener DR, Rosenbaum JL. The cilium secretes bioactive ectosomes. Curr Biol (2013) 23:906-911
247. Wren KN, Craft JM, Tritschler D, Schauer A, Patel DK, Smith EF, Porter ME, Kner P, Lechtreck KF. A differential cargo-loading model of ciliary length regulation by IFT. Curr Biol (2013) 23(24):2463-2471
248. Wu X, Karin M. Emerging roles of Lys63-linked polyubiquitylation in immune responses. Immunol Rev (2015) 266(1):161-174
249. Xie R, Nguyen S, McKeehan WL, Liu L. Acetylated microtubules are required for fusion of autophagosomes with lysosomes. BMC Cell Biol (2010) 11:89
250. Yan Y, Flinn RJ, Wu H, Schnur RS, Backer JM. hVps15, but not $Ca^{2+}$/CaM, is required for the activity and regulation of hVps34 in mammalian cells. Biochem J (2009) 417: 747–755
251. Yang Z and Klionsky DJ. Mammalian autophagy: core molecular machinery and signaling regulation. Curr Opin Cell Biol (2010) 22:124-131
252. Yang Z, Klionsky DJ. An overview of the molecular mechanism of autophagy. Curr Top Microbiol Immunol (2009) 335:1-32.
253. Young ARJ, Chan EYW, Hu XW, Ko ¨chl R, Crawshaw SG, High S, Hailey DW, Lippincott-Schwartz J, Tooze SA. Starvation and ULK1-dependent cycling of mammalian Atg9 between the TGN and endosomes. J Cell Sci (2006) 119:3888-3900
254. Zaffagnini G, Martens S. Mechanisms of selective autophagy. J Mol Biol (2016) 428 (9PtA):1714-1724
255. Zanchetta ME, Meroni G. Emerging Roles of the TRIM E3 Ubiquitin Ligases MID1 and MID2 in Cytokinesis. Frontiers in physiology (2019) 10, 274.
256. Zanchetta ME, Napolitano LMR, Maddalo D, Meroni G. The E3 ubiquitin ligase MID1/TRIM18 promotes atypical ubiquitination of the BRCA2-associated factor 35, BRAF35. Biochimica et biophysica acta Molecular cell research (2017) 1864, 1844-1854.

257. Zhang W, Taylor SP, Nevarez L, Lachman RS, Nickerson DA, Bamshad M, Krakow D, Cohn DH. IFT52 mutations destabilize anterograde complex assembly, disrupt ciliogenesis and result in short rib polydactyly syndrome. Hum Mol Genet (2016) 25:4012-4020
258. Zhao B, Li L, Lei Q, Guan K-L. The Hippo-YAP pathway in organ size control and tumorigenesis: an updated version. Genes Dev (2010) 24:862-874
259. Zimmerman K, Yoder BK. Snapshot: sensing and signalling by cilia. Cell (2015) 161(692–692):e691
260. Zuo X, Guo W, Lipschutz JH. The exocyst protein sec10 is necessary for primary ciliogenesis and cystogenesis in vitro. Mol Biol Cell (2009) 20:2522-2529